PREDICTION OF SOUND TRANSMISSION CHARACTERISTICS OF MULTIPLE ELASTOMERIC BULB SEALS

A THESIS SUBMITTED TO

THE GRADUATE SCHOOL OF NATURAL AND APPLIED SCIENCES

OF

MIDDLE EAST TECHNICAL UNIVERSITY

BY

BURAK NEBİL BARUTÇU

IN PARTIAL FULFILLMENT OF THE REQUIREMENTS

FOR

THE DEGREE OF MASTER OF SCIENCE

IN

MECHANICAL ENGINEERING

JUNE 2017

Approval of the thesis:

PREDICTION OF SOUND TRANSMISSION CHARACTERISTICS OF MULTIPLE ELASTOMERIC BULB SEALS

submitted by **BURAK NEBİL BARUTÇU** in partial fulfillment of the requirements for the degree of **Master of Science in Mechanical Engineering Department, Middle East Technical University** by,

Prof. Dr. Gülbin Dural Ünver
Dean, Graduate School of **Natural and Applied Sciences** _____

Prof. Dr. Tuna Balkan
Head of Department, **Mechanical Engineering** _____

Prof. Dr. Mehmet Çalışkan
Supervisor, **Mechanical Engineering Dept., METU** _____

Examining Committee Members:

Assoc. Prof. Dr. Ergin Tönük
Mechanical Engineering Dept., METU _____

Prof. Dr. Mehmet Çalışkan
Supervisor, **Mechanical Engineering Dept., METU** _____

Asst. Prof. Gökhan O. Özgen
Mechanical Engineering Dept., METU _____

Asst. Prof. Kerem Bayar
Mechanical Engineering Dept., METU _____

Asst. Prof. Dr. Bülent İrfanoğlu
Mechatronics Engineering Dept., Atılım University _____

Date: 22.06.2017

I hereby declare that all information in this document has been obtained and presented in accordance with academic rules and ethical conduct. I also declare that, as required by these rules and conduct, I have fully cited and referenced all material and results that are not original to this work.

Name, Last name : Burak Nebil Barutçu
Signature :

ABSTRACT

PREDICTION OF SOUND TRANSMISSION CHARACTERISTICS OF MULTIPLE ELASTOMERIC BULB SEALS

Barutçu, Burak Nebil

M. Sc., Department of Mechanical Engineering

Supervisor: Prof. Dr. Mehmet Çalışkan

June 2017, 103 pages

Prevention of transmitted sound through car doors is a critical issue; as doors are the weakest parts of a car assembly in terms of sound isolation performance. Main path for sound transmission is through the seals between the car body and the door. Hence, the examination of sound transmission loss characteristics of seals between the car body and door is important to improve the sound isolation characteristics of the door assembly. The aim of this research is prediction of the sound transmission characteristics of multiple elastomeric bulb seals used between the car door and body. Generally, two bulb seals are used; the first one is attached to the main body of the

car and the other is attached to the door. Those elastomeric sealants should be examined together to improve the total sound insulation performance.

Prediction of sound transmission characteristics of multiple elastomeric bulb seal system is the main objective of this research. This assessment includes four main steps. The first step is validating the deformation analysis by comparing the force vs opening curves of the bulb seals with the analyses results. The second step is prediction of the deformed form of those multiple seal system. The third step involves validation of acoustical simulations. The final step is about estimation of transmission loss of the assembly of two deformed bulb seals, based on the deformation analysis conducted in the second step. Sound transmission loss values are examined to predict the sound insulation performance of the sealing system.

Keywords: Hyperelastic materials, nonlinear FEA, multiple bulb seals system, sound transmission loss, force – opening curve

ÖZ

ELASTOMER YAPIDAKİ ÇOKLU BALON FİTİLLERİNİN SES GEÇİŞ KAYBI KARAKTERİSTİĞİNİN DEĞERLENDİRİLMESİ

Barutçu, Burak Nebil

Yüksek Lisans, Makina Mühendisliği Bölümü

Tez Yöneticisi: Prof. Dr. Mehmet Çalışkan

Haziran 2017, 103 sayfa

Ses geçirgenliği konusunda otomobillerin en zayıf noktaları araç kapıları olduğundan dolayı, araç kapılarından geçen sesin önlenmesi önemli bir konu olmaktadır. Ses geçişinin en fazla gerçekleştiği nokta araç gövdesi ve kapı arasındaki boşluktur. Bu nedenle araç kapısı ve gövdesi arasındaki fitillerin ses yalıtımı yetkinliğinin geliştirilmesi büyük önem arz etmektedir. Bu çalışmanın amacı, otomobil gövde ve kapısı arasında kullanılan elastomer yapıdaki çoklu balon fitil sisteminin ses geçiş kaybı karakteristiğinin değerlendirilmesidir. Genellikle, otomobillerde biri gövde üzerinde, diğeri kapı üzerinde olmak üzere iki tane balon fitil kullanılmaktadır. Toplam ses geçiş kaybının geliştirilebilmesi için bu iki fitilin oluşturduğu sistem birlikte değerlendirilmelidir.

Çalışma dört ana başlıktan oluşmaktadır. Birinci bölüm, deneyler sonucunda elde edilen kuvvet – açıklık eğrileri ile analiz sonucunda elde edilen kuvvet – açıklık eğrilerinin karşılaştırılması ile deformasyon analizlerinin ve hiperelastik malzeme modellerinin doğrulanmasını içermektedir. İkinci bölümde durağan yapısal analizler kullanılarak otomobil gövdesi ve kapısı arasında bulunan fitillerin deforme olmuş geometrilerinin elde edilmesi bulunmaktadır. Üçüncü adım ise kullanılabilecek akustik benzetim modelinin doğrulanmasını, son kısım da ikinci adımda yapılan analizler sonucunda elde edilen deforme olmuş iki fitil yapısının akustik analizler ile ses geçiş kaybı performansının hesaplanmasını içermektedir. Ses yalıtım performansının tahmin edilebilmesi için ses geçiş kaybı değerleri incelenmiştir.

Anahtar Kelimeler: Hiperelastik malzemeler, doğrusal olmayan sonlu eleman analizi, çoklu balon fitiller, ses geçiş kaybı, kuvvet – açıklık eğrisi

To My Loved Parents, My Handsome Brother

and My Precious Wife…

ACKNOWLEDGEMENTS

I would like to express my deepest gratitude to Prof. Dr. Mehmet Çalışkan for his endless and invaluable support, encouragements, guidance throughout the research and writing of this thesis.

In addition, I would like to express sincere appreciation to Asst. Prof. Dr. Gökhan Özgen for conducting hyperelastic and viscoelastic material tests and for his support, guidance and insight on the static deformation analyses of sealants.

This thesis work was sponsored by TOFAŞ, STANDARD PROFİL and OTEST companies. I would like to thank specifically TOFAŞ and STANDARD PROFİL companies for supplying the force deflection and sound transmission test results, rubber material and sealant samples.

Moreover, I would like to thank Serkan Atamer and M. Hakan Kandemir for their support on simulations.

Most special thankfulness is to my special woman Cansu, for her presence, for making my life such meaningful. Even more, this accomplishment would not have been possible without her. Lastly, but not least, I must express my very profound gratitude to my family for their eternal trust and love.

TABLE OF CONTENTS

LIST OF TABLES

LIST OF FIGURES

LIST OF SYMBOLS

1,2,3	: Principal material coordinates
I_n	: Strain invariants in (n) direction
W	: Strain energy function
C_{ij}	: Hyperelastic material constants
λ_i	: Stretch ratios in (i) direction
L_i	: Instantaneous gage length
ϵ_n	: Engineering strain in (n) direction
J	: Jacobian measuring dilatancy
μ	: Shear modulus
f	: Frequency in [Hz]
L_0	: Initial gage length
th_i	: Instantaneous material thickness
th_0	: Initial material thickness
σ_n	: Engineering stress in (n) direction
t	: Time
ω	: Frequency in $[rad/s]$
E'	: Storage modulus of elasticity
E''	: Loss modulus of elasticity
E^*	: Complex modulus of elasticity
η	: Loss factor
ρ_i	: Density of (i)th medium
c_i	: Speed of sound in (i)th medium
τ	: Transmission coefficient
p_i	:Wave equation of incident wave

p_r	:Wave equation of reflected wave
p_t	:Wave equation of transmitted wave
T_0	:Reference temperature
T_A	:Slope
e_{abs}	:Absolute error
e_{rel}	:Relative error

LIST OF ABBREVIATIONS

MR	: Mooney-Rivlin model
FE	: Finite element
FEA	: Finite element analysis
SEA	: Statistical energy analysis
TOFAŞ	: Turkish Automotive Company
TL	: Transmission loss
LC	: Load case
TFMM	: Transfer function matrix method

CHAPTER 1

INTRODUCTION

Elastomeric bulb seals are widely used in automotive and construction industry as a sealing system to decrease transmission of noise, water and heat from one medium to another. Therefore, their insulation performance characterization becomes important day by day.

Bulb seals are the major components to fill the openings between the door and body frames. As the leakage area increases, the sound transmission from one medium to another increases drastically. Therefore, mechanical behavior and the sound insulation performance of the bulb seal system should be depicted thoroughly.

In the automotive industry, interior sound quality is one of the most important parameters at the design stage of new high – end vehicles. There are two primary noise generation mechanisms, first one is the aspiration through the small leaks and the second one is the structural transmission of sound due to flow – induced mechanical vibrations of bulb seals. In cases where the seals are incapable of blocking the flow through the gaps, intense aspiration noise can be produced [1]. Especially, while an automobile cruising at speeds over $120\ km/h$, due to leakage of the wind noise, sound insulation performance of the sealing system in the middle – to – high frequency range is very crucial [2].

As in the case of the automotive industry, sound quality of the interior mediums is an important phenomenon also in the construction industry. Moreover, it is regulated by means of policies to increase the acoustical comfort in the hotels, office areas, hospitals, residences, schools etc. In terms of sound transmission elimination, operable elements like doors and windows are the weakest elements and the sealing system between the door and the frame is the weakest link in the door structures. Additionally, acoustical doors are very important architecturally, as in recording studios, conference halls as well as hotel room doors and doors to dwellings [3].

By considering the needs of these two mentioned industries, it can be stated that study on the sound insulation performance of the sealing system composed of bulb seals is very crucial and this task can be achieved by means of finite element analysis. As the final shape of the bulb sealants is not the same as the initial shape, analyses should be conducted in two main steps. In the first step, the deformed geometries should be obtained by means of quasi – static structural simulations. After that, acoustical analysis should be performed by using these deformed geometries in order to get the insulation performance during the utilization.

The aim of this study is characterization of the sealing system of an automobile, which consists two different elastomeric bulb sealants, in terms of sound isolation. This study is performed by finite element analysis in two main parts. In the first part, depiction of hyperelastic material property of the sealants and obtaining deformed geometry is aimed. In the second part, acoustical simulations are conducted in order to characterize the sound isolation performance of the overall system.

In the first part, non – linear material properties of the bulb sealants are defined by hyperelastic material models and quasi – static structural analysis is performed.

However, the very first thing is obtaining a correct model for the deformation analysis. This step is completed, by performing experiments on individual sealants and comparing the force vs opening curves of the experimental results with the simulation results. After acquiring correct simulation model, analysis is carried on the actual sealing system with two individual bulb sealants.

As the second step, acoustical simulations are performed. Same with the deformation analysis, correct acoustical model should be verified. This step is achieved in different ways. Firstly, simulation of a simplified model is performed and those results are compared with results of an analytical method, which is called as transfer function matrix method. Secondly, acoustical measurements are conducted and sound transmission loss vs frequency curves of experimental results are compared with simulation results. As the final step, acoustical simulation is carried on the actual sealant system and effects of possible sound transmission paths are identified.

This thesis contains five main parts. In the first chapter, aim of the thesis and the main motivation of the study have been explained. In the second chapter, properties of the hyperelastic materials are depicted and studies directly related with the characterization of the sound transmission performance of bulb sealants in literature are summarized. Additionally, basic information about sound transmission is supplied in this literature review chapter. In the third chapter non – linear deformation analyses are explained. This chapter covers the definition of hyperelastic material models, validation analyses and non – linear static structural analysis of the sealant system. In the fourth chapter, acoustical analyses have been explained. Validation analyses and experimental results are covered as well as the simulations of the actual sealant system. Moreover, finite element models with the material definitions and possible transmission paths of the insulation system are described in this chapter. Last chapter includes discussion of the results and conclusion.

CHAPTER 2

LITERATURE REVIEW

2.1 HYPERELASTIC MATERIALS

Hyperelastic materials can be viewed as a special form of the elastomeric materials. In their molecular composition, long chains of crossed linked molecules and chemical bonds exist at those entanglement points, which make the material stronger. The most important property of the hyperelastic materials is the nonlinear relationship between strain and stress in the static loading cases. The molecular chains of the hyperelastic materials illustrated in Figure 2-1 are randomly oriented. When the material deforms, those randomly oriented chains orient themselves and revert back as the load on the material removed. As a consequence of this, the relation between stress and strain changes as the deformation changes and this phenomenon makes the hyperelastic materials nonlinear. This nonlinear relationship between the stress and strain can be expressed by curve fitting on the experimental data of the stress and strain by employing the hyperelastic material models [4]. In the dynamic cases, these elastomeric materials are described as viscoelastic materials. Material properties of viscoelastic materials are highly depend on excitation frequency and temperature.

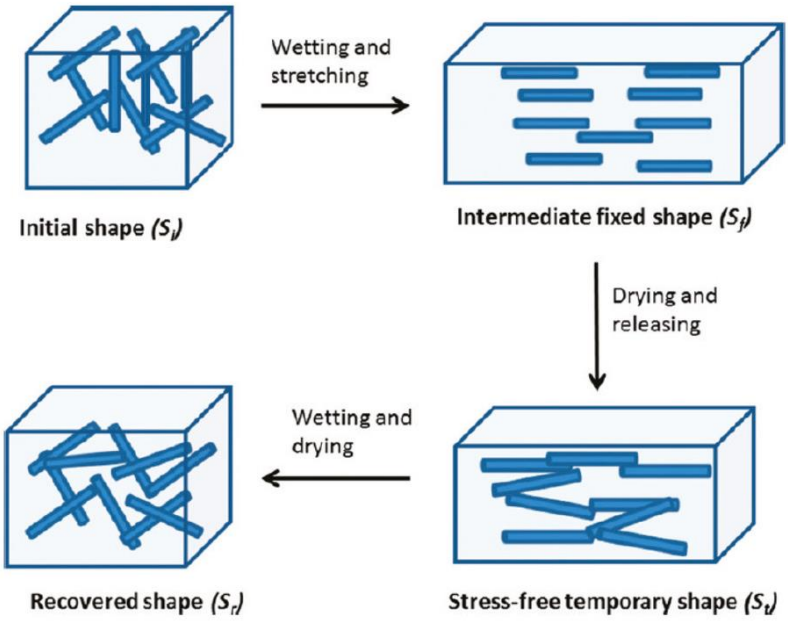

Figure 2-1 General chain structure of hyperelastic materials [4]

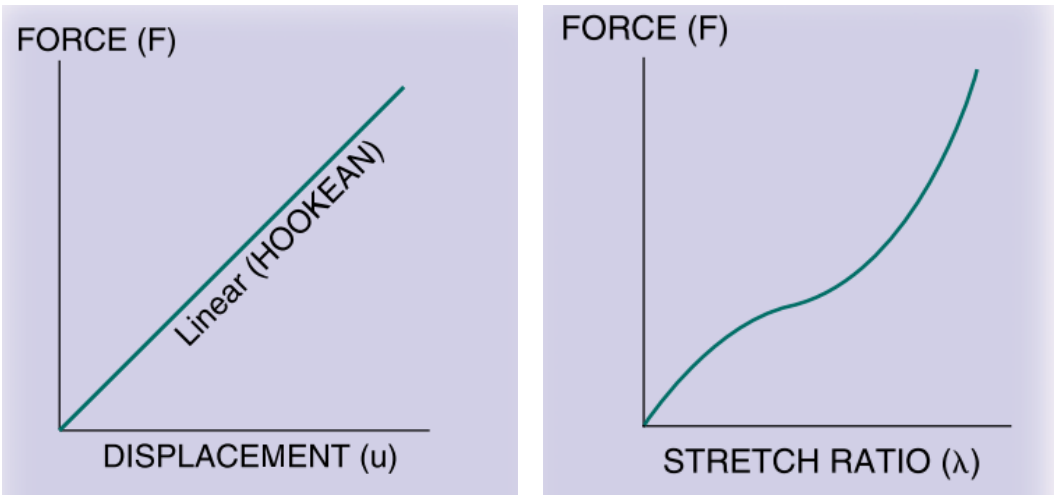

(a) (b)

Figure 2-2 (a) Linear force – displacement relation (b) Nonlinear force – extension relation [5]

Nonlinear hyperelastic material models are mainly based on the weighted averaging of the strain invariants, I_1, I_2 and I_3, to be able to get the strain energy functions, W. Furthermore, the stress – strain relation can be calculated from the strain energy function by the following formula [4], [6].

$$\sigma_{ij} = \frac{\partial W}{\partial \epsilon_{ij}} \tag{2-1}$$

Moreover, strain invariants are calculated by using the stretch ratios and they can be expressed as:

$$I_1 = \lambda_1^2 + \lambda_2^2 + \lambda_3^2 \tag{2-2}$$

$$I_2 = \lambda_1^2\lambda_2^2 + \lambda_2^2\lambda_3^2 + \lambda_3^2\lambda_1^2 \tag{2-3}$$

$$I_3 = \lambda_1^2\lambda_2^2\lambda_3^2 \tag{2-4}$$

where the stretch ratios are defined as:

$$\lambda_i = \frac{L_i + \Delta L_i}{L_i} = 1 + \epsilon_i; \qquad i = 1,2,3 \tag{2-5}$$

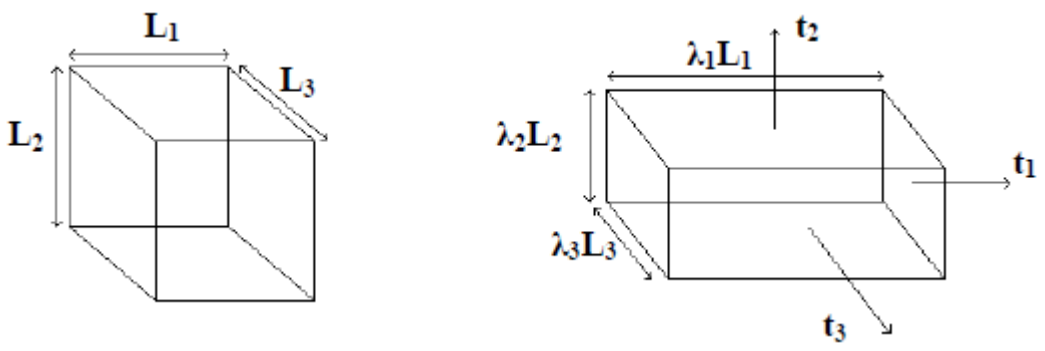

Figure 2-3 Definition of the stretch ratios [6]

Furthermore, ϵ_i can be defined as the engineering strain [6].

There are various types of hyperelastic material models to describe the relation between the stress and strain by defining the strain energy functions. In the section named as "HYPERELASTIC MATERIAL MODELS", "Neo – Hookean Model, Mooney – Rivlin Model, Yeoh Model, Ogden Model and Double Transition (15 – Parameter) Model" are described extensively.

Another important property of the hyperelastic materials is the frequency and temperature dependency of its material properties. As a result of the material nonlinearity, hyperelastic materials' complex moduli are highly dependent on the frequency and temperature to which the material is exposed [6], [7]. For uniaxial cases, standard viscoelastic state equations can be written as follows:

$$\sigma(t) + \sum_{k=1}^{K} b_k \frac{d^k \sigma}{dt^k} = E_0\, \varepsilon(t) + \sum_{j=1}^{J} E_j \frac{d^j \varepsilon}{dt^j} \qquad (2\text{-}6)$$

In the case of harmonic excitations, stress and strain functions can be formulated in terms of time as follows:

$$\sigma(t) = \sigma_0 e^{i\omega t} \tag{2-7}$$

$$\epsilon(t) = \epsilon_0 e^{i\omega t} \tag{2-8}$$

State equation of viscoelastic materials, which are exposed to harmonic excitations, can be obtained by putting equations (2-7) and (2-8) into the equation (2-6) as follows:

$$\sigma_0 = \frac{\varepsilon_0\left(E_0 + \sum_{j=1}^{J} E_j (i\omega)^j\right)}{1 + \sum_{k=1}^{K} b_k (i\omega)^k} = \frac{\varepsilon_0\, E_0\, \left(1 + \sum_{j=1}^{J} a_j (i\omega)^j\right)}{1 + \sum_{k=1}^{K} b_k (i\omega)^k} \tag{2-9}$$

Equation (2-9) can be simplified in terms of magnitudes of strain and stress as follows:

$$\sigma_0 = (E' + iE'')\, \varepsilon_0 \tag{2-10}$$

In equation (2-10), E' and E'' terms represent storage modulus and loss modulus, respectively. For metals, storage modulus is constant and frequency dependency of shear modulus is very low. However, for the viscoelastic materials (i.e. hyperelastic materials) both constants depend on frequency.

Additionally, frequency dependency of the stress – strain relation can be represented by using complex modulus, which is formulated below.

$$\sigma_0 = \tilde{E}^*(i\omega)\varepsilon_0 = (E' + iE'')\,\varepsilon_0 \tag{2-11}$$

In different form;

$$\tilde{E}^* = E'(\omega)\big(1 + i\eta(\omega)\big) \tag{2-12}$$

where $\eta(\omega)$ represents loss factor.

$$\eta(\omega) = \frac{E''(\omega)}{E'(\omega)} \tag{2-13}$$

In the hyperelastic material models, the weighted average of the strain invariants can be formed by determining the material constants and they can be calculated by curve fitting the model on to the material test results. Therefore, obtaining the stress – strain relationship by conducting tests on the material is the major step. Moreover, since the complex modulus values of the hyperelastic materials are highly dependent on the frequency, additional to the quasi – static tests, "Complex Modulus Tests" should be performed. In the section named as "HYPERELASTIC MATERIAL TESTS", "Uniaxial Tensile Test, Uniaxial Compression Test, Planar Shear Test, Volumetric Compression Test and Complex Modulus Tests" will be depicted deeply.

2.1.1 HYPERELASTIC MATERIAL MODELS

In this section, mathematical models, which relate the engineering stress and engineering strain and frequency and temperature dependent material properties of the hyperelastic materials, are examined. These models are simply curve fitting functions on the experimental results for different loading conditions. "Neo –

Hookean Model, Mooney – Rivlin Models, Yeoh Model, and Ogden Model" are used to describe the nonlinear relationship between stress and strain. "Double Transition (15 – Parameter) Model and Arrhenius Shift Factor Equation" can be used to predict the complex modulus values of the elastomeric materials in dynamic cases.

2.1.1.1 Neo – Hookean Model

The strain energy function in the Neo – Hookean model is expressed in terms of first strain invariant and a material constant; therefore, this model is the simplest material model to depict the relation between the stress and strain characteristics of hyperelastic materials [4].

$$W = C_{10}(I_1 - 3) \tag{2-14}$$

The model has high performance in terms of experimental fit up to 40% strain in uniaxial tension and up to 90% strains in simple shear. Moreover, equation (2-14) is derived from the thermodynamics and statistical mechanics [4].

2.1.1.2 Mooney – Rivlin Models

The earliest theory of nonlinear elasticity is set forth by Mooney. This model is composed of both first and second strain invariants and two material constants [5].

$$W = C_{10}(I_1 - 3) + C_{01}(I_2 - 3) \tag{2-15}$$

The material model Mooney – Rivlin is a phenomenological theory and it shows a good agreement with 100% strains in tensile test. However, it is insufficient in describing the compression mode of deformation. Furthermore, the Mooney – Rivlin model fails to describe the stiffening of the material at large strains. This model has been derived by assuming the material as incompressible and isotropic. In addition, the Hooke's law is obeyed in simple shear [4].

To overcome the defects of the Mooney – Rivlin model Tschoegl suggest that using high order terms in the generalized Mooney – Rivlin strain energy function gives better agreement with the experimental data. [8] As a result of this fact, some additional models, based on the Mooney – Rivlin model, have been proposed as: [5]

Three term Mooney – Rivlin Model:

$$W = C_{10}(I_1 - 3) + C_{01}(I_2 - 3) + C_{11}(I_1 - 3)(I_2 - 3) \tag{2-16}$$

Signiorini Model:

$$W = C_{10}(I_1 - 3) + C_{01}(I_2 - 3) + C_{20}(I_1 - 3)^2 \tag{2-17}$$

Third Order Invariant Model:

$$W = C_{10}(I_1 - 3) + C_{01}(I_2 - 3) + C_{11}(I_1 - 3)(I_2 - 3) + C_{20}(I_1 - 3)^2 \tag{2-18}$$

Third Order Deformation (or James – Green – Simpson) Model:

$$W = C_{10}(I_1 - 3) + C_{01}(I_2 - 3) + C_{11}(I_1 - 3)(I_2 - 3) + C_{20}(I_1 - 3)^2 + C_{30}(I_1 - 3)^3 \tag{2-19}$$

Although, increasing the order of the strain energy function yields a better performance by capturing more infection points in stress – strain curve, which can be seen in Figure 2-4; this may result in unstable energy function, which may yield non – physical results [4].

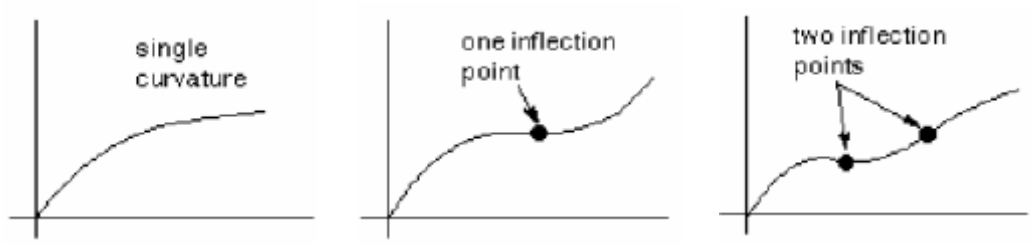

(a) (b) (c)

Figure 2-4 Stress – strain curves obtained by (a), Two – Term MR; (b), Five – Term MR; (c), Nine – Term MR [4]

2.1.1.3 Yeoh Model

Yeoh model depends on the assumption that the second strain invariant is constant with strain. As a result of this fact, the strain energy function only depends on the first strain in variant and it can be formulated as: [5]

$$W = C_{10}(I_1 - 3) + C_{20}(I_1 - 3)^2 + C_{30}(I_1 - 3)^3 \qquad (2\text{-}20)$$

The main advantage of the Yeoh model is that various modes of deformation can be analyzed by using only uniaxial tensile test results of a material.

2.1.1.4 Ogden Model

Ogden model describes the energy function as separable functions of principal stretches. It can be formulated as:

$$W = \sum_{n=1}^{N} \frac{\mu_n}{\alpha_n} J^{-\alpha_n/3} \left(\lambda_1^{\alpha_n} + \lambda_2^{\alpha_n} + \lambda_3^{\alpha_n} - 3\right) + 4.5K\left(J^{-\frac{1}{3}} - 1\right)^2 \qquad (2\text{-}21)$$

where J is the Jacobian measuring dilatancy and it is depicted as the determinant of the deformation gradient [5].

Actually, the Neo – Hookean and Mooney – Rivlin models are the special forms of the Ogden model. Moreover, it gives good experimental fit in simple tension up to 700%. Furthermore, Ogden model should also be taken into consideration for compressible materials [5].

2.1.1.5 Double Transition (15 – Parameter) Model and Arrhenius Shift Factor Equation

As it is stated earlier, modulus and loss factor values of viscoelastic materials are highly dependent on frequency and temperature. Unlike the previously mentioned mathematical models for quasi – static loadings, double transition model along with the Arrhenius shift factor equation is used to predict the shear modulus and loss factor of the material in dynamic cases for different environmental (i.e. different temperatures) and loading conditions (i.e. different frequencies) [9].

Material tests in order to obtain complex modulus values can be conducted at discrete frequency values and in limited number of temperatures. In order to obtain material properties at a temperature and frequency that was not in the measured data set, new parameter is utilized that combines temperature and frequency, which is named as reduced frequency. By using this reduced frequency parameter, modulus and loss factor values obtained for different temperatures and frequencies can be represented in continuous form, which is named as master curve. Furthermore, double transition model can be fitted on to this continuously represented data to obtain mathematical expression of the modulus and loss factor values of a material. By using this mathematical expression, material properties can be predicted for different frequency and temperature values. In Figure 2-5, storage modulus test data and master curves can be seen. Frequency is denoted as ω and $\alpha_T\omega$ represents reduced frequency in Figure 2-5 [9].

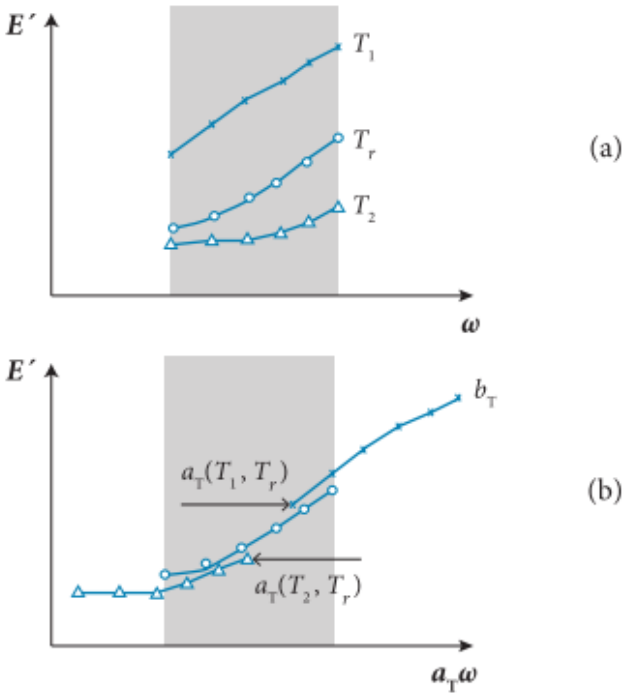

Figure 2-5 (a), Isotherms of storage modulus at temperaturesT_1, T_2 and T_3; (b), Isotherms of storage modulus after application of the shift factor (i.e. master curve of storage modulus [10]

Function of the shift factor can be obtained by using Arrhenius shift factor equation as follows:

$$\ln\big(\alpha(T)\big) = T_A\left(\frac{1}{T} - \frac{1}{T_0}\right) \tag{2-22}$$

where T_0 is an arbitrary reference temperature and T_A is the slope of the line and is related to the activation energy of the material. It should be noted that all temperatures are in absolute degrees (Kelvin scale) [9].

After obtaining the master curves for both modulus and loss factor, frequency dependent mathematical expressions of double transition model (or 15 – parameter model), can be used to modulus and loss factor values for different frequencies.

2.1.2 HYPERELASTIC MATERIAL TESTS

2.1.2.1 Uniaxial Tension Test

Uniaxial tensile test has been conducted to get the initial material stiffness, Young's modulus, material yield point and the failure stress and strain by examining the stress – strain curve. Specimen should only be exposed to simple tension without any shear or compression strains. Thus, the length of the material should be 10 times longer than its width or thickness whichever is higher [4].

Stretch and stress values can be calculated by the following formulas.

$$\lambda_2 = \lambda = L/L_0 \tag{2-23}$$

$$\lambda_1 = \lambda_3 = \sqrt{A/A_0} \tag{2-24}$$

$$\sigma_2 = \sigma = F_p/A_0 \tag{2-25}$$

$$\sigma_1 = \sigma_3 = 0 \tag{2-26}$$

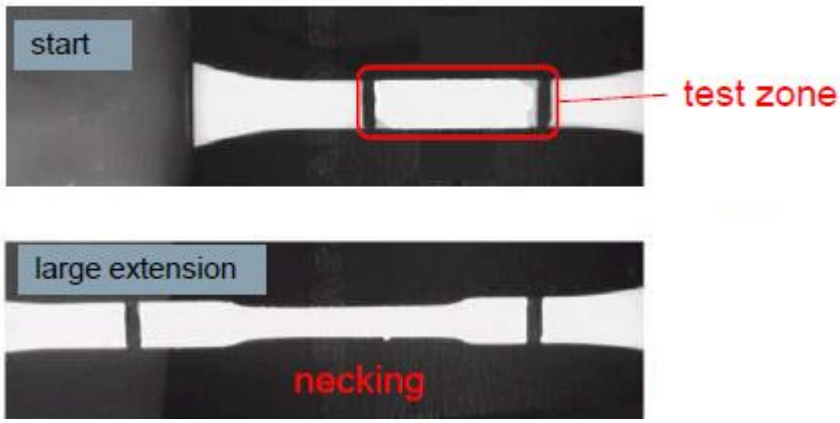

Figure 2-6 Uniaxial Tensile Test Scheme [11]

2.1.2.2 Uniaxial Compression Test

Uniaxial compression test has very similar features with the uniaxial tension test. As the material should only be exposed to pure compression strains, the specimen needs to be compressed between two platens without friction between the platens and the specimen [4].

Stretch and stress values can be obtained from

$$\lambda_2 = \lambda = L/L_0 \tag{2-27}$$

$$\lambda_1 = \lambda_3 = \sqrt{A/A_0} \tag{2-28}$$

$$\sigma_2 = \sigma = F_p/A_0 \tag{2-29}$$

$$\sigma_1 = \sigma_3 = 0 \tag{2-30}$$

Figure 2-7 Uniaxial Compression Test Fixture [11]

2.1.2.3 Planar Shear Test

At the planar shear test, the specimen is exposed to pure shear at 45° angle to the stretching direction. Therefore, the width of the material should at least 10 times longer than the length in the stretching direction [4].

Stretch and stress values can be calculated from

$$\lambda_1 = 1 \tag{2-31}$$

$$\lambda_2 = \lambda = L/L_0 \tag{2-32}$$

$$\lambda_3 = th/th_0 \tag{2-33}$$

$$\sigma_1 \neq 0 \tag{2-34}$$

$$\sigma_2 = \sigma \tag{2-35}$$

$$\sigma_3 = 0 \tag{2-36}$$

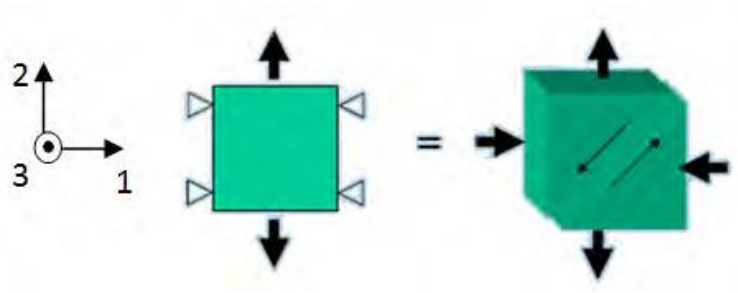

Figure 2-8 Coordinates of planar shear test [4]

2.1.2.4 Volumetric Compression Test

From the volumetric compression test, compressibility property of the material can be obtained. Eight specimens with 3 mm diameter and 2 mm thickness, which are stacked and lubricated, compressed in a fixture. The slope of the stress – strain curve

gives the bulk modulus of the material. The following formulas yield the stretch and stress values [4].

$$\lambda_1 = \lambda_2 = 1 \tag{2-37}$$

$$\lambda_3 = L/L_0 \tag{2-38}$$

$$\sigma_1 = \sigma_2 = \sigma_3 = -|F_p/A_0| \tag{2-39}$$

where A_0 is the cross – sectional area of the plunger and F_p is the force on the plunger.

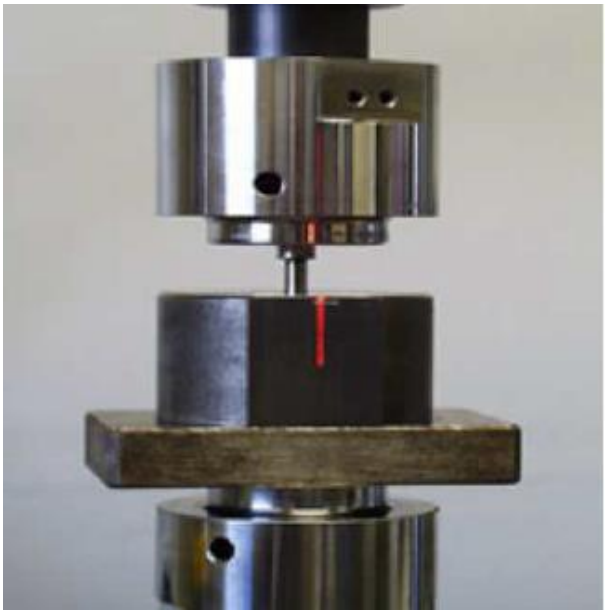

Figure 2-9 Volumetric compression test [11]

2.1.2.5 Complex Modulus Tests

Complex modulus tests are conducted in a sealed medium. Stress and strain values are measured to get loss factor and modulus values for different frequencies at different temperatures. Tests can be conducted according to the standards listed as:

- ISO 18437-4 Mechanical vibration and shock – Characterization of the dynamic mechanical properties of viscoelastic materials – Part 4: Dynamic stiffness method
- ASTM D 5992 – Standard Guide for Dynamic Testing of Vulcanized Rubber and Rubber – like Materials Using Vibratory Methods
- ISO 10112 – Damping Materials – Graphical Presentation of Complex Modulus
- ISO 6721-1:2011 Plastics – Determination of Dynamic Mechanical Properties – Part 1: General Principles

Figure 2-10 DMA machine for complex modulus test

Complex modulus tests are conducted to a narrow frequency and temperature range and double transition model along with the Arrhenius shift factor equation is applied in order to predict the complex modulus values for different frequencies and temperatures.

2.2 ACOUSTICS

2.2.1 SOUND TRANSMISSION LOSS

When an acoustic wave becomes incident onto a boundary between two media, it splits into two waves, first one is the reflected wave and the second one is the transmitted wave [3]. Schematic representation of a transmission of a normally incident wave from one medium to another can be illustrated in Figure 2-11.

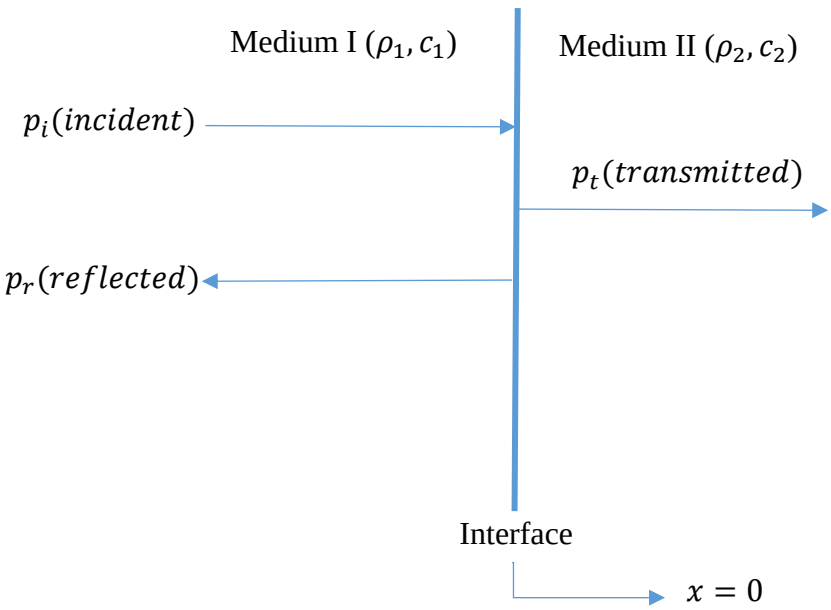

Figure 2-11 Schematic representation of transmission of a normally incident wave through two media

Sound transmission coefficient based on power can be defined as follows:

Reflection Coefficient Based on Power

$$\gamma = \frac{Intensity\ of\ Reflected\ Wave}{Intensity\ of\ Incident\ Wave} \tag{2-40}$$

Transmission Coefficient Based on Power	$\tau = \dfrac{Intensity\ of\ Transmitted\ Wave}{Intensity\ of\ Incident\ Wave}$	(2-41)

Moreover, below mentioned two boundary conditions should also be satisfied to be able express the transmission coefficients analytically.

1) Equality of pressures at all interfaces.

2) Equality of normal components of particle velocity at all interfaces.

In the case of normal transmission through three media whose scheme can be illustrated in Figure 2-12, the above – mentioned boundary conditions should be satisfied at all two interfaces.

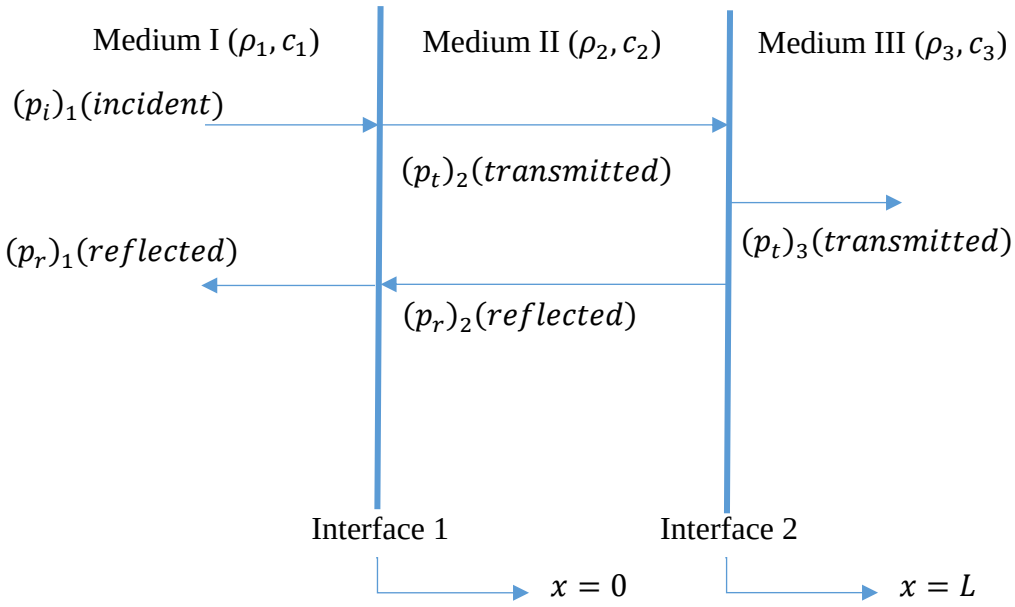

Figure 2-12 Schematic representation of transmission of a normally incident wave through three media

For the three media case, the wave expressions can be written as follows:

$$(p_i)_1 = P_{i1} e^{j(\omega t - k_1 x)} \tag{2-42}$$

$$(p_r)_1 = P_{r1} e^{j(\omega t + k_1 x)} \tag{2-43}$$

$$(p_t)_2 = P_{t2} e^{j(\omega t - k_2 x)} \tag{2-44}$$

$$(p_r)_2 = P_{r2} e^{j(\omega t + k_2 x)} \tag{2-45}$$

$$(p_t)_3 = P_{t3} e^{j(\omega t - k_2 (x - L)} \tag{2-46}$$

Then, by using wave equations and applying two boundary conditions on two interfaces separately, sound transmission coefficient can be obtained for three media case as follows:

$$\tau = \frac{I_{t3}}{I_{i1}} = \frac{|P_{t3}|^2 / 2\rho_3 c_3}{|P_{i1}|^2 / 2\rho_1 c_1} \tag{2-47}$$

$$\tau = \frac{4\rho_1 c_1 \rho_3 c_3}{(\rho_3 c_3 + \rho_1 c_1)^2 (\cos(k_2 L))^2 + \left(\rho_2 c_2 + \frac{\rho_1 c_1 \rho_3 c_3}{\rho_2 c_2}\right)^2 (\sin(k_2 L))^2} \tag{2-48}$$

After obtaining the sound transmission coefficients of the waves transmission loss or sound radiation index can be calculated by formula [12].

$$TL\ [dB] = -10\log(\tau) \tag{2-49}$$

2.2.2 SOUND TRANSMISSION LOSS ANALYSES

Many studies are presented in the literature related with the sound transmission characterization of the elastomeric bulb seals. There are two main noise generation mechanisms related with the elastomeric bulb seals. The first one is the aspiration noise, which penetrates through the openings between the car body and seals, and the other one is the flow – induced mechanical vibrations of the bulb. Aspiration noise is the most important noise source if there are gaps between the car body and the sealant. Therefore, dynamic characteristics of the sealing systems, excited by the unsteady surface pressure due to the turbulent flow over the vehicle, should be analyzed deeply. Since conducting experiment on the vehicles during the drive or in the wind tunnels is costly and time consuming, finite element analyses methods are used to calculate acoustical characteristics of these sealing systems under different circumstances.

The comparison with the calculated sound transmission loss using different mathematical models with the experimental results acquired from the reverberation room tests were done by Park et al. Moreover, the sealant and air layers were modeled by using finite element methods and transfer function matrix method. In their studies, the validation was done by comparing the sound transmission loss of a simple model, which can be seen in Figure 2-13, calculated with finite element analysis and the transfer function matrix method [13].

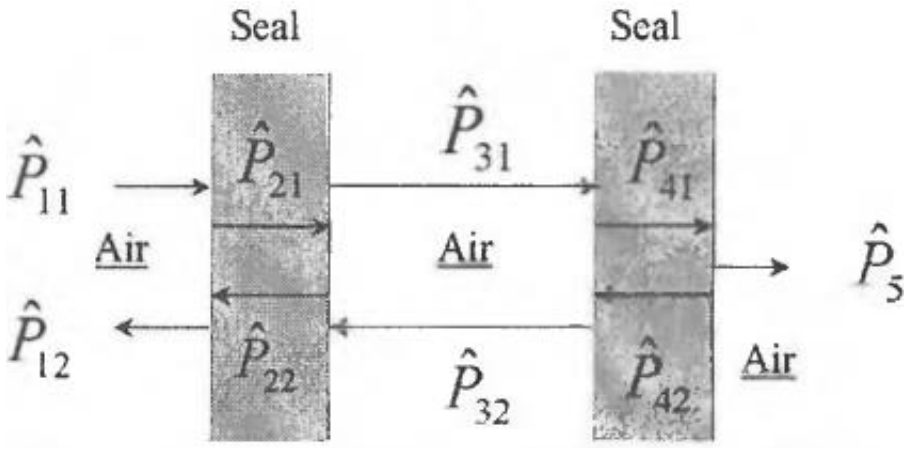

Figure 2-13 Simple seal model [13]

Both results were calculated with finite element analysis and transfer function matrix compared in Figure 2-14 in terms of sound transmission loss for two different bulb seals that have different densities. According to Park and his friends, dip points in the sound transmission loss vs frequency graph is due to the resonance frequencies of the mass – air – mass interaction. As the last step of their study, the experimental results of a simple sealant model, which can be seen in Figure 2-15, were compared with the calculated results. The calculated results do not show much similarity, although there is good correlation between the analytical calculations and the finite element analysis. According to them, the reason is the use of constant material properties in the analytical and finite element methods as well as the simplicity of the analytical and finite element models [13].

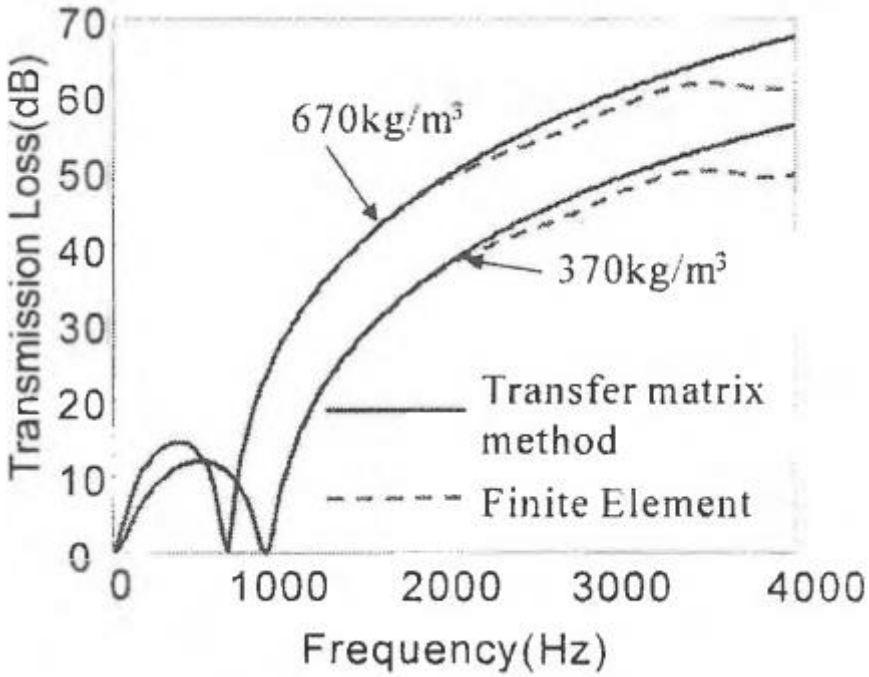

Figure 2-14 Comparison of results of finite element analysis with transfer function matrix method of simple model [13]

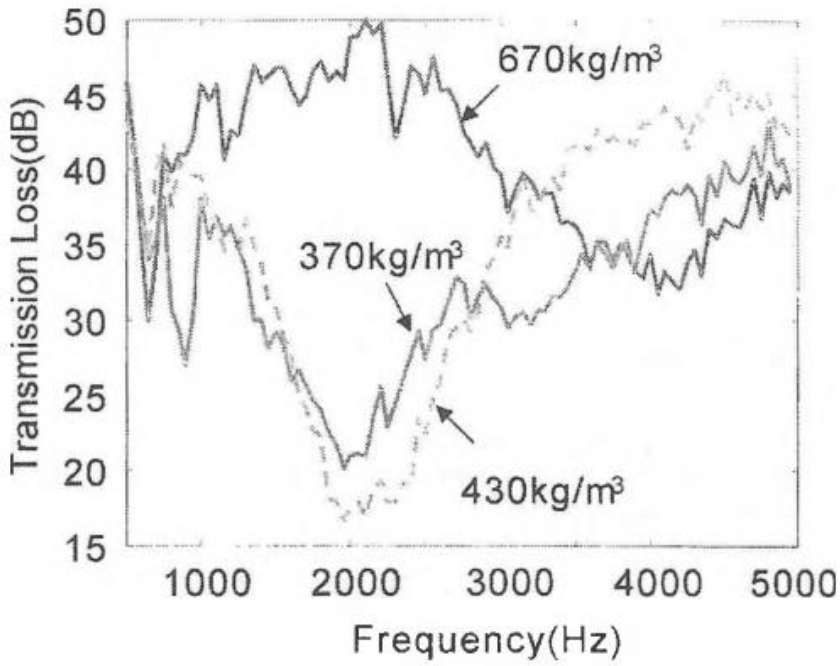

Figure 2-15 Reverberation room experiment results of simple model [13]

In another article by Park et al., the dynamic characterization of sealing system was carried to next level by analyzing a complex bulb seal, which is used in the sealing systems of a vehicle. The purpose is to validate their studies with the reverberation room experiments. In addition, the transverse velocity along the seal wall was measured by a laser vibrometer to be able to describe the vibration characteristics of the bulb seal [1].

In the finite element analysis, firstly, static analysis was simulated to get the deformed geometry of the seal and then perturbation analysis was conducted on the deformed geometry on ABAQUS environment. Acoustic fluid – solid interactions were modelled and pressure waves were defined as inputs. This choice of the input as pressure waves eliminates the need of the air layers that cover the input region of the bulb seal and reduces the simulation time [1].

At the beginning, onset of analysis of the complex seal geometry, three different simple models, whose sound transmission loss values can be predicted by the transfer function matrix method, were constructed. The numerical analysis was validated for these models by comparing the results of the simulation with the results of the analytical method. Geometries of simple models can be seen in Figure 2-17 [1].

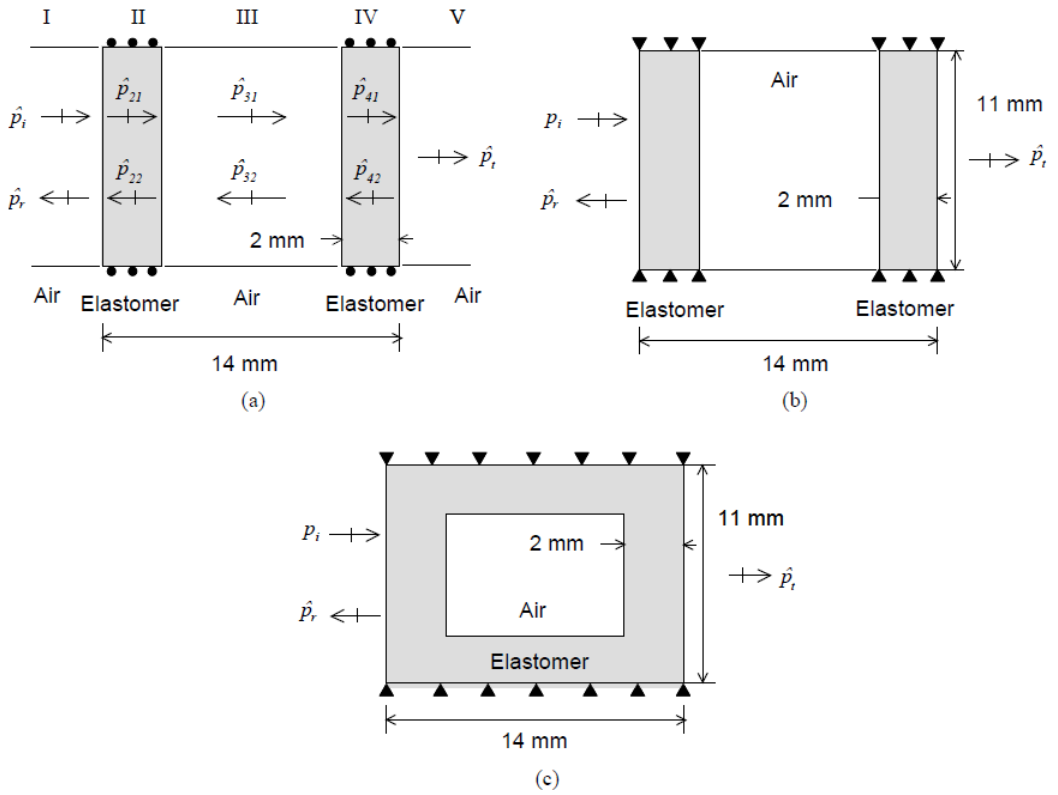

Figure 2-16 Geometries of simplified models – (a), double membrane model; (b), double membrane model with fixed displacement boundary conditions at their ends; (c), rectangular model [1]

In Figure 2-17 the comparison between the results of finite element analysis and transfer function matrix method can be displayed [1].

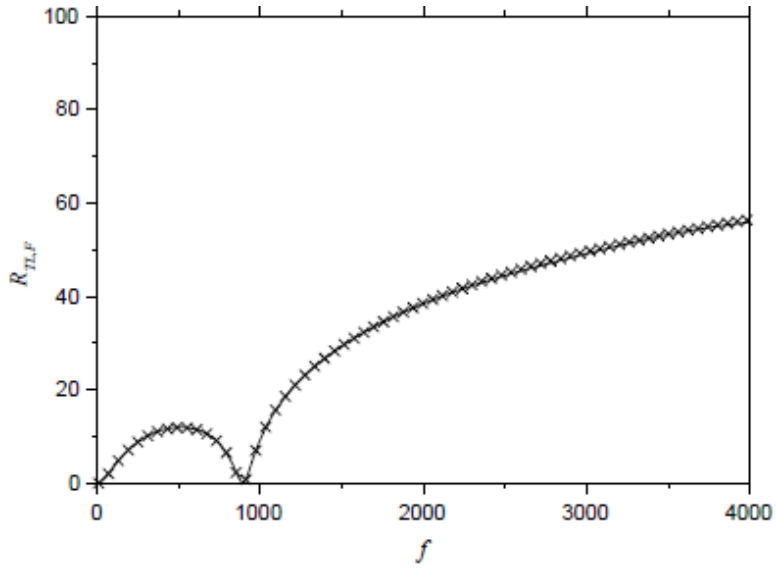

Figure 2-17 Sound transmission loss predictions for a simplified dual – membrane model – (x), transfer function matrix method; (----), FE analysis [1]

Results of the rectangular model for different $c_L/(hf)$ values can be illustrated in Figure 2-18.

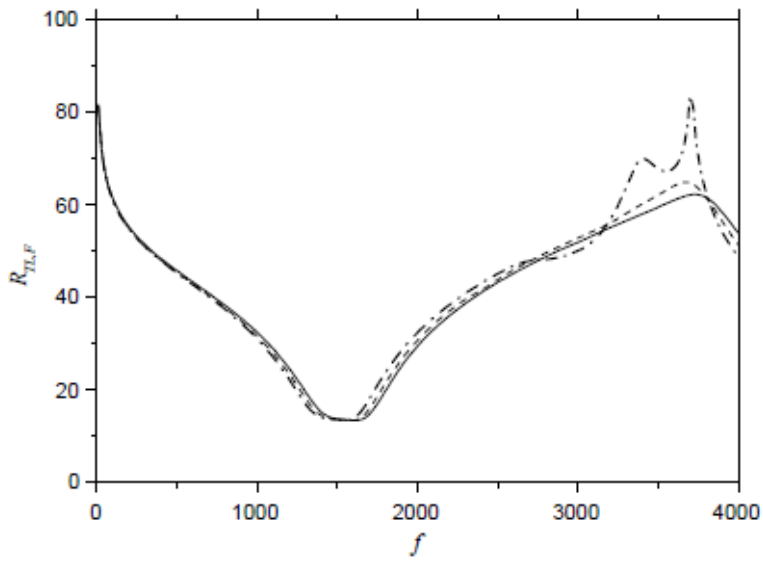

Figure 2-18 Sound transmission loss predictions for a rectangular model with value of $c_L/(hf)$ – (—·—·—·—), 21.5; (- - - - -), 41; (———) 82.[1]

After validating the numerical analysis with the analytical methods, the sound transmission loss values of complex geometry were analyzed for different compression ratios. Comparison of the results of the analyses and experiments can be inspected in Figure 2-19.

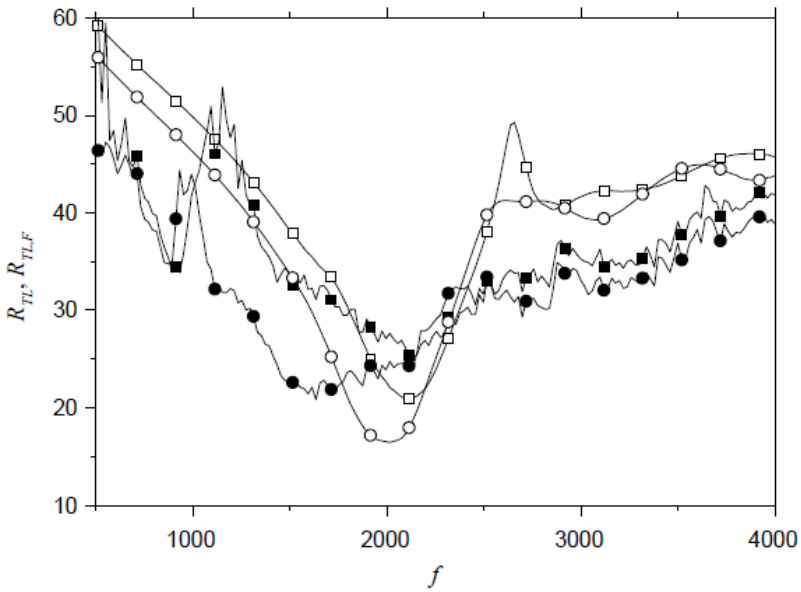

Figure 2-19 Comparison of results of analysis with the experiments for different CR values – (—■—), experiment results for CR value of %22.5; (—□—), analysis results for CR value of %22.5; (—●—), experiment results for CR value of %16.9; (—○—), analysis results for CR value of %16.9.[1]

It was stated that experimental results and results of analysis display similar trends, by Park and his friends. According to this study, sound transmission loss characteristics of a bulb seal should be investigated in three different regions, stiffness – controlled region, resonant region and mass – controlled region. Region, which corresponds to the frequencies lower than the mass – air – mass resonance, called as

stiffness – controlled region and region with higher frequencies called as mass – controlled region. These regions can clearly be traced in Figure 2-20. [1]

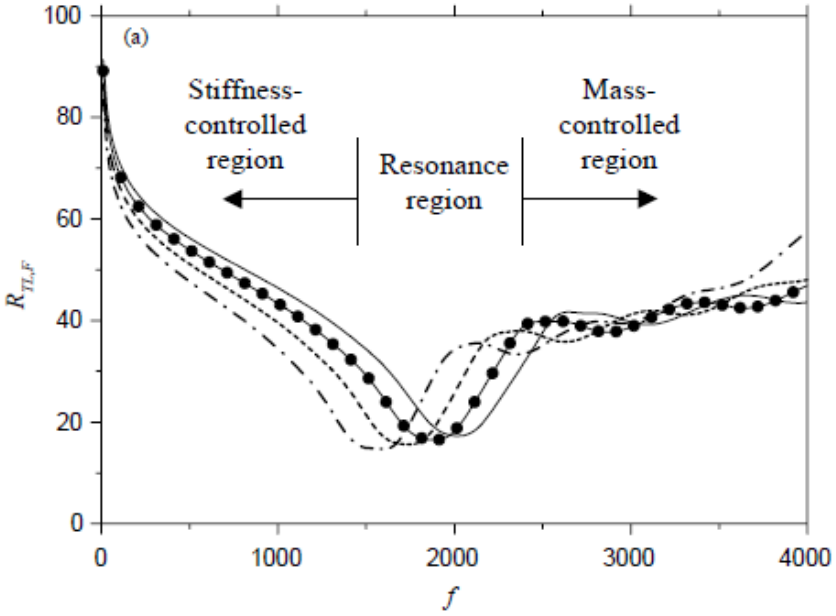

Figure 2-20 Regions of transmission loss vs frequency graph [1]

Finite element analyses by using 2D models and by considering nonlinear hyperelastic materials was carried out by B. Andro et al. Firstly, different complex seal geometries were deformed between two plates and deformed shapes were obtained. Then, an acoustical analysis was performed by finite element method in order to predict the sound transmission loss characteristics. Two methods were used to validate the deformation analysis. In the first one, the deformed geometries of the analysis and the experiments were compared. As a second validation step, the calculated reaction forces on the upper plate by using simulations were compared with the experiments. After getting close trends for the comparison of the reaction forces of the experiments and the deformation analyses; the deformed geometry was exported and acoustical simulations were conducted [2].

In acoustical analysis, 2D models were preferred, and initial conditions and boundary conditions were defined as stated in Figure 2-21. At the end, sensitivity analysis was performed to distinguish the effects of compression ratio, material properties and different seal geometries on the sound transmission loss [2].

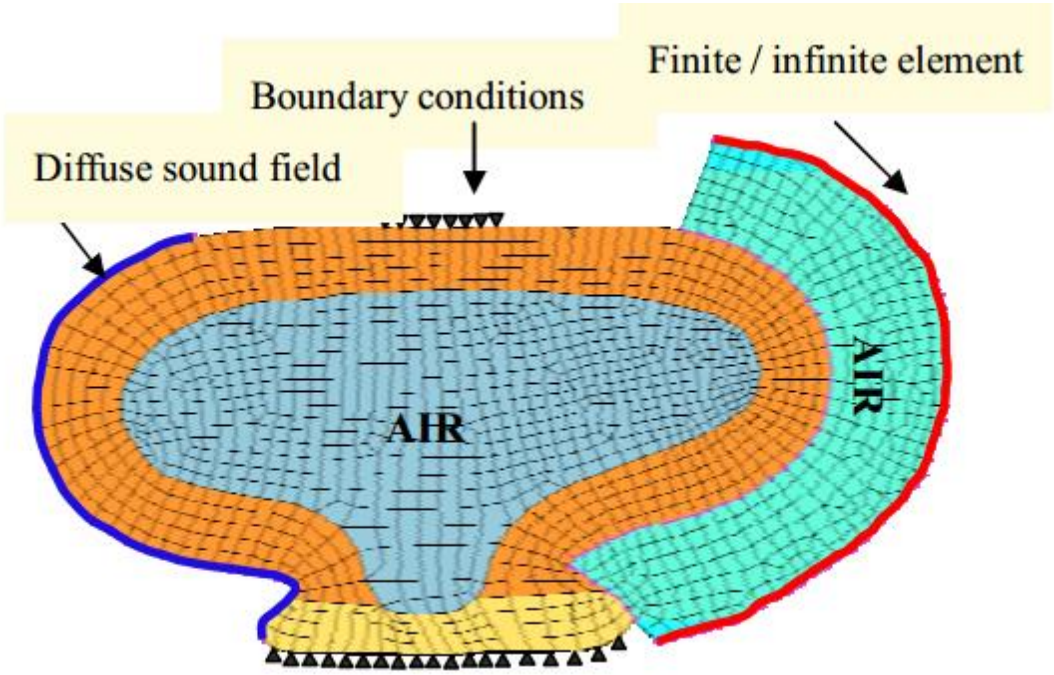

Figure 2-21 Initial conditions and boundary conditions of acoustic model [2]

A study on Hybrid FE – SEA model was employed by Cordioli et al. to predict the sound transmission loss of a car door seal. At the beginning, a full nonlinear deformation/contact analysis was performed to estimate the deformed geometry of the door seal in actual conditions. Then, the geometry was utilized in a vibro – acoustical analysis to predict the sound transmission loss of the seal. The channel between the door and the car structure where the seal is located was also modeled. In addition, the estimated sound transmission loss values was compared with the experimental data [14].

In this article, 3D models were employed with modeling of a portion of the car door sealant only, which is exposed to the sound waves directly. The deformed and undeformed geometries of their seal as well as their Hybrid FE – SEA model can be seen in Figure 2-22 and Figure 2-23, respectively [14].

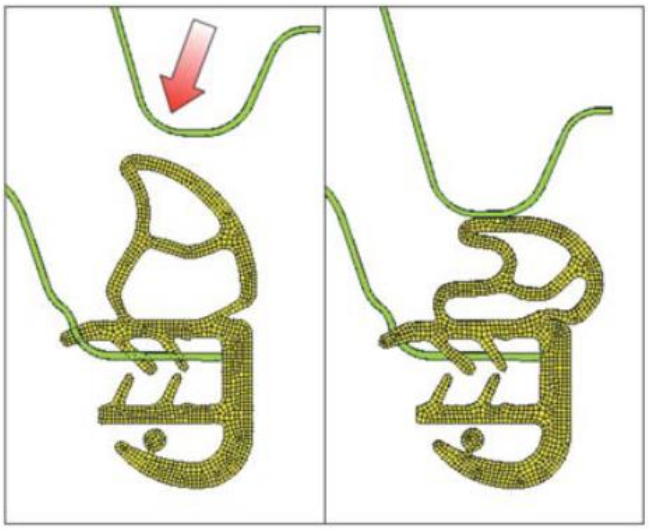

Figure 2-22 Undeformed and deformed geometries of the seal [14]

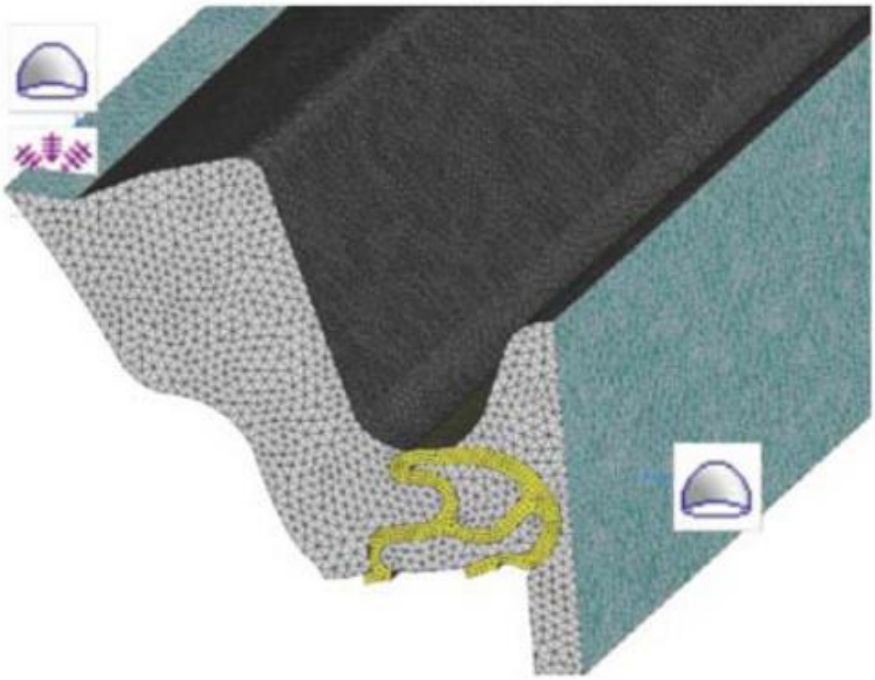

Figure 2-23 Hybrid FE – SEA model of the sealing system [14]

Up to this point, all of the articles covered are related with the sound transmission characteristics of single bulb seal. However, in actual cases sealing systems on the car door contain two bulb seals. The validity of the finite element methods on sound transmission loss was examined by simulating simple models as well as complex sealing systems that contains multiple bulb sealants by Gur et al. Effects of material properties, geometries of the bulb seals on sound transmission were also examined in their study. In addition, the effect of pre – stress on the sound transmission loss was also depicted. According to the article, pre – stress on the deformed bulb seals was found not to have any significant effect on the sound insulation performance of the sealing system. Since incorporating the sealant pre – stress to the acoustic analysis is lengthy and time consuming, transmission loss analysis can be performed without considering the pre – stress on the sealing system [15].

Most important parameters that affects the sound transmission characteristic of seals are material properties, geometry and position of the bulb seal. By accumulated knowledge, Gur and his friends were performed simulations on a system, which contains multiple sealants. Deformation analysis was performed at the beginning as well as the acoustical analysis was simulated on a reduced model. Undeformed and deformed geometries can be seen in Figure 2-24. Moreover, acoustic model can be seen in Figure 2-25. If acoustical model examined deeply, it can be noticed that Gur et al. used only a portion of the door seal [15].

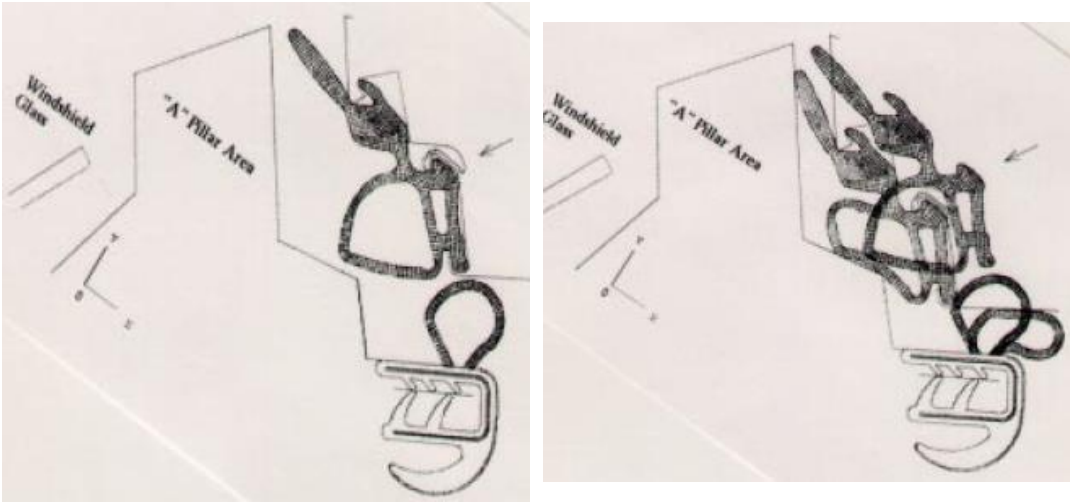

(a) (b)

Figure 2-24 (a), Undeformed geometry; (b), deformed geometry of sealing system [15]

Figure 2-25 Acoustical model of the sealing system [15]

CHAPTER 3

QUASI – STATIC DEFORMATION ANALYSES

This chapter covers details of the quasi – static deformation analyses such as the material definitions, mesh generations, boundary conditions for both validation and analysis of systems with multiple sealants along with the results. There are two main steps. The first one is associated with deciding on the method to be employed in the deformation analysis by validating them with experimental results and the second one involves with the deformed geometry of the sealants.

In the multiple sealant system, there are two bulb seals, whose sectional view can be seen in Figure 3-1. The lower seal is named as “The Primary Seal” and the upper seal is named as “The Secondary Seal”. All of the geometries used in this thesis are obtained from Turkish automotive company, TOFAŞ, which is the fifth largest industrial enterprise of Turkey.

Specifications of the workstation on which the analyses are performed are,

- 64 Gb ram
- 3.10 GHz processor with 32 cores
- 256 Gb SSD
- 1 Tb HDD

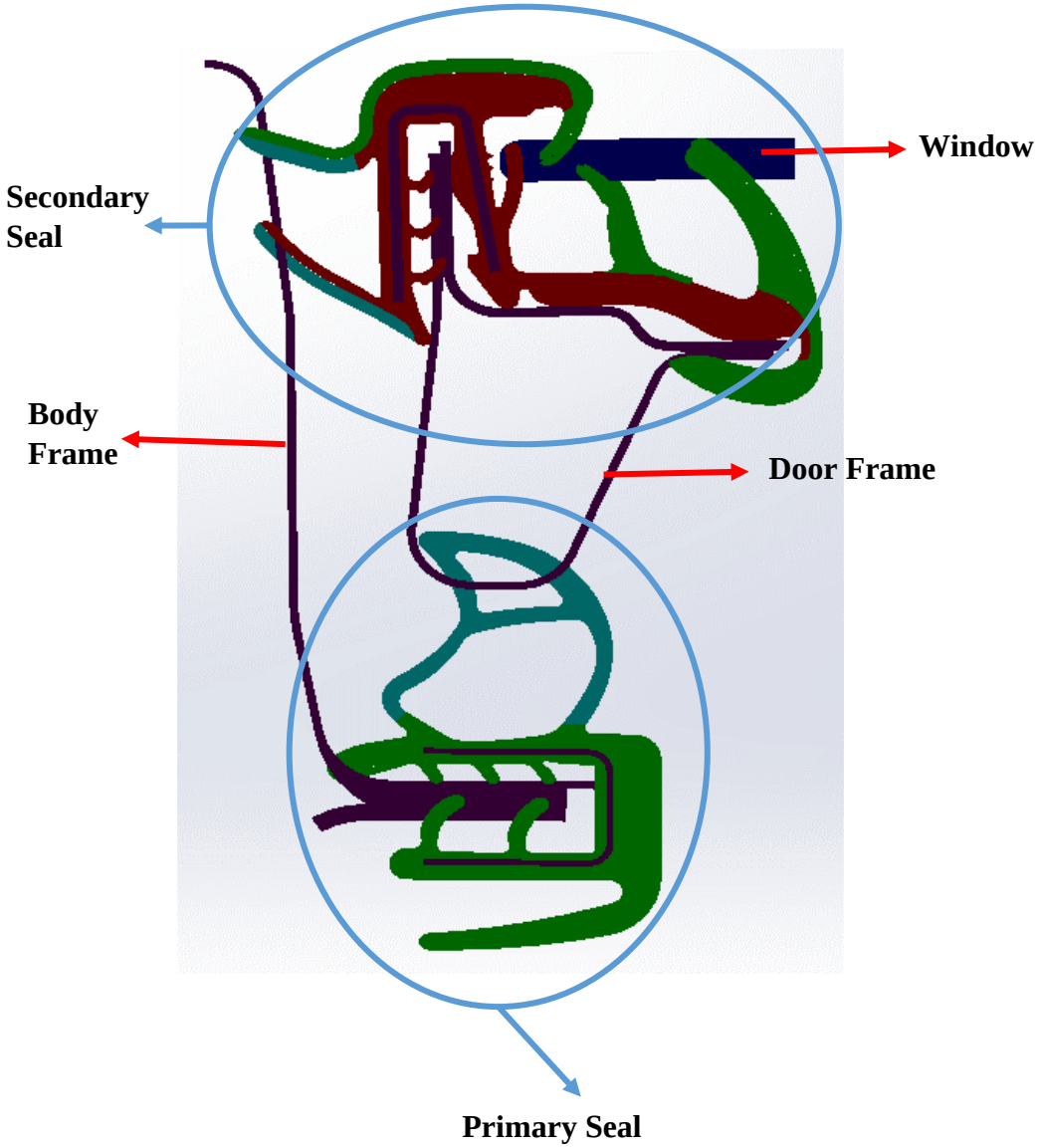

Figure 3-1 Unprocessed multiple seal system geometry

3.1 VALIDATION OF ANALYSIS METHOD

Before going into details of the deformation analysis of the system with multiple sealants, the very first step is validation of the analysis. In this validation step, correct hyperelastic material models should be decided as well as the analysis methods. In other words, the objectives of these validation simulations are deciding on the correct material models and generating correct simulation models.

Validation of the deformation analysis has been conducted by comparing the results of three different tests; two of them is carried on the primary seal and the last test is performed on the secondary seal by TOFAŞ. Those tests are chosen according to the deformation types of this sealant system. Force vs opening curves are taken into account as the comparable data.

3.1.1 GEOMETRY AND MODEL GENERATION

Sketches of the test setups, which was supplied by TOFAŞ, can be seen in Figure 3-2 and Figure 3-3.

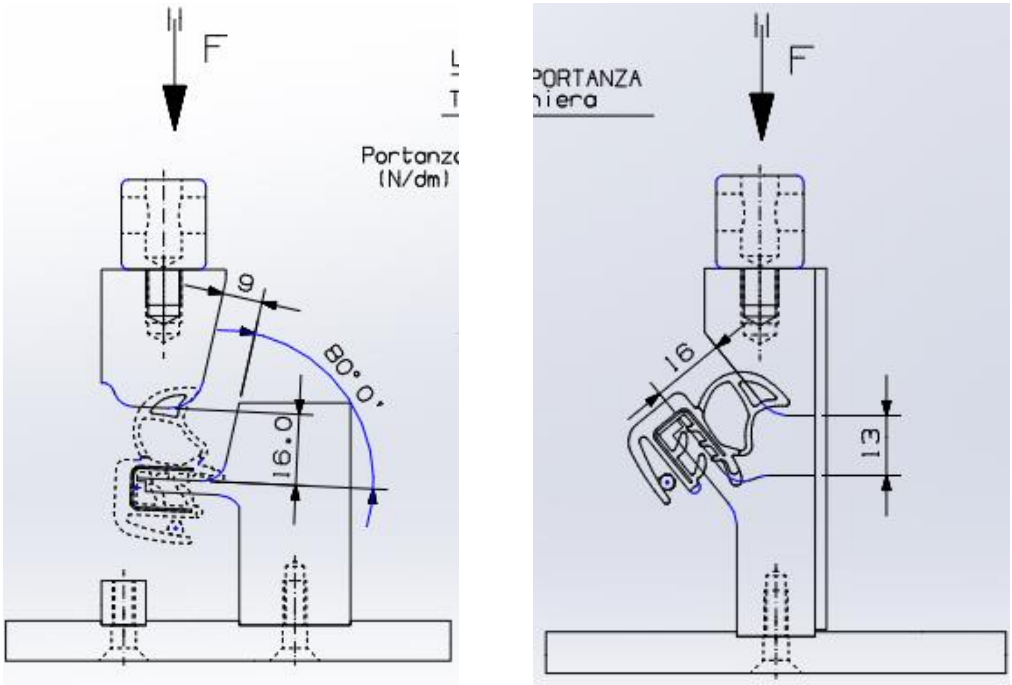

(a) (b)

Figure 3-2 Sketches of tests which will be performed on primary seal – (a), 1st Test; (b), 2nd (Inclined) Test

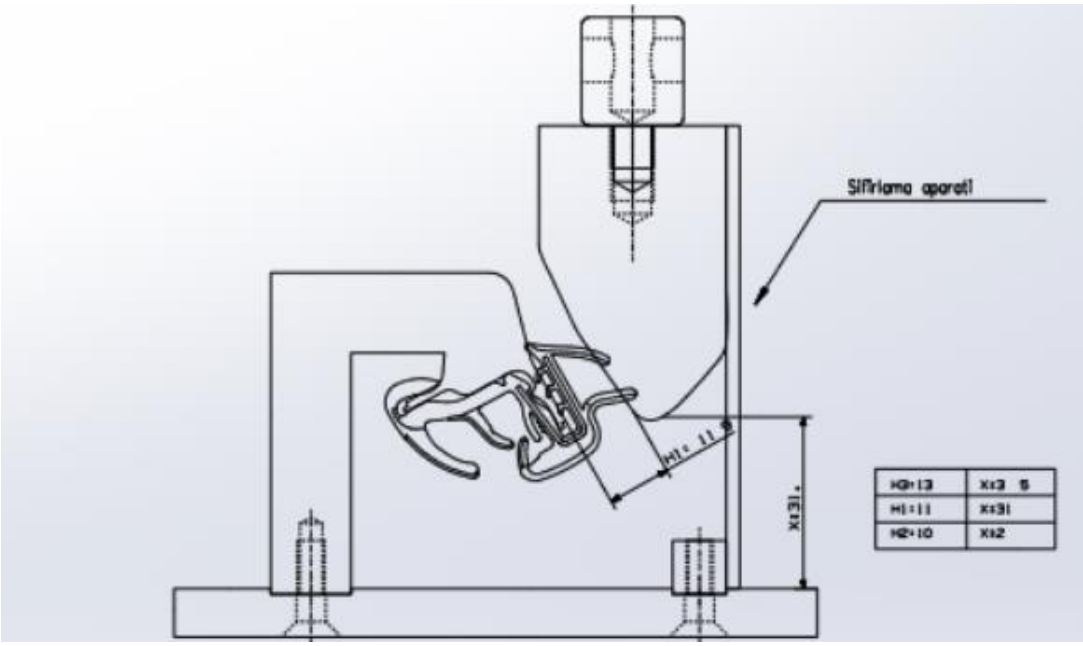

Figure 3-3 Sketch of test setup of secondary seal (3rd Test)

2D geometries of those test setups have been created from those sketches by using SolidWorks 2016. All of the analyses have been performed by 2D models. Created geometries can be seen in Figure 3-4. Furthermore, “Plain Strain” assumption is made for the 2D deformation simulations.

Analyses have been performed on the Marc – Mentat platform. Created geometries meshed and displacement boundary conditions applied. All of the tests have been simulated in two load cases; first one is for mounting the seal geometry and second load case is for deforming the seals. Estimates of displacement values that should be defined as boundary conditions were picked from the sketches of the test setups. Meshed geometries and details of the models can be examined in Figure 3-5.

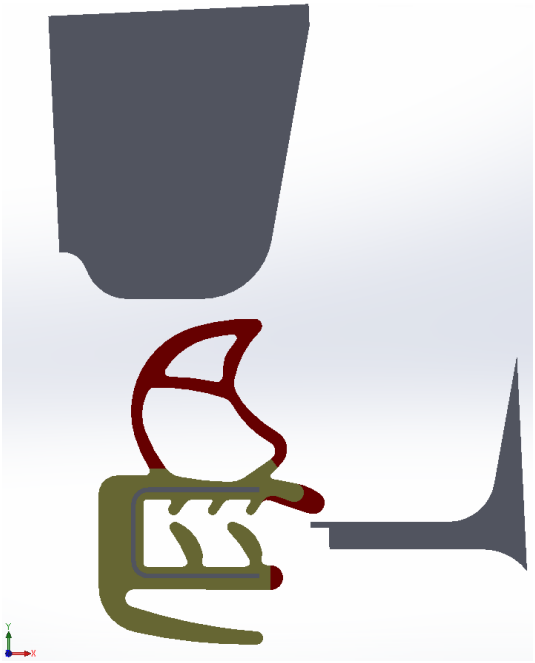

(a)

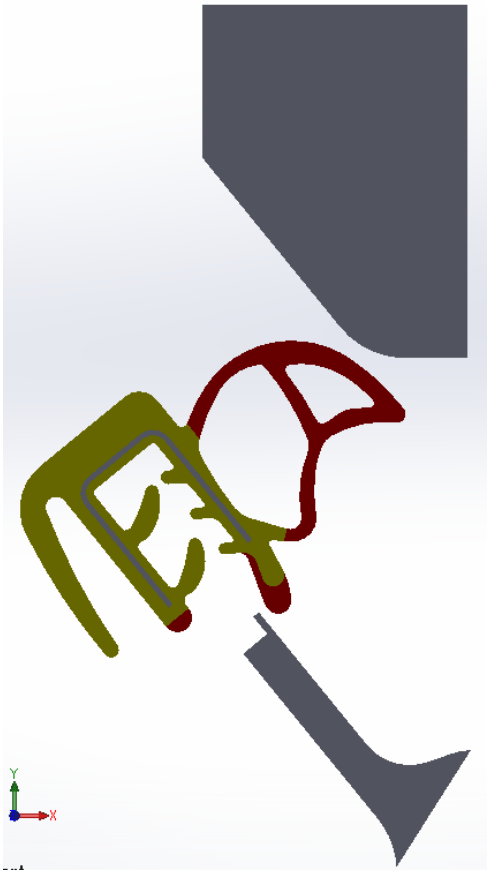

(b)

(c)

Figure 3-4 Geometries of test setups – (a), 1st Test; (b), 2nd Test; (c), 3rd Test

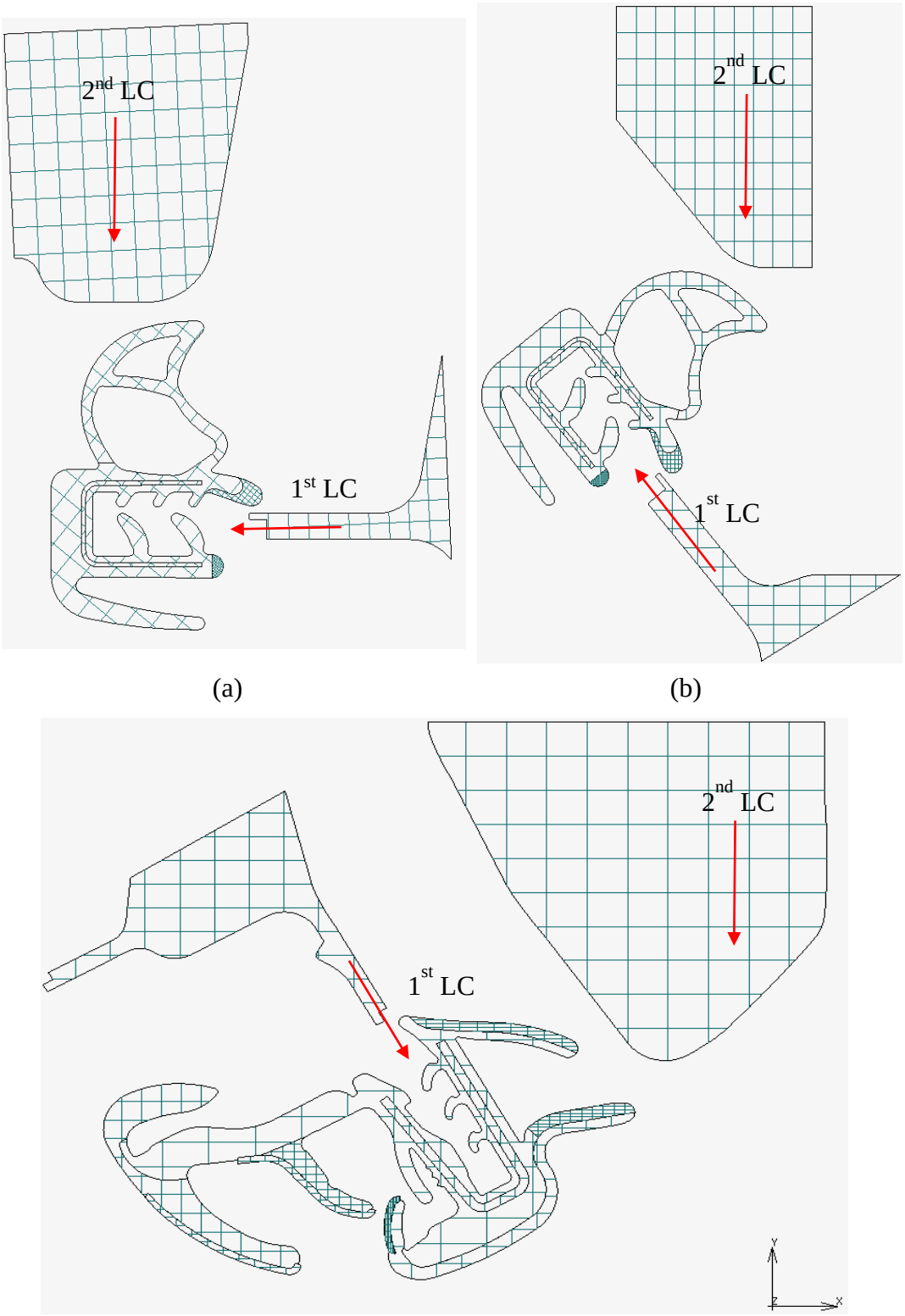

Figure 3-5 Models of test setups – (a), 1st Test; (b), 2nd Test; (c), 3rd Test

In order to understand the effect of friction forces between the contacting bodies, two different cases have been modelled for these tests. In the first case, friction forces are not considered; however, in the second case, coulomb friction of $\nu = 0.3$ is defined between the contacting bodies.

3.1.2 MATERIALS

Two types of materials have been assigned for each tests, one is steel and the other one is material configuration of the elastomers. Rubber components composed of five different materials, which are "SPAF650, SPAF750, EPDM TA20-65, EPDM TA20-70, and EPDM TA20-80". In order to obtain the stress – strain relationship and apply the hyperelastic material models "Uniaxial Tension Test" and "Shear Test" are performed on the samples of those materials. However, samples can only be obtained for "SPAF650, TA20-65 and TA20-80" materials from Turkish Automobile Company.

Ten different material models were applied on the results of the uniaxial tension test and shear test by considering two different error types such as "Absolute Error" and "Relative Error" which are formulated as follows, respectively:

$$e_{abs} = Actual\ Value - Measured\ Value \tag{3-1}$$

$$e_{rel} = e_{abs}/Measured\ Value \tag{3-2}$$

Best model, which can be used to present the material behavior of the elastomer, is selected by considering three different criteria as follows:

1. Hyperelastic material model should give similar trend and close results with the experimental results.

2. Results calculated from the specified mathematical model should be physically meaningful. In other words, calculated stress values should have non – negative values.
3. The model should have the minimum error value with respect to others.

For the TA20-65 material, Table 3-1 presents the calculated error values for different material models.

Table 3-1 Calculated error values for TA20-65 material

Model Applied	**Absolute Error**	**Relative Error**
Neo – Hookean	401.2	418.174
Mooney Rivlin – 2 Term	260.171	152.889
Mooney Rivlin – 3 Term	79.0728	152.704
Signiorini	56.233	150.598
Second Order Invariant	20.5793	81.6098
Third Order Deformation	12.3523	80.8513
Yeoh	14.5275	174.6625
Ogden – 1st Order	880.87	166.342
Ogden – 2nd Order	20.9798	148.992
Ogden – 3rd Order	23.0982	145.879

According to Table 3-1, the third order deformation model with absolute error criteria has minimum error; however, as the strain values increase, the calculated stresses

increase sharply and gives astronomical values. On the contrary, Yeoh model gives relatively similar trend with the experimental results and its error is very close to the error of the third order deformation model. Thus, Yeoh model with absolute error criteria is chosen for the TA20-65 material. Figure 3-6 presents the results of both experiments and Yeoh model for TA20-65 material.

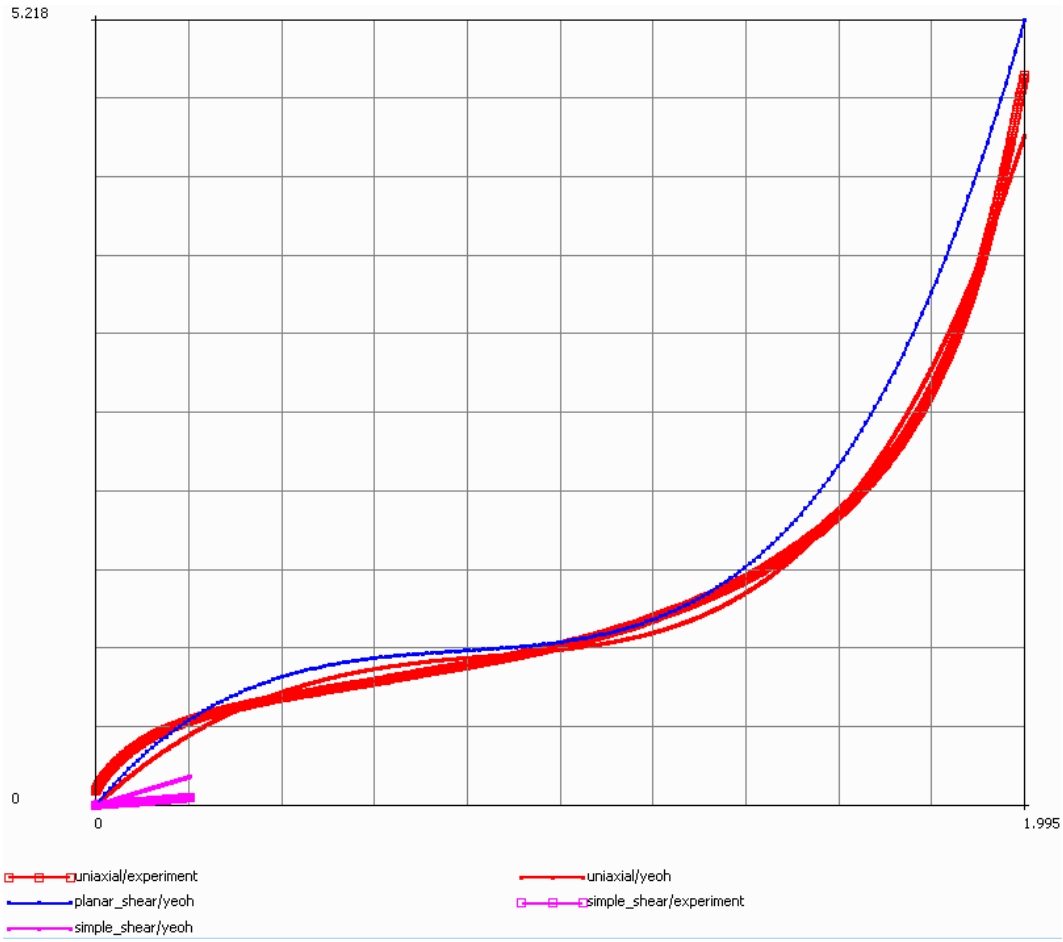

Figure 3-6 Stress – strain relation of TA20-65 material

Similarly, material model for the SPAF650 is chosen according to the criteria specified earlier. Table 3-2 presents the calculated error values for different material models. Moreover, it is indicated that the minimum error can be predicted by third order deformation model and the second one is the Yeoh model with absolute error

criteria. However, those two models give very high stress values as the strain increasing as in the case of TA20-65 material. Thus, the 3rd order Ogden model with absolute error criteria is chosen to describe the stress – strain relationship of SPAF650 material, because this model gives the best curve fit with minimum error. Figure 3-7 presents the relation between stress and strain for both experiments and material model.

Table 3-2 Calculated error values for SPAF650 material

Model Applied	Absolute Error	Relative Error
Neo – Hookean	75.0827	146.81
Mooney Rivlin – 2 Term	50.307	142.381
Mooney Rivlin – 3 Term	11.4885	129.103
Signiorini	8.40013	122.34
Second Order Invariant	5.01709	83.816
Third Order Deformation	2.43937	83.0578
Yeoh	3.50488	99.119
Ogden – 1st Order	471.843	1341.43
Ogden – 2nd Order	5.36868	97.7359
Ogden – 3rd Order	4.89898	94.5146

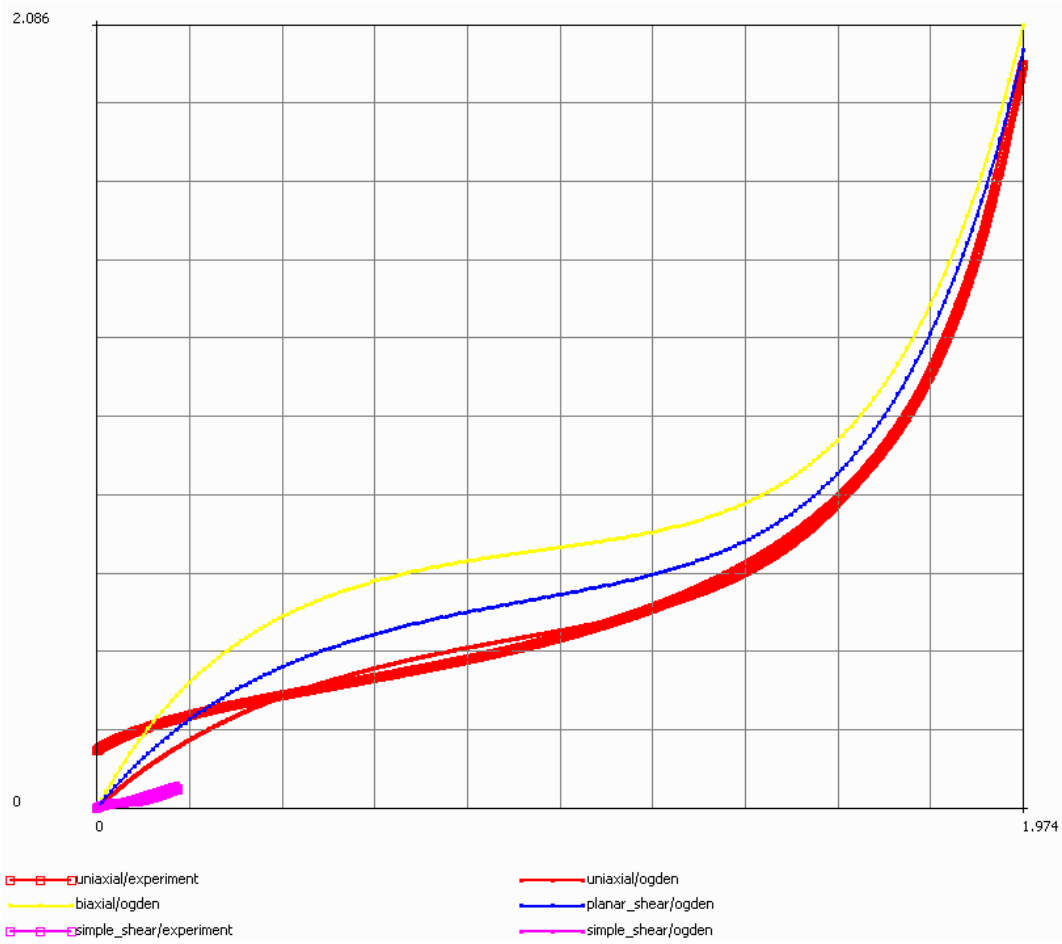

Figure 3-7 Stress – strain relation of SPAF650 material

As material samples for tests cannot be obtained for SPAF750 material, experimental results of SPAF650 material is used by multiplying its test data with the density ratios (i.e. $0.75/0.65$) of two materials. Moreover, hyperelastic material models have been applied on those modified test data in order to estimate the material properties of SPAF750. Table 3-3 indicates the calculated errors for SPAF750 material. As it is expected, this material has the same properties as the SPAF650. In other words, the lowest error values are calculated by using the third order deformation and Yeoh models; however, stress values increase sharply while the strain values are also keep on increasing. Best curve fit is obtained by using a 3rd order Ogden model with

absolute error criteria, which results in the third lowest error. Figure 3-8 presents stress vs strain graph of both curve fitted and test data.

Table 3-3 Calculated error values for SPAF750 material

Model Applied	Absolute Error	Relative Error
Neo – Hookean	134.735	157.547
Mooney Rivlin – 2 Term	87.4801	151.903
Mooney Rivlin – 3 Term	20.2066	134.825
Signiorini	14.5891	126.734
Second Order Invariant	8.01311	84.3052
Third Order Deformation	3.41674	83.936
Yeoh	5.22593	99.8218
Ogden – 1st Order	164.988	144.521
Ogden – 2nd Order	7.77116	99.4333
Ogden – 3rd Order	7.06875	94.664

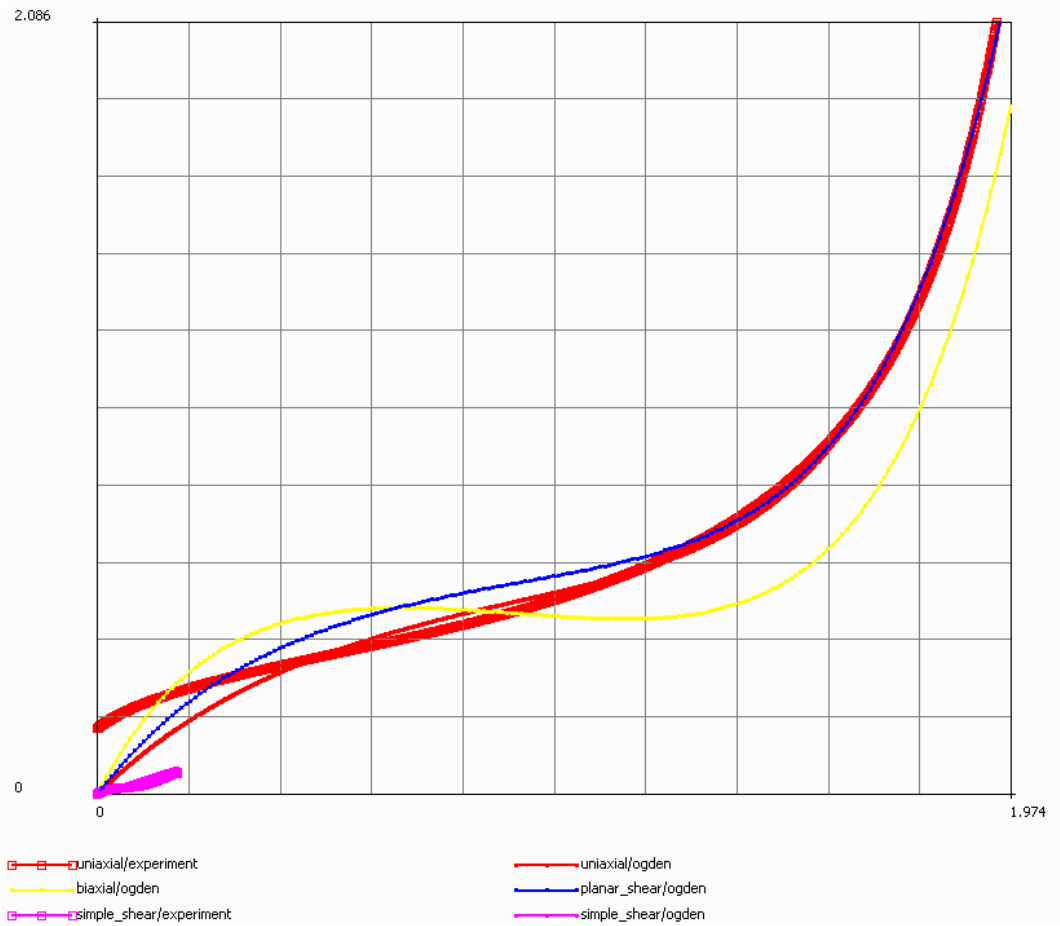

Figure 3-8 Stress – strain relation of SPAF750 material

Last hyperelastic material considered is TA20-80. For this material, calculated errors for different hyperelastic material models are tabulated in Table 3-4. According to this table, minimum error values can be achieved by applying third order deformation model with absolute error criteria. However, with this model calculated stress values got negative (i.e. non – physical) values for planar shear. Second minimum error value can be calculated if second order invariant model is used. Nevertheless, this model also gives negative shear stress values and it cannot be used to describe the behavior of the elastomer TA20-80. Therefore, next model with the lowest error, which is the Yeoh model with absolute error criteria, is chosen. This model gives best curve fit on the experimental results with physical stress quantities. Stress vs strain

graph for both experimental and the curve fitted model can be examined in Figure 3-9.

Table 3-4 Calculated error values for TA20 – 80 material

Model Applied	**Absolute Error**	**Relative Error**
Neo – Hookean	261.945	331.819
Mooney Rivlin – 2 Term	169.814	113.741
Mooney Rivlin – 3 Term	77.5762	112.001
Signiorini	58.6979	113.658
Second Order Invariant	13.0826	76.9887
Third Order Deformation	11.1133	70.0734
Yeoh	16.8578	142.698
Ogden – 1st Order	287.106	136.676
Ogden – 2nd Order	17.3861	101.207
Ogden – 3rd Order	17.4243	105.113

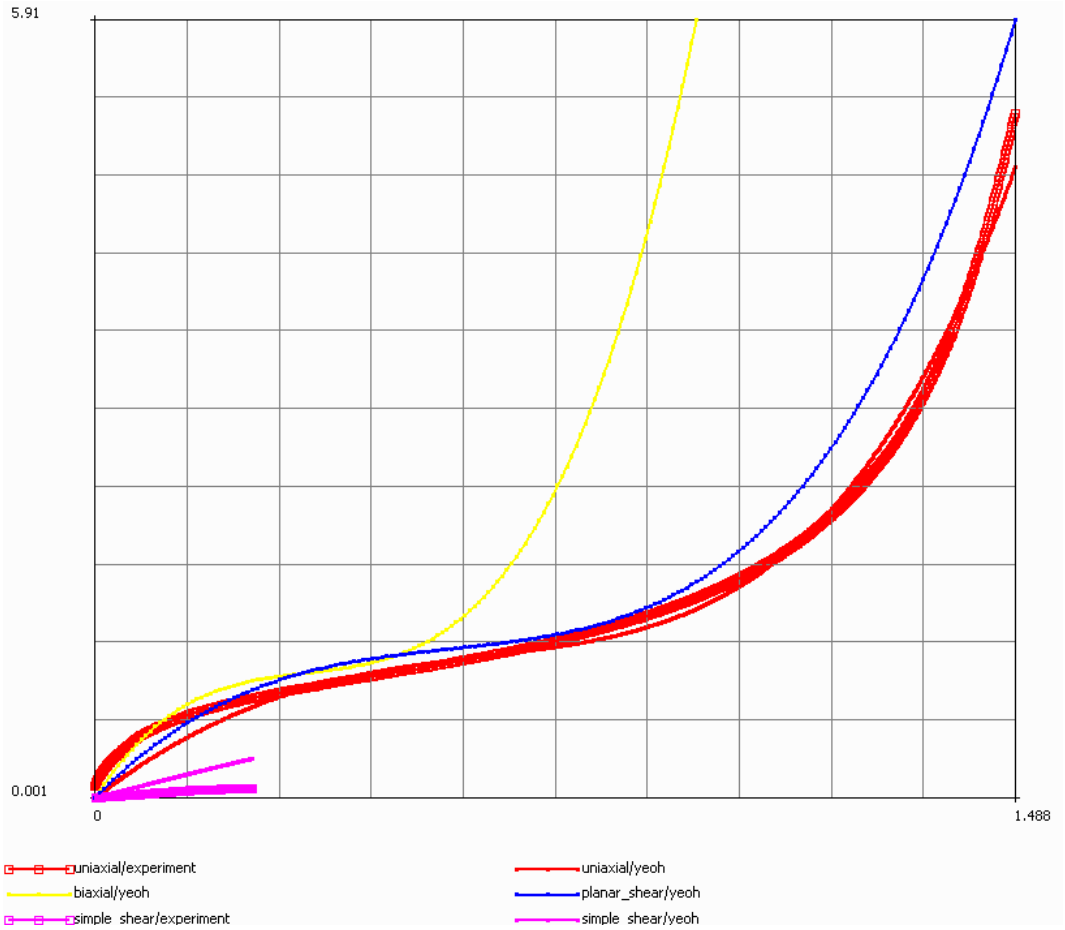

Figure 3-9 Stress – strain relation of TA20-80 material

Related coefficients correspond to the applied hyperelastic material models are presented in the below tables, Table 3-5, Table 3-6 and Table 3-7.

Table 3-5 Calculated coefficients for the 3rd order Ogden model of SPAF650

SPAF650	Moduli	Exponents
1	47.119	-0.0111492
2	3.51286	0.373022
3	$8.75E-06$	12.005

Table 3-6 Calculated coefficients for the 3rd order Ogden model of SPAF750

SPAF750	Moduli	Exponents
1	152.192	0.0579541
2	108.788	-0.0734758
3	$8.87E-06$	12.1173

Table 3-7 Calculated coefficients for Yeoh model of TA20-65 and TA20-80

	TA20-65	TA20-80
$C10$	0.475165	0.602777
$C20$	-0.07388	-0.14147
$C30$	0.009658	0.032541

Assigned material configuration for the test simulations of the primary and secondary sealants can be examined in Figure 3-10 and Figure 3-11.

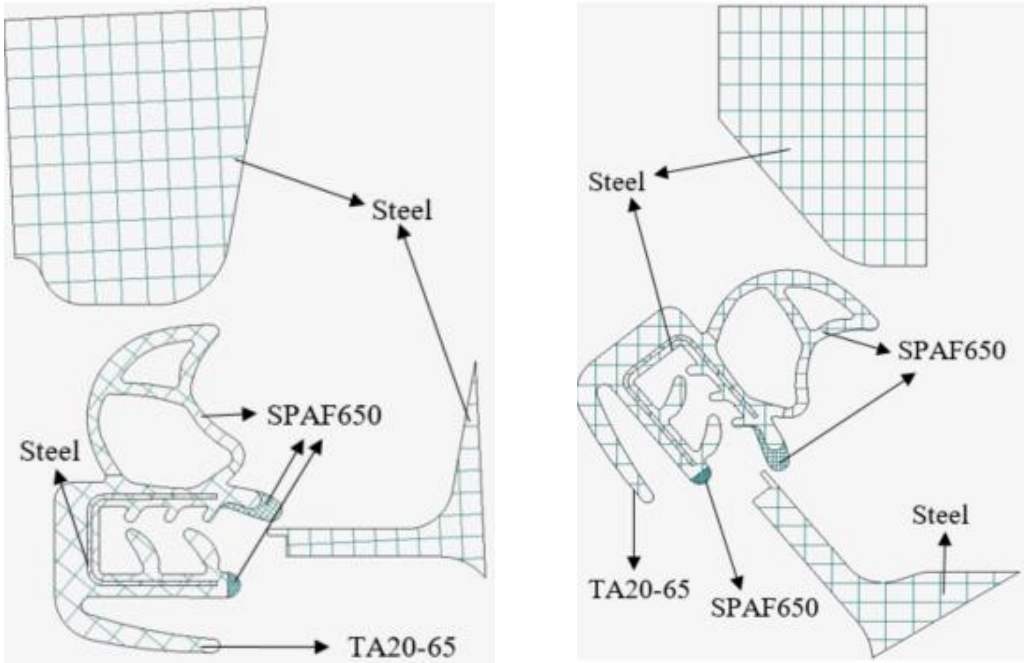

(a) (b)

Figure 3-10 Assigned material configuration for simulations of the – (a), 1st Test; (b) 2nd Test

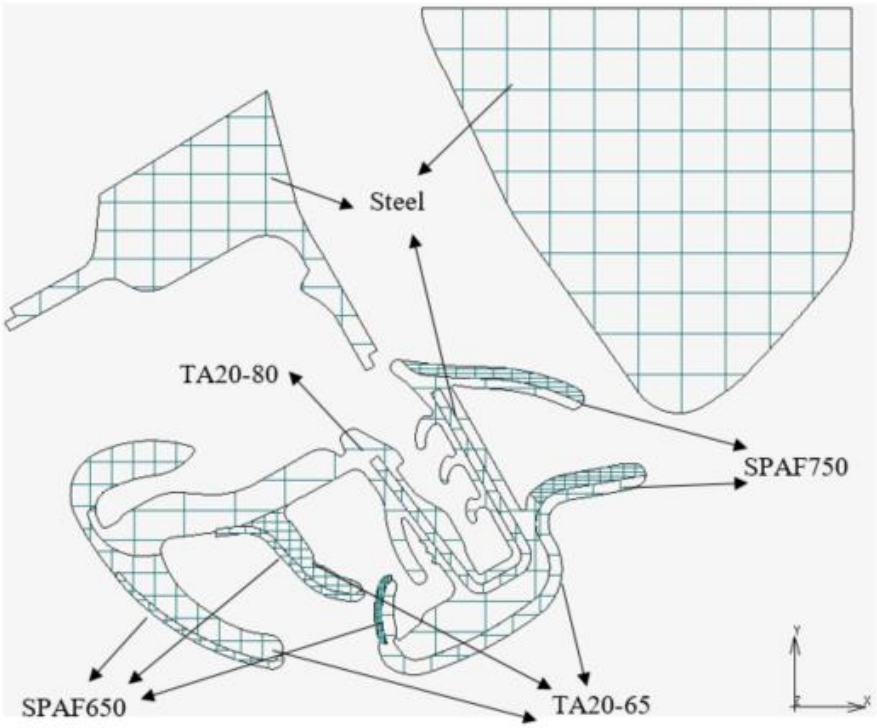

Figure 3-11 Assigned material configuration for simulations of the 3rd Test

3.1.3 RESULTS

The validity of the deformation analysis has been approved by comparing the force vs opening curves for both experiments and simulations. “Equivalent Von Misses stress, equivalent elastic strain and displacement” results are presented in Figure 3-12, Figure 3-13 and Figure 3-14.

During these simulations, low strain with large deflections assumption is made for the elastic components. If the Figure 3-13 examined, it can be seen that the maximum strain level is approximately 4% which means that the low strain assumption is corrected.

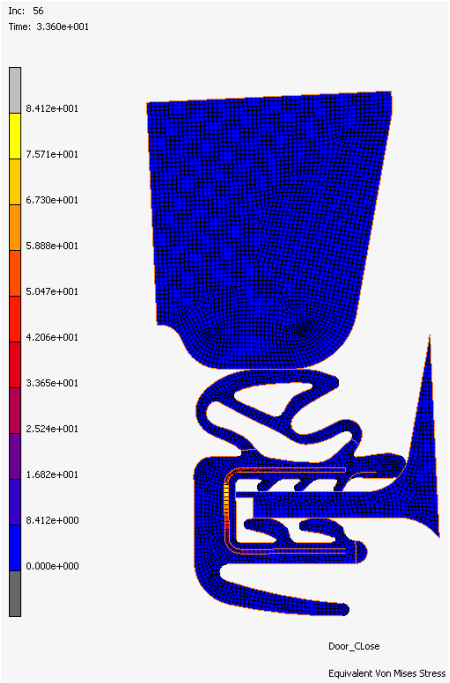

(a)

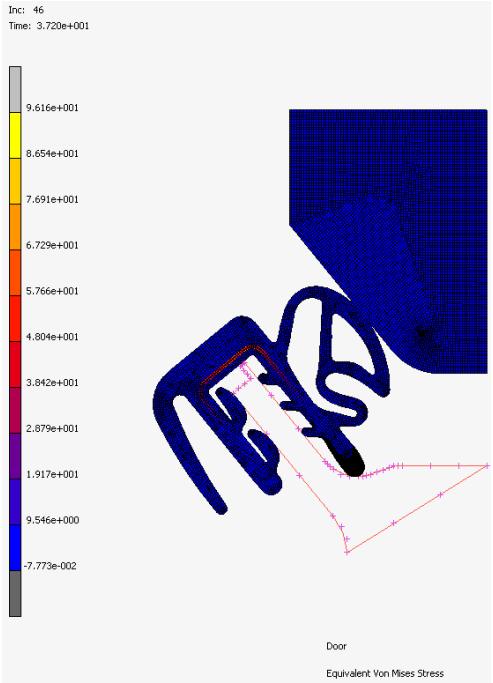

(b)

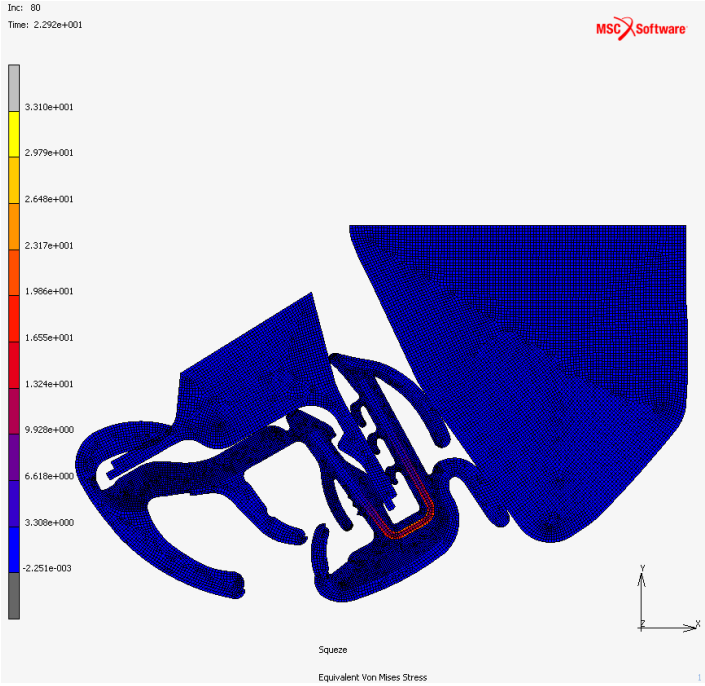

(c)

Figure 3-12 Equivalent Von Misses stress results of the – (a), 1st Test; (b), 2nd Test; (c), 3rd Test

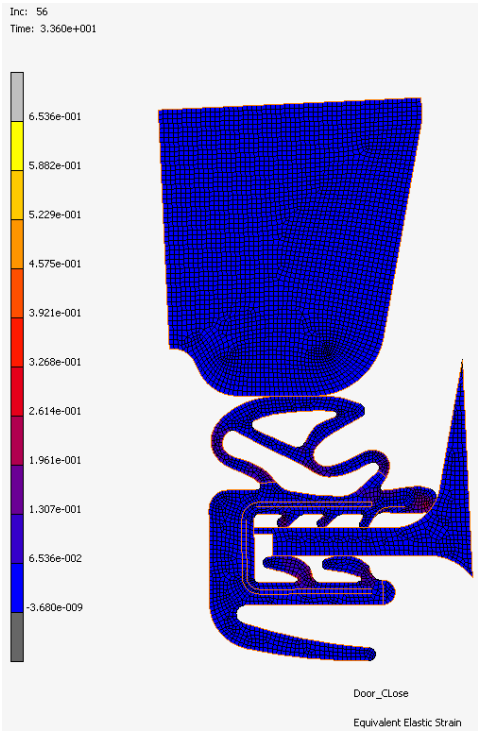

(a)

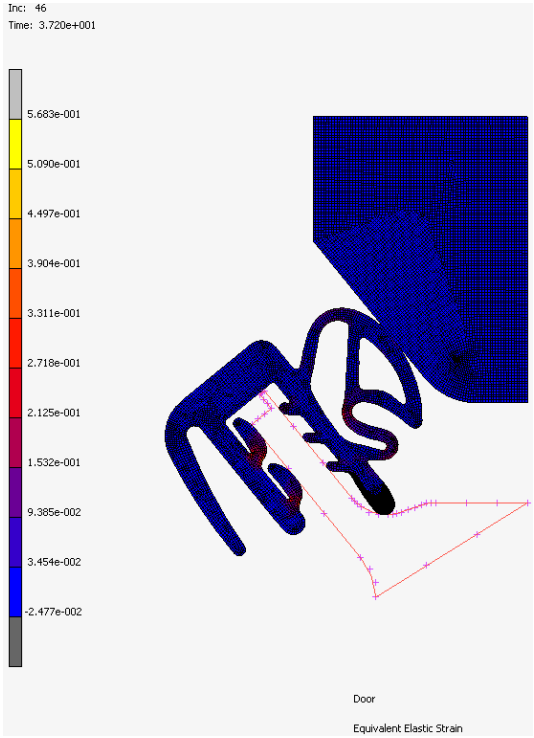

(b)

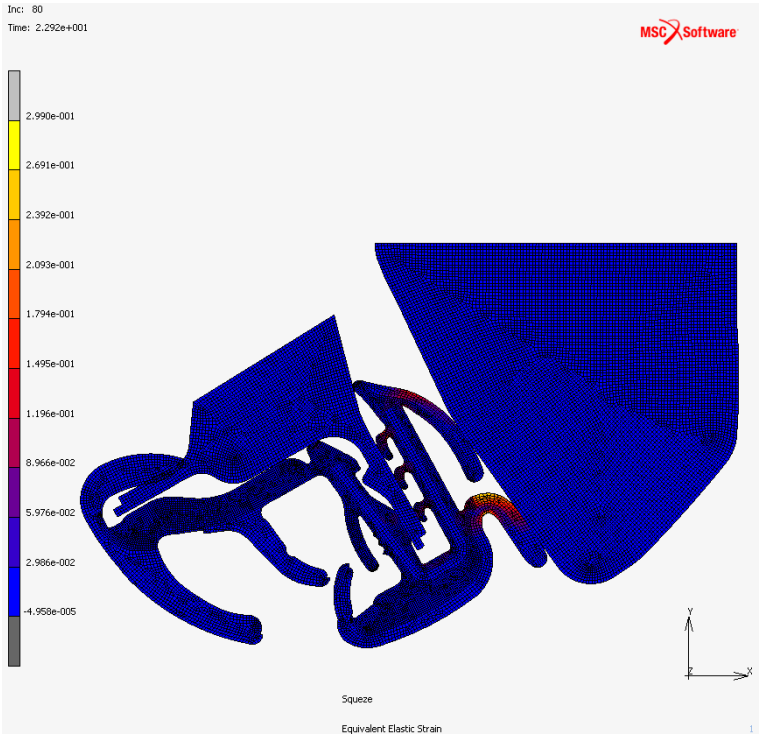

(c)

Figure 3-13 Equivalent elastic strain results of the – (a), 1st Test; (b), 2nd Test; (c), 3rd Test

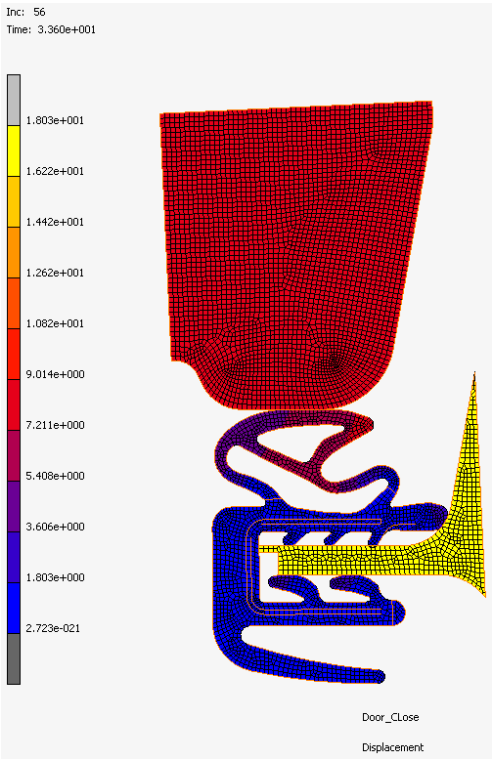

(a)

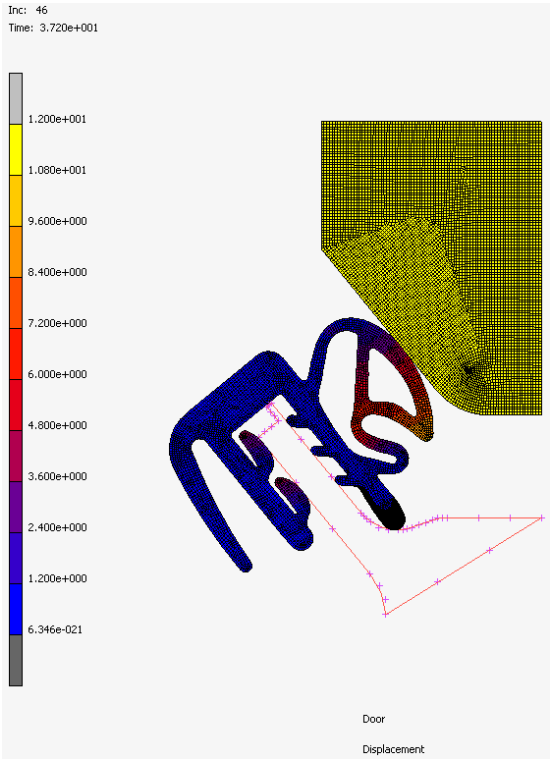

(b)

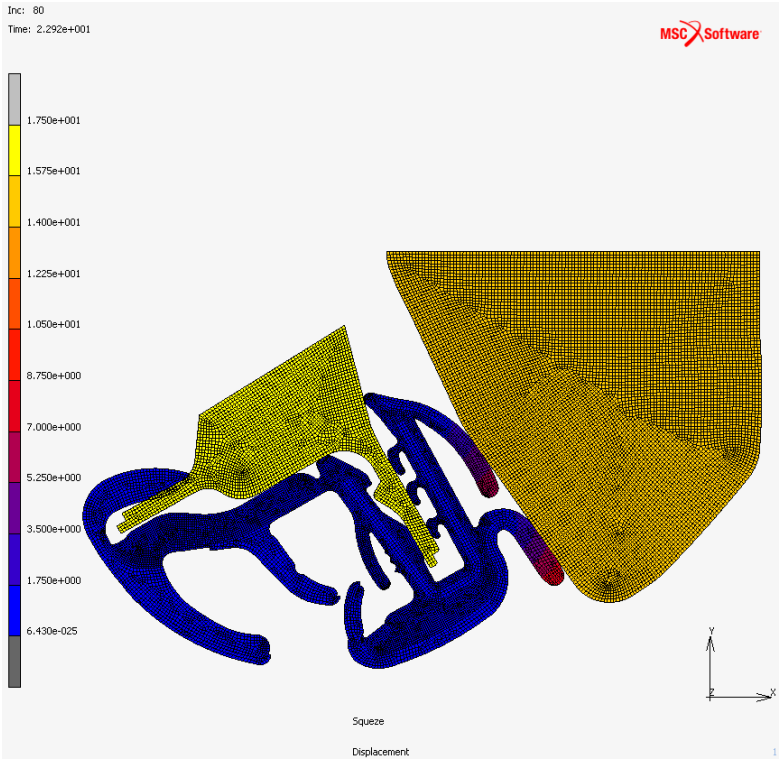

(c)

Figure 3-14 Displacement results of the – (a), 1st Test; (b), 2nd Test; (c), 3rd Test

Force vs opening curves for both experiments and simulations have been plotted in Figure 3-15, Figure 3-16 and Figure 3-17. Test results can only be obtained for the 1st and 3rd tests.

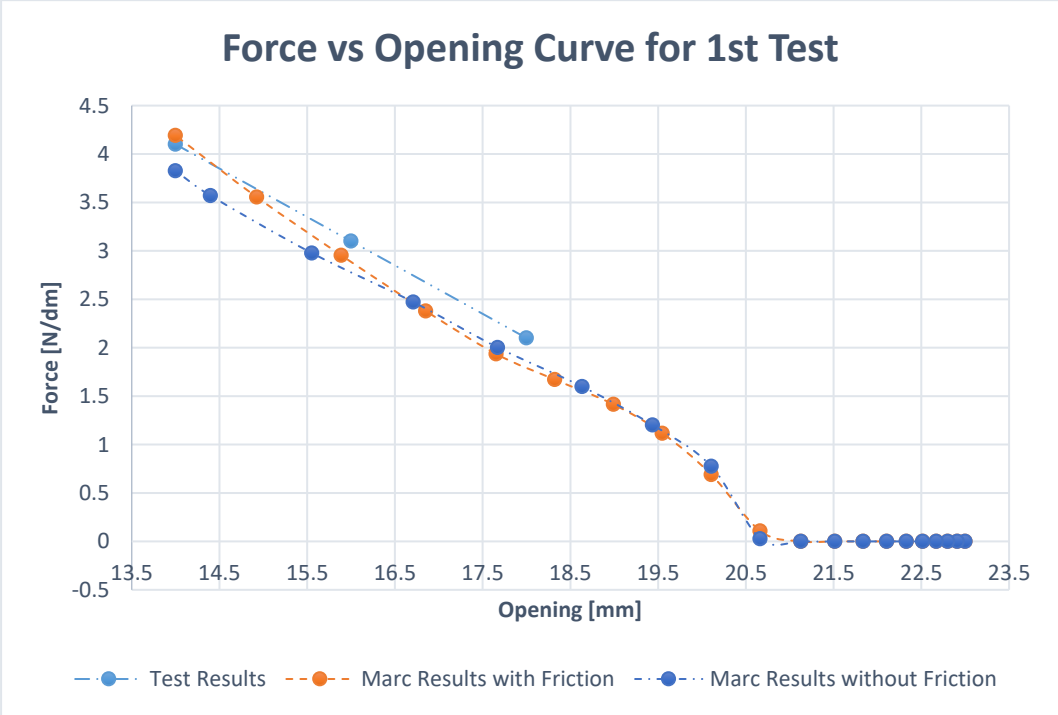

Figure 3-15 Force [N] vs opening [mm] results of the 1st Test

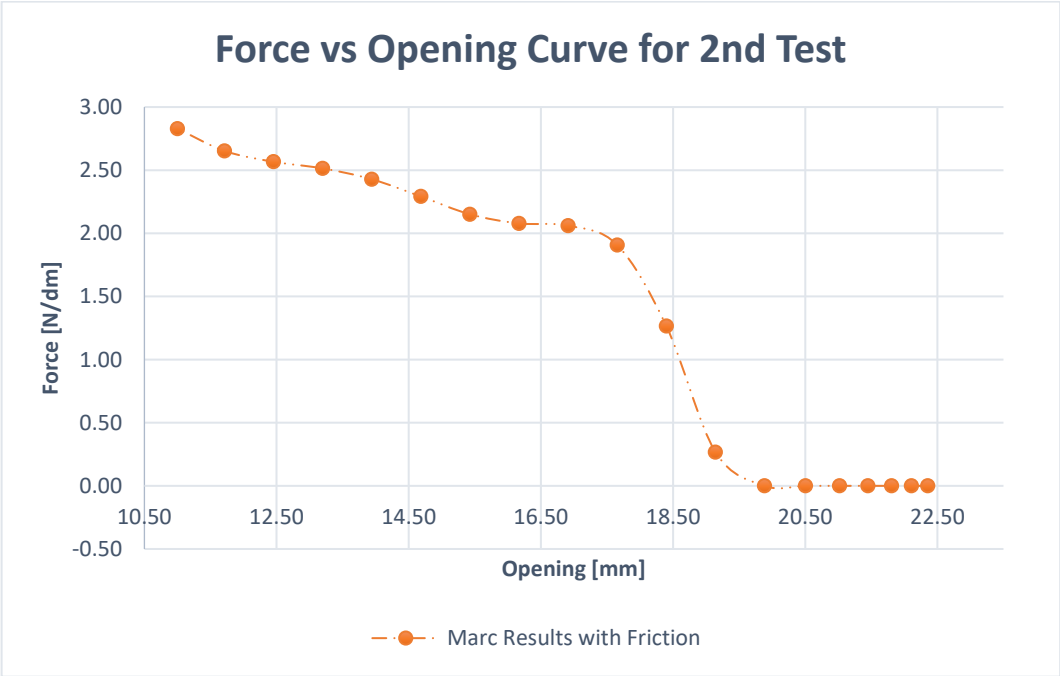

Figure 3-16 Force [N] vs opening [mm] results of the 2nd Test

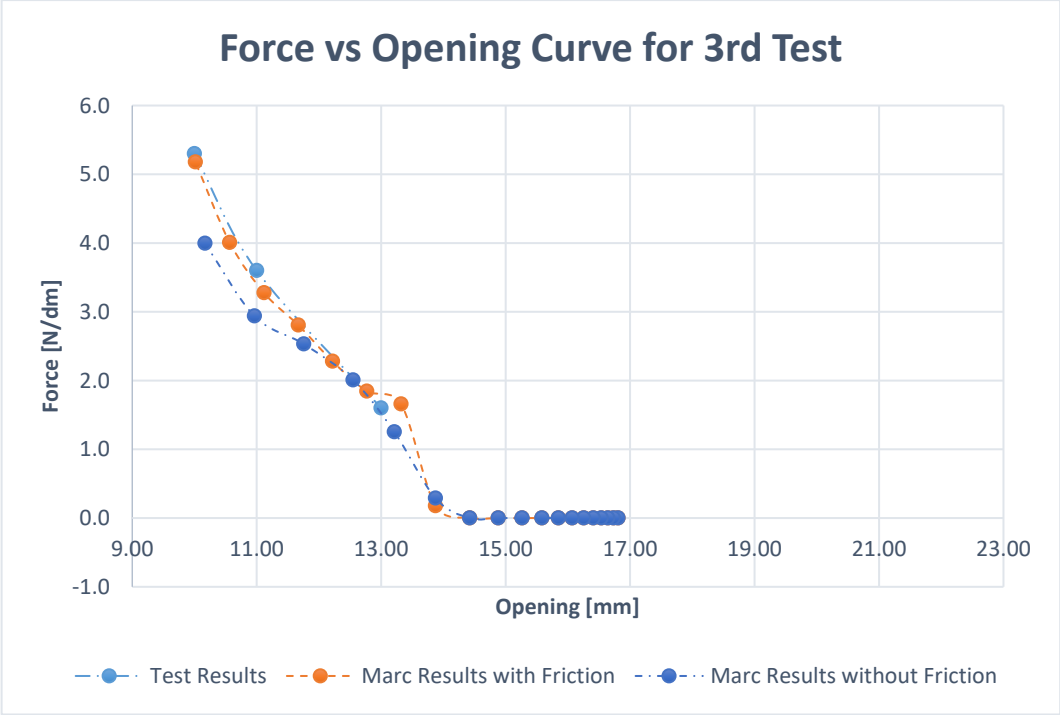

Figure 3-17 Force [N] vs opening [mm] results of the 3rd Test

When results of the 1st test are examined, it can clearly be seen that the calculated force values for changing displacements are very close to the experimental results. Moreover, in the case where the frictional effects are taken into account the reaction force values are slightly increased as it is expected and the results become more realistic for that case. Similarly, on the 3rd test one can figure out the same behaviors with the 1st test. These calculated values are very close to the experimental results and considering friction force makes the simulation closer to the test conditions in real world. Since the test results for the inclined test of the primary sealant (i.e. the 2nd Test) cannot obtained, comparison of simulations with the actual conditions cannot be performed. Nevertheless, if the trends of the 1st and 2nd test results, it is reasonable to state that the 2nd Test simulations can be accepted. Although all of the surface components are meshed, rigid and non – deformable bodies may not be meshed and can be defined as rigid geometry. Moreover, meshing of the rigid components may lead misleading results in some cases. However, during these analyses, force values are compared with the experimental results. Within the light of all of these statements, it is judicious to aver that the deformation simulations are validated and deformed geometry of the multiple seal system can be obtained by using the specified material models, considering friction and forming the simulation models similar with the test simulation models on the Marc environment with same assumptions.

3.2 ANALYSIS OF SEALANT SYSTEM COMPOSED OF MULTIPLE BULB SEALS

As it is depicted earlier, deformed geometry should be obtained to be able to carry on with the acoustical analysis by performing static deformation analysis on the system with multiple sealants. In this section, details of the deformation analysis of sealant system will be presented.

3.2.1 GEOMETRY, MESH GENERATION AND MODELING

Simulations of the multiple sealant system are performed based on the validation analyses. Same material models are used as well as the mesh resolution and contact definitions. Geometry of the multiples sealant system is obtained from the 3D model of a passenger car door, which can be examined in Figure 3-18.

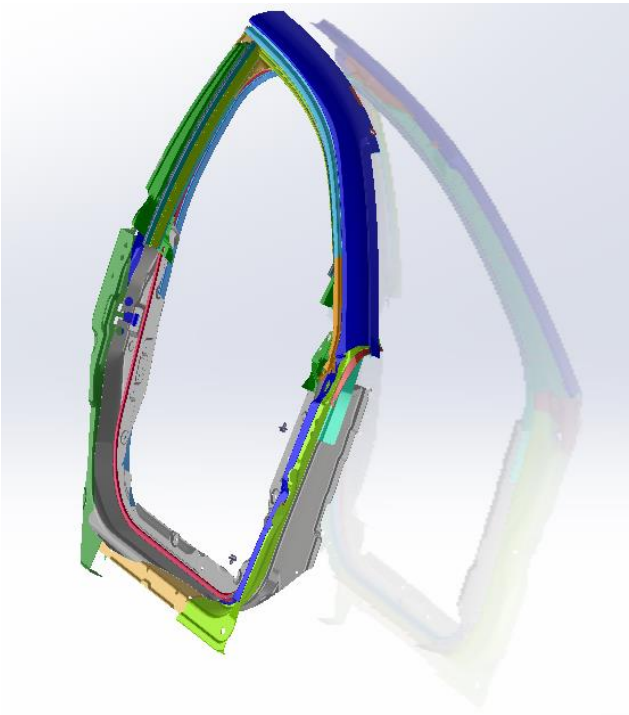

Figure 3-18 3D geometry of a passenger car

2D sealant geometry have been obtained from the section of the passenger car where the wind noise leakage is dominant and it is presented in Figure 3-19 as well as the cross sectional view.

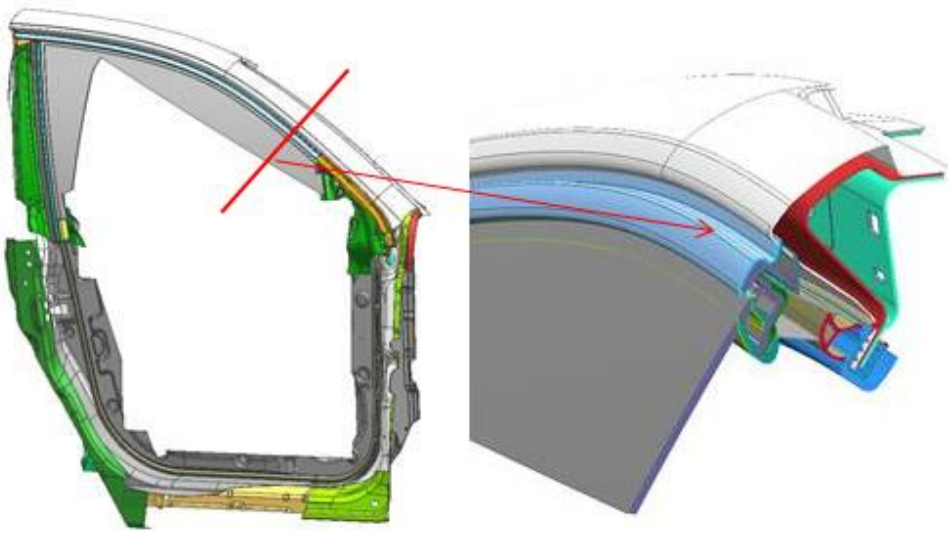

Figure 3-19 Cut section and cross sectional view of the sealant system.

2D geometry (cross section) of the sealant system is formed as it is demonstrated in Figure 3-20 where the mounted configuration is displayed. However, as the mounting can only be done on the CAD software, elastomer geometries in their undeformed formation. Hence, this geometry should be prepared for the deformation analysis by forming the unmounted formation through moving parts. By this way, the amount of displacement that should be defined as boundary condition is specified. Unmounted formation of the system can be seen in Figure 3-21. Deformation analysis for multiple seal system is performed in multiple loaded cases and type of the frictional contact is defined between the contacting bodies.

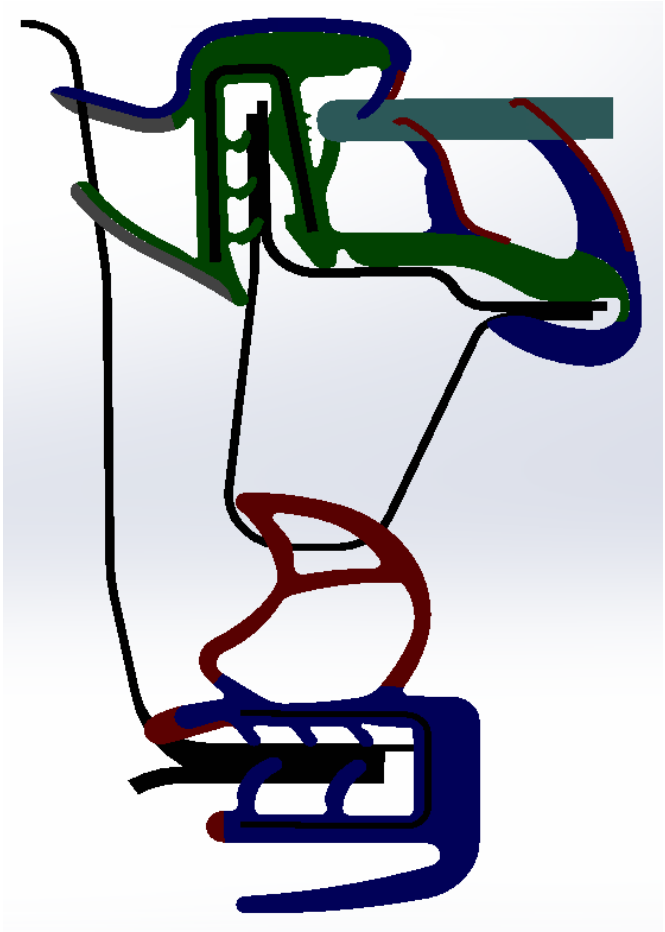

Figure 3-20 Cross sectional view of the 2D sealant system

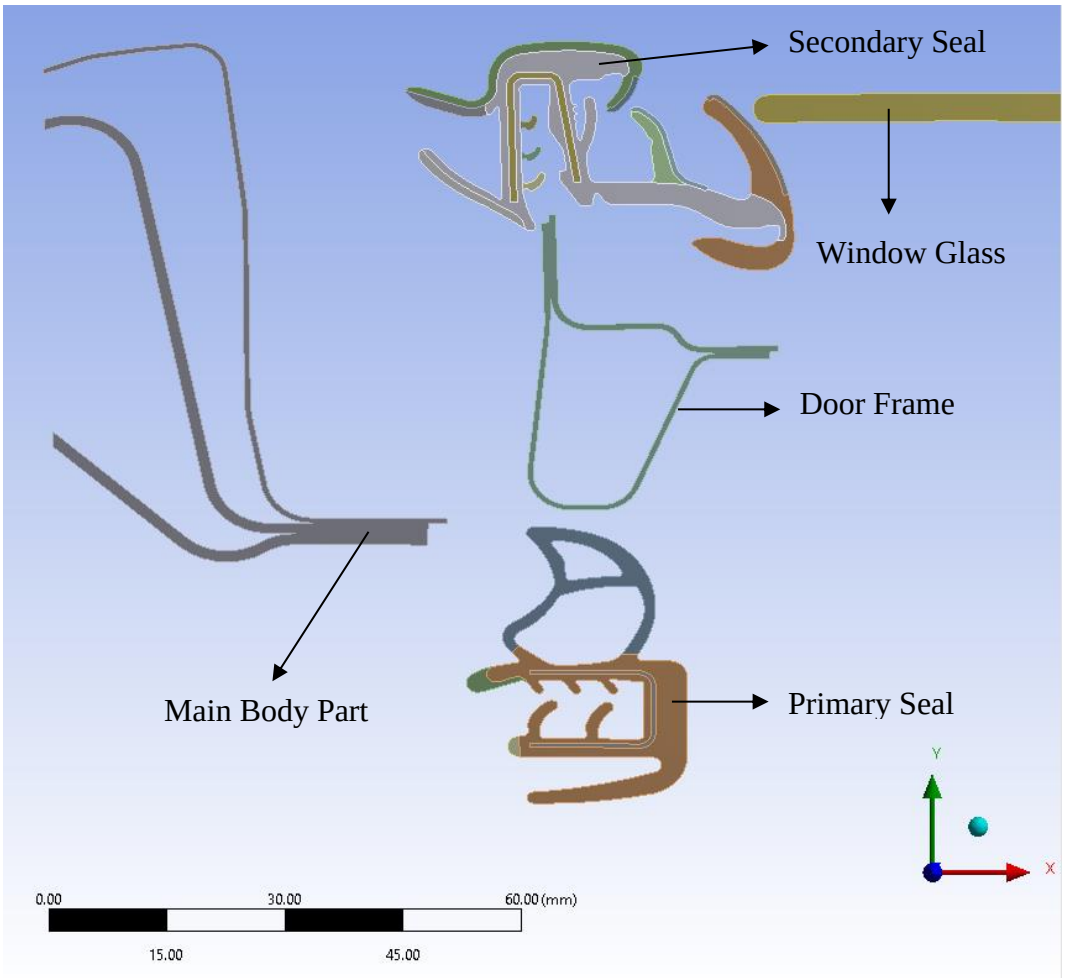

Figure 3-21 Unmounted form of the 2D sealant system geometry

The same mesh size is used as in the case of validation analyses and simulations are performed on Marc – Mentat program. Meshed model can be examined in Figure 3-22.

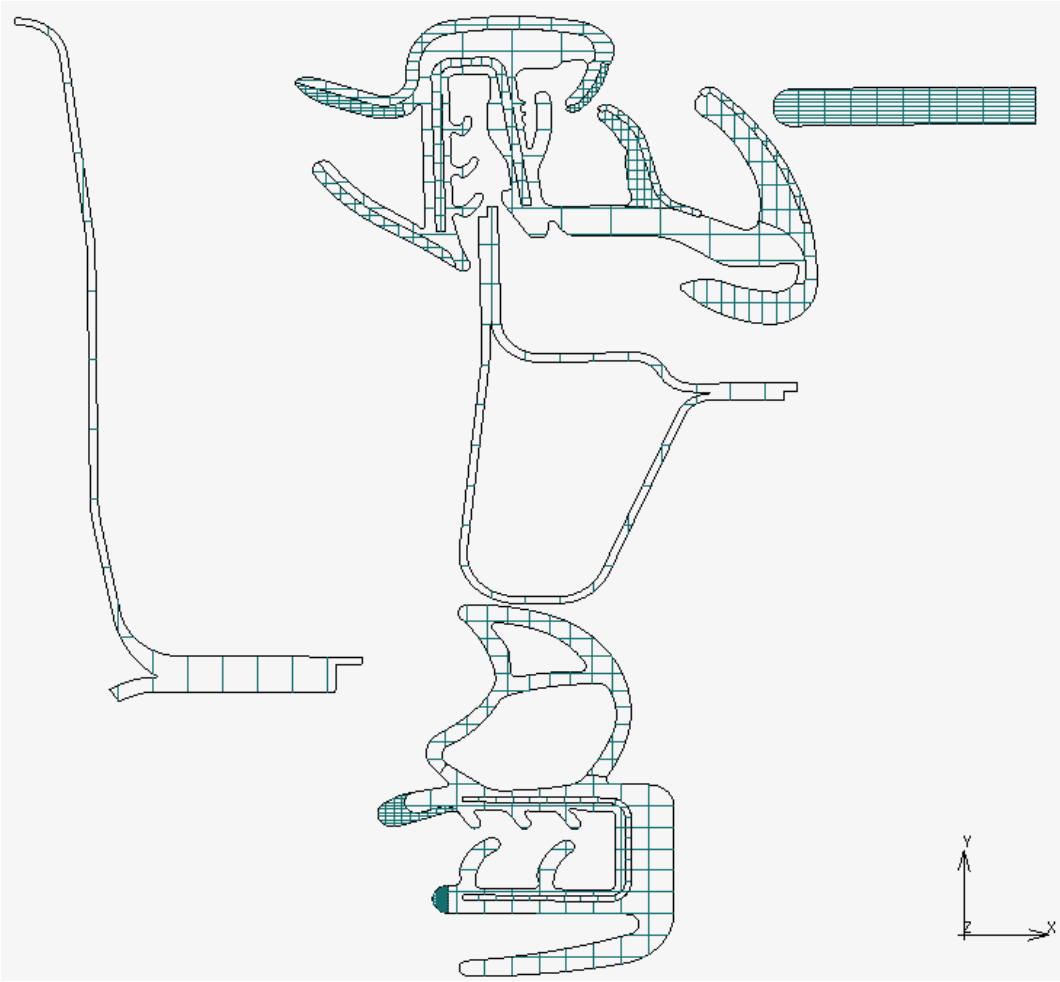

Figure 3-22 Meshed model of multiple seal system

3.2.2 RESULTS

Deformed geometry is calculated and it is presented in Figure 3-23 as a result of the deformation analysis of the multiple sealant system. This mounted form of the sealant system is exported by calculating a new position of each node by disturbing them by an amount of calculated displacement. Exported 2D cross sectional view, which can be seen in Figure 3-24, is imported into SolidWorks 2016. As it is expected, the deformed formation of the primary and secondary sealants is very similar to the results of the validation analyses.

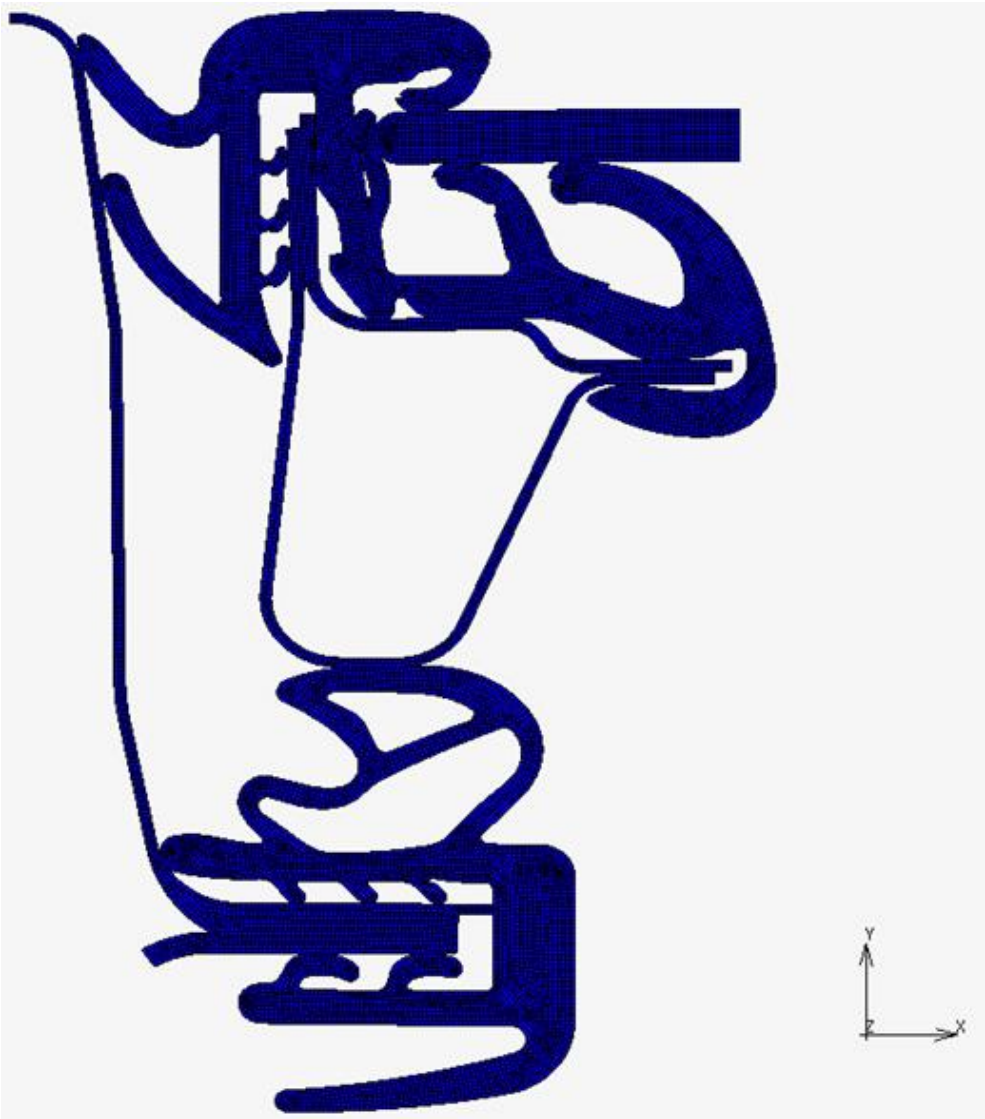

Figure 3-23 Deformed result of the simulations

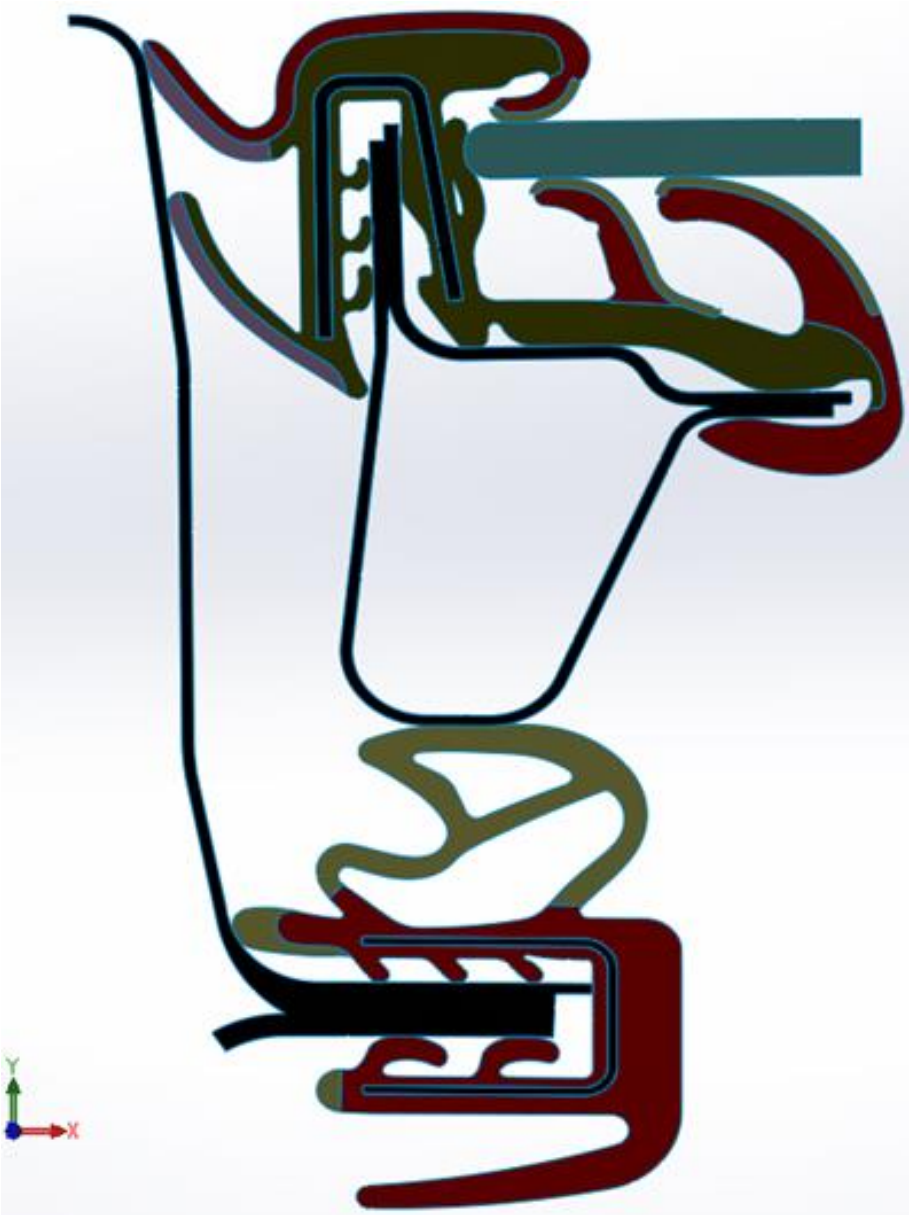

Figure 3-24 2D cross sectional view of sealant system

CHAPTER 4

ACOUSTICAL SIMULATIONS

4.1 VALIDATION OF ANALYSIS METHOD

The very first step of the acoustical analyses is the validation as in the case of the deformation analyses. This step is accomplished by comparing the analytical results of the previously mentioned ideal models, which are formed by Park et al. [1], with the simulation results as well as conducting tests on the primary and secondary sealants and comparing the simulation results with the experimental results. Acoustical simulations have been performed on the Actran 15.1 and MSC Apex Fossa is used as the pre – processor.

4.1.1 SIMULATION OF THE SIMPLIFIED MODEL

Simulation for an ideal, simplified model has been performed and sound transmission loss is calculated by both the results of the analyses and the transfer function matrix method. Dual – membrane model is chosen as the simplified model, as the set of equations governing the final relationship between the incident, transmitted, and reflected pressure amplitudes are supplied in the Park's article [1]. The sketch corresponding to the dual – membrane model can be seen in Figure 2-16.

4.1.1.1 Geometry, Mesh Generation and Modelling

Geometry of the simplified model is generated according to its sketch. Dual – membrane model is a simplified structure of a sealant geometry. Two independent sealant membranes are separated by an air gap. The elastomer membranes are free to move along the direction of wave propagation. The elastomer thickness in the model is $2\,mm$ and the thickness of the air layer between the membranes is $10\,mm$. Geometry of the dual – membrane model can be seen in Figure 4-1.

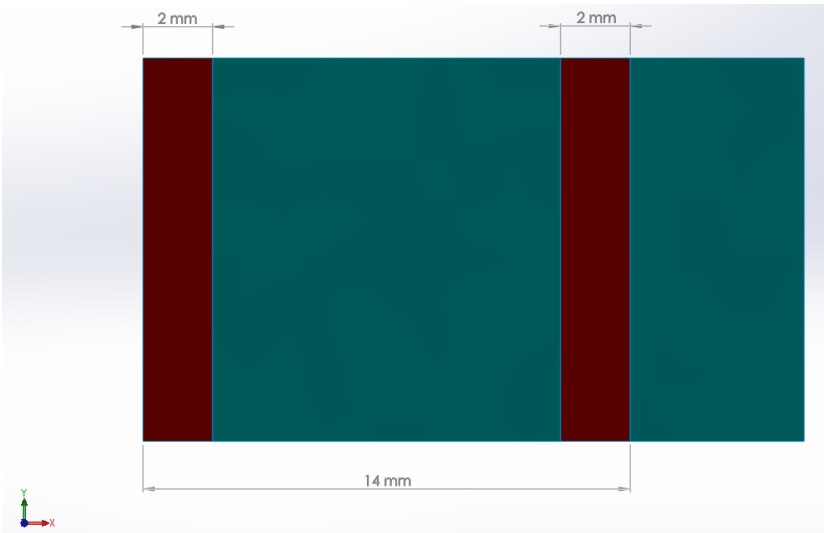

Figure 4-1 Dual – membrane model geometry

As the elastomer material, an isotropic material is used for both sealants. The material density is reported to be $\rho_s = 370\ kg/m^3$ and Poison's ratio is declared as $\nu = 0.4$. Moreover, constant Young's modulus with a value of $E = 2.3\,MPa$ has been assigned. Energy dissipation due to material damping has been neglected in both acoustical analyses. Air with mass density of $1.225\ kg/m^3$ is assigned as the fluid. Also, the speed of sound is defined as $340\ m/s$.

This verification analyses have been performed frequencies from $1\ Hz$ to $5000\ Hz$ as in the case of Park et al.'s article. Furthermore, $1\ mm$ mesh size is chosen to be able to get at least six elements per wavelength, which results fine enough mesh resolution for the highest frequency of interest. Applied boundary conditions and meshed geometry are presented in Figure 4-2.

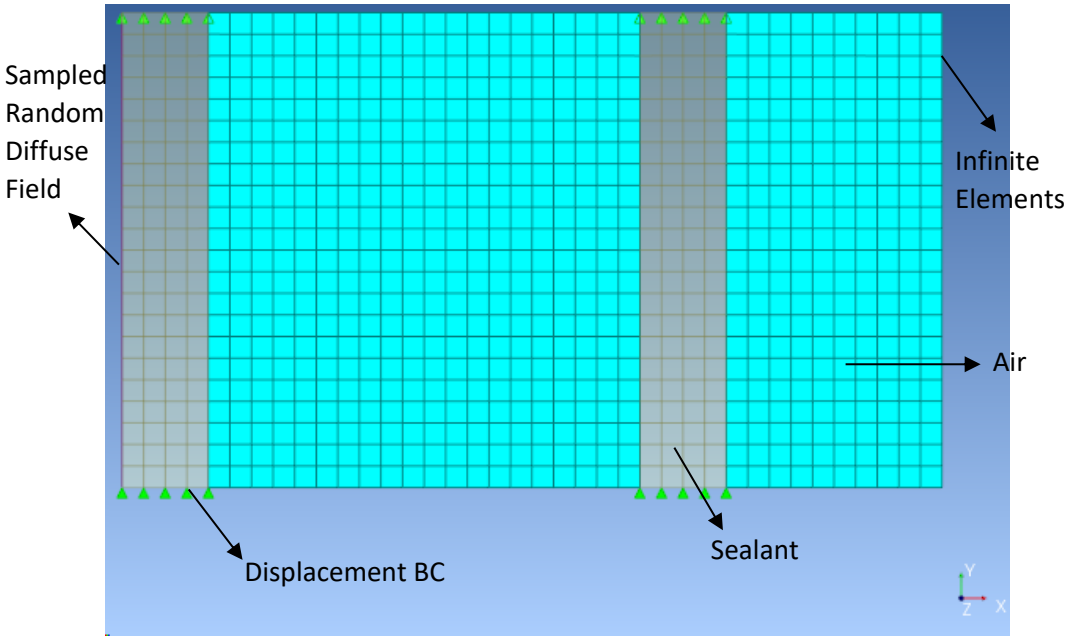

Figure 4-2 Dual – membrane model

4.1.2 TEST SIMULATIONS ON SEALANTS

Acoustical tests are conducted on the primary and secondary sealants to obtain their individual sound transmission performances. Test setup can be seen in Figure 4-3.

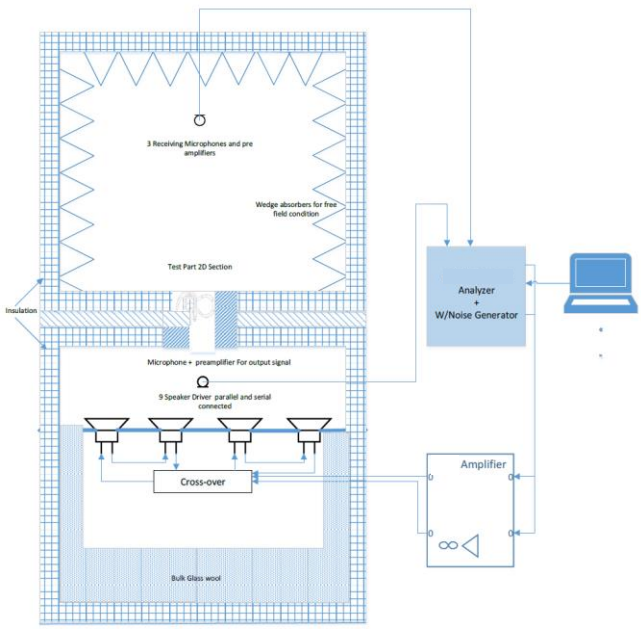

Figure 4-3 Sketch of the acoustical test setup

Loudspeakers have been used as sound sources for generation of a nearly diffuse sound field. In the receiver room anechoic conditions have been formed. Furthermore, "Sampled Random Diffuse Field" is used as the excitation boundary condition and "Infinite Elements" are assigned to the side of the air layer to get anechoic conditions on the receiver portion. Fluid – solid interactions are automatically constructed on Actran software. Furthermore, if nothing is assigned for a boundary it is treated as rigid surface with zero transmission. In addition, analyses have been performed from $100\ Hz$ to $5000\ Hz$ with $5\ Hz$ frequency resolution and power spectral density is calculated by averaging 50 samples.

4.1.2.1 Geometry and Mesh Generation

Sealant geometries for these tests have been obtained by sampling the cases in the literature review and the photographs of the sealants, which are mounted to the test setups. Related photographs can be seen in Figure 4-4.

(a) (b)

Figure 4-4 Mounted sealants for acoustical analyses – (a), Primary Seal; (b) Secondary Seal

Acquired geometries can be examined in Figure 4-5.

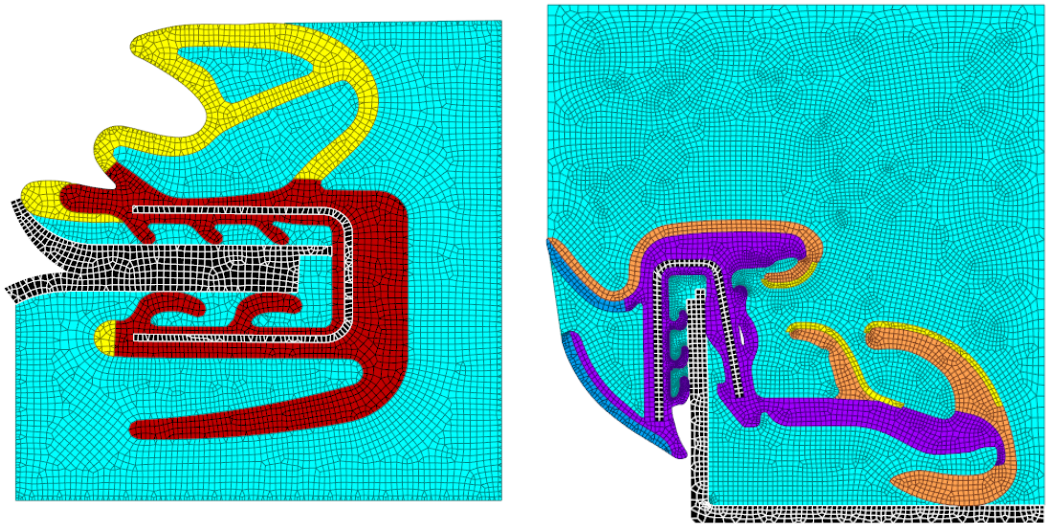

(a) (b)

Figure 4-5 Analyses geometries of sealants – (a), Primary Seal; (b) Secondary Seal

4.1.2.2 Materials

Samples for some of the materials are obtained and complex modulus tests have been performed on those samples to get the complex modulus of the materials for different frequencies. On the test results, double transition model along with the Arrhenius shift factor equation has been applied and mathematical expressions, which can be used to calculate the complex modulus of the materials for different frequencies beyond the limits of the complex modulus test, are obtained. Reference temperature and slope are taken as $T_0 = 383\,K$ and $T_A = 12500$ in Arrhenius shift factor equation.

As in the case of the hyperelastic materials tests, samples only for "SPAF650, TA20-65 and TA20-80" materials can be acquired.

Since coefficients for the SPAF750 material cannot be calculated, complex moduli correspond to the SPAF650 material are multiplied with the density ratio of two materials $(0.75/0.65)$. Moreover, SPAF650 material has been assigned rather than the flock material. Details of the material configuration used in the simulations is demonstrated in Figure 4-6.

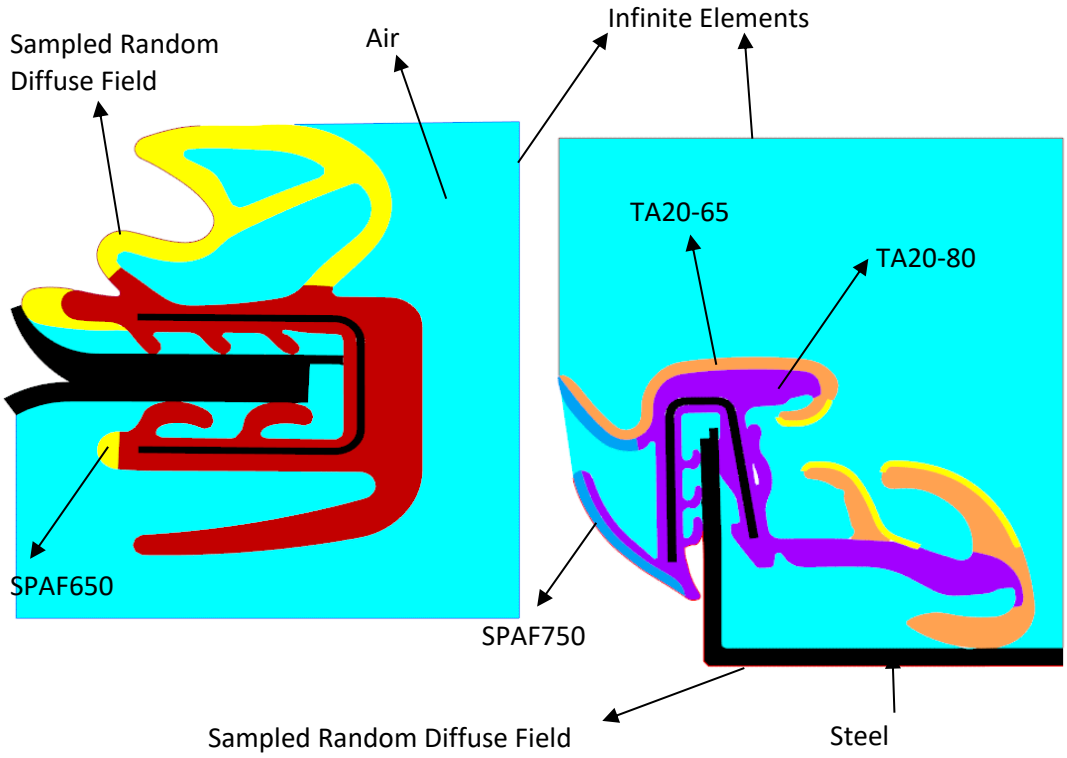

Figure 4-6 Assigned material configuration of sealant acoustical simulations

4.1.3 RESULTS OF VALIDATION ANALYSES

Sound transmission loss is predicted from incident power supplied by the sampled random diffuse field and the radiated power from the infinite elements. Moreover, sound transmission loss for the simplified dual – membrane model has been obtained by the equations of the transfer function matrix method with the applied material coefficients during the ideal model simulations. Before going into details of the result comparison, it should be noted that in the calculations of the ideal dual – membrane model, plane wave assumption has been made for both transmitted and reflected sound waves. Moreover, different from the analytical calculations, diffuse field conditions have been assigned in the simulations. Figure 4-7 illustrates the predicted

sound transmission loss values of the simplified dual – membrane model by the transfer function matrix method.

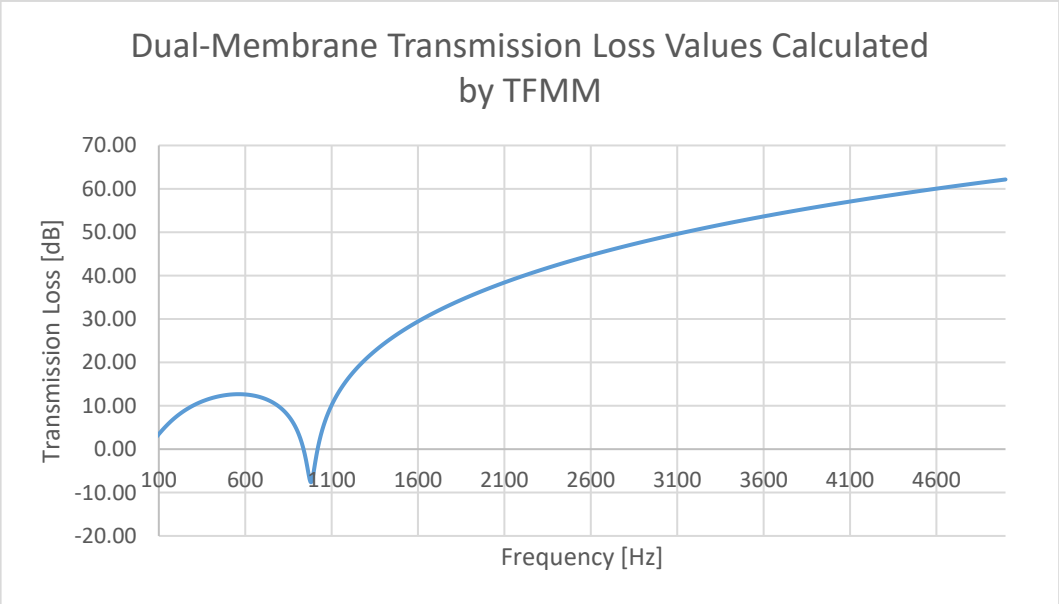

Figure 4-7 Sound transmission loss vs frequency graph of simplified dual – membrane model which is calculated by transfer function matrix method

On the other hand, simulation results for the same simplified dual – membrane model can be examined in Figure 4-8.

It can be said that those two graphs have similar trends and close results for mid – to – high frequencies. However, for the low – frequency range the predicted sound transmission loss values from the simulation results are nearly $15\ dB$ higher than the results of the transfer function matrix method. Resonance frequency calculated from the simulation results is very close to the analytical result. One is $971\ Hz$ and the other one is $975\ Hz$, respectively. According to the Park's article this resonance frequency corresponds to the mass – air – mass resonance frequency of the seal. At this resonance frequency, the seal behaves as two masses connected with a spring

element. For the dual – membrane model, the mass – air – mass resonance frequency, f_0, is: [1]

$$f_0 = \frac{1}{2\pi}\sqrt{\frac{\rho c^2}{L}\left(\frac{d_1 + d_2}{\rho_s d_1 d_2}\right)} \tag{4-1}$$

For the given dimensions and material properties, calculated resonance frequency is $974.52\ Hz$. This calculated resonance frequency is very close to the resonance frequency obtained from the acoustical simulations.

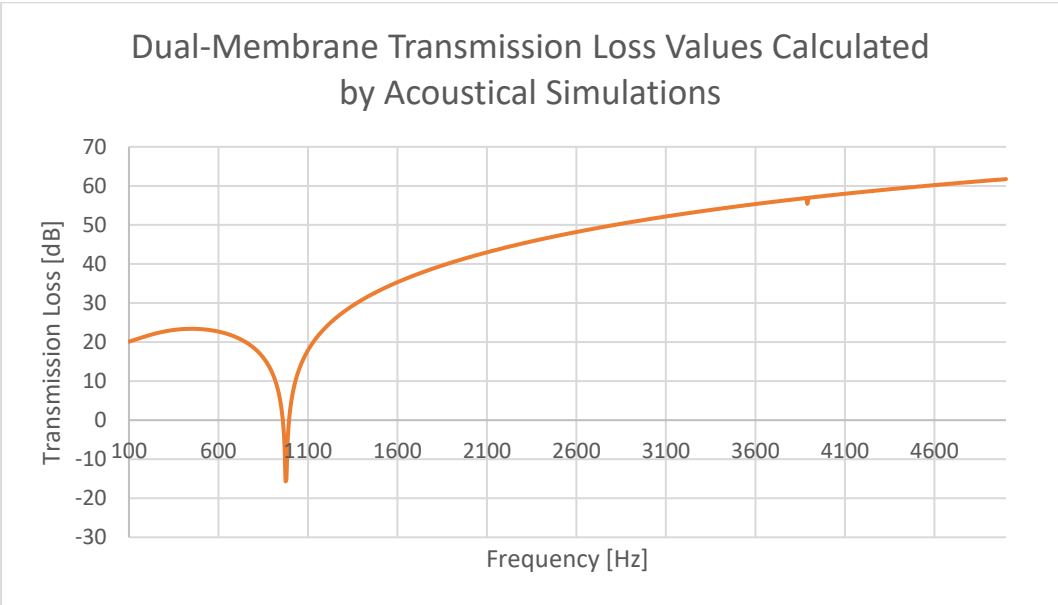

Figure 4-8 Sound transmission loss vs frequency graph of simplified dual – membrane model which is obtained from simulations

There exists dissimilar points between the results of the transfer function matrix method and the acoustical simulations. This comparison shows that the proposed

model for the acoustical analyses can be used to estimate the sound transmission loss of different sealant geometries.

Second simulation has been done on the primary seal. Simulation results are compared with the acoustical test results mentioned earlier. Figure 4-9 represents results of the test and simulation.

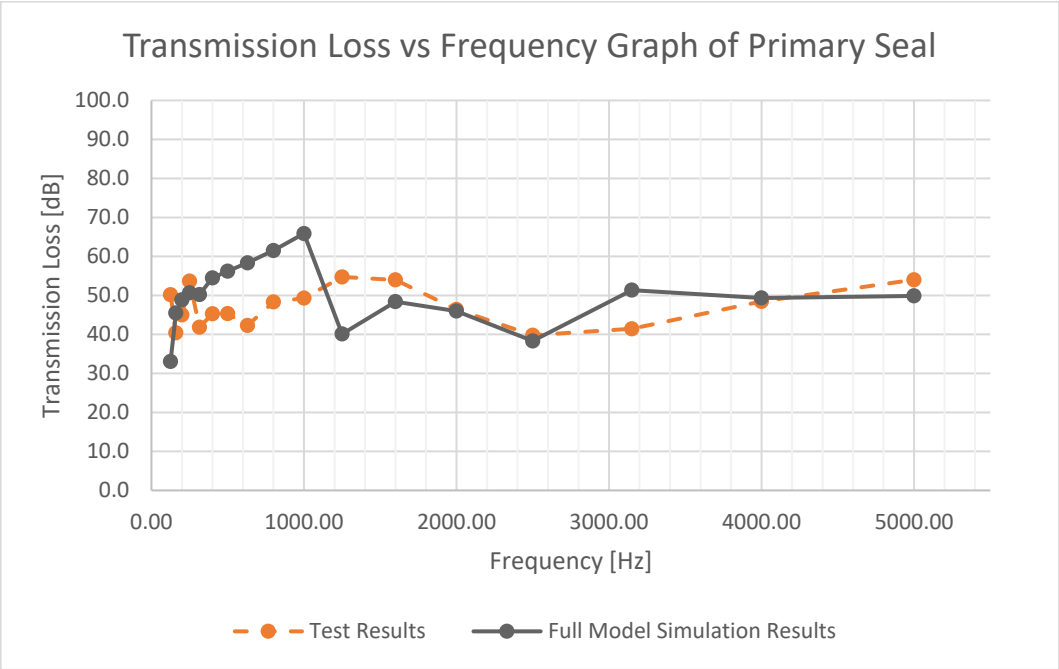

Figure 4-9 Sound transmission loss vs frequency graph of results of acoustical simulation and test for primary seal

The calculated sound transmission loss values for primary seal test is represented in 1/3 octave band center frequencies. Comparison of the test results and simulation results yields that the calculated sound transmission loss values possess similar trends for mid – frequency and high frequency ranges. However, for the low – frequency range, simulation results display high transmission loss values, as it is expected. It is reasonable to state that the applied model can be used to estimate the sound

transmission loss for middle – to – high frequency ranges, not for the low frequency range. It should be noted that for the TA20-70 material, TA20-65 material has been assigned.

The same model has been applied to the acoustical simulations of the secondary seal. Like the primary seal, the results are compared with the experimental values to determine the validity of the applied model. Comparison of the sound transmission loss values for the secondary seal is presented in Figure 4-10 for 1/3 octave band center frequencies.

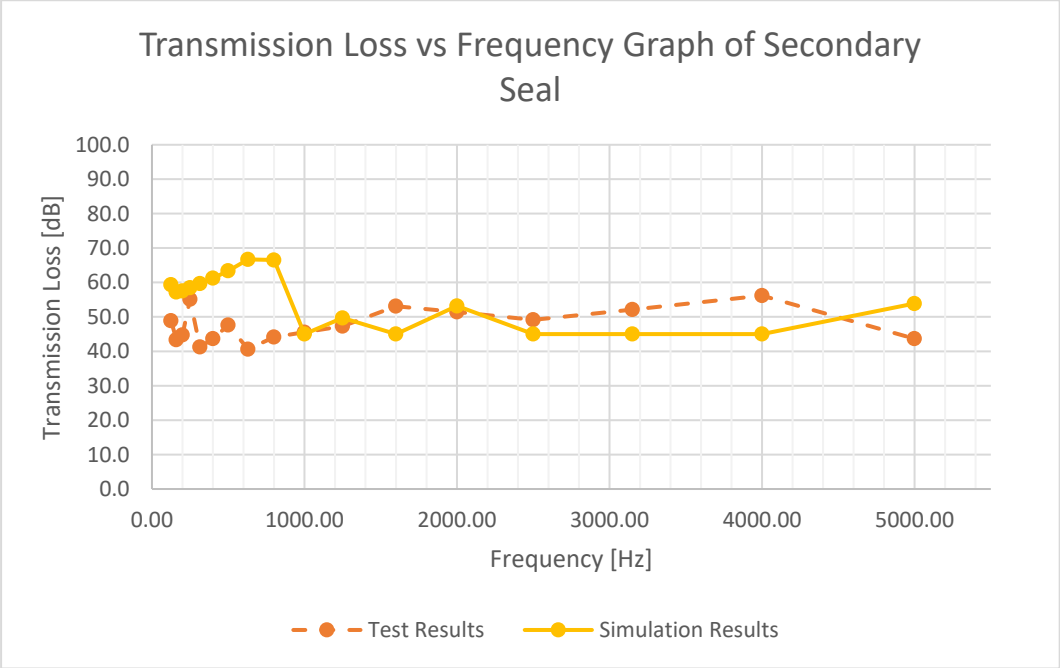

Figure 4-10 Sound transmission loss vs frequency graph of results of acoustical simulation and test for secondary seal

Similar to the results of the primary seal and simplified dual – membrane model, calculated sound transmission loss values for the low – frequency range results in higher transmission loss values. On the contrary, for the middle and high frequency

ranges test and simulation results have the same trend. The calculated values are close to the test results, although some of the material properties have been estimated or other materials' properties are assigned.

Comparison of the sound transmission loss values for three different simulations for validation yields that the proposed model for the acoustical tests can be used to estimate the sound transmission performance of a system that consists of hyperelastic materials. Although estimated transmission loss values corresponds to the lower frequencies are higher than the analytical results or the test results; close results can be observed for mid – to – high frequency range. Therefore, this model can be used to estimate the sound transmission performance of the overall sealant system composed of two different bulb seals.

4.2 ANALYSIS OF MULTIPLE SEAL SYSTEM

In this section acoustical analysis performed on the sealing system of a passenger car, which consists of two different sealants, is depicted. Since the elastic strain levels are below the 5% in the deformation analyses, the effects of preload is negligible and not considered in the acoustical simulations.

4.2.1 GEOMETRY, MESH GENERATION AND MODELING

Geometry for the acoustical analysis is obtained from the results of the deformation analysis. The exported geometry from Marc – Mentat platform is processed by SolidWorks 2016. Necessary air layers have been added into the geometry. Final form can be seen in Figure 4-11.

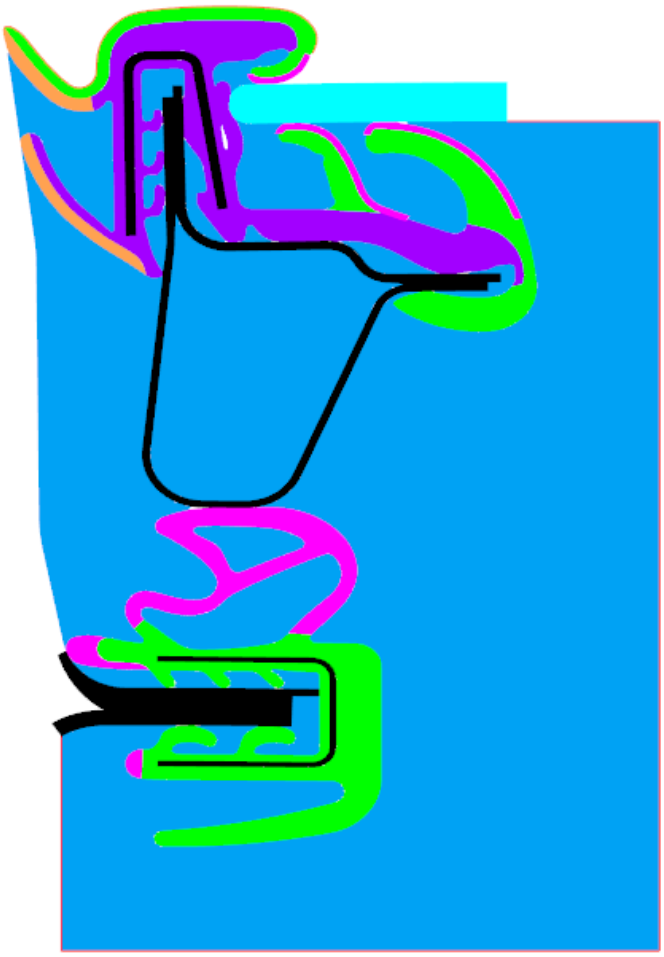

Figure 4-11 Double sealant system geometry for acoustical simulations

MSC Apex Fossa is used as pre – processor. Line elements and surface elements are created with 1 mm mesh size. Linear elements are used. After the mesh generation step, it is imported into Actran software to create acoustical simulation model. Same acoustical model with the validation analyses have been used. Simulations are performed from 100 Hz to 5000 Hz with 5 Hz frequency increments on Actran 15.1. Sampled random diffuse field is used with fifty samples as the excitation boundary condition. On the receiver side, infinite elements are employed. Boundary conditions and assigned materials can be examined in Figure 4-12.

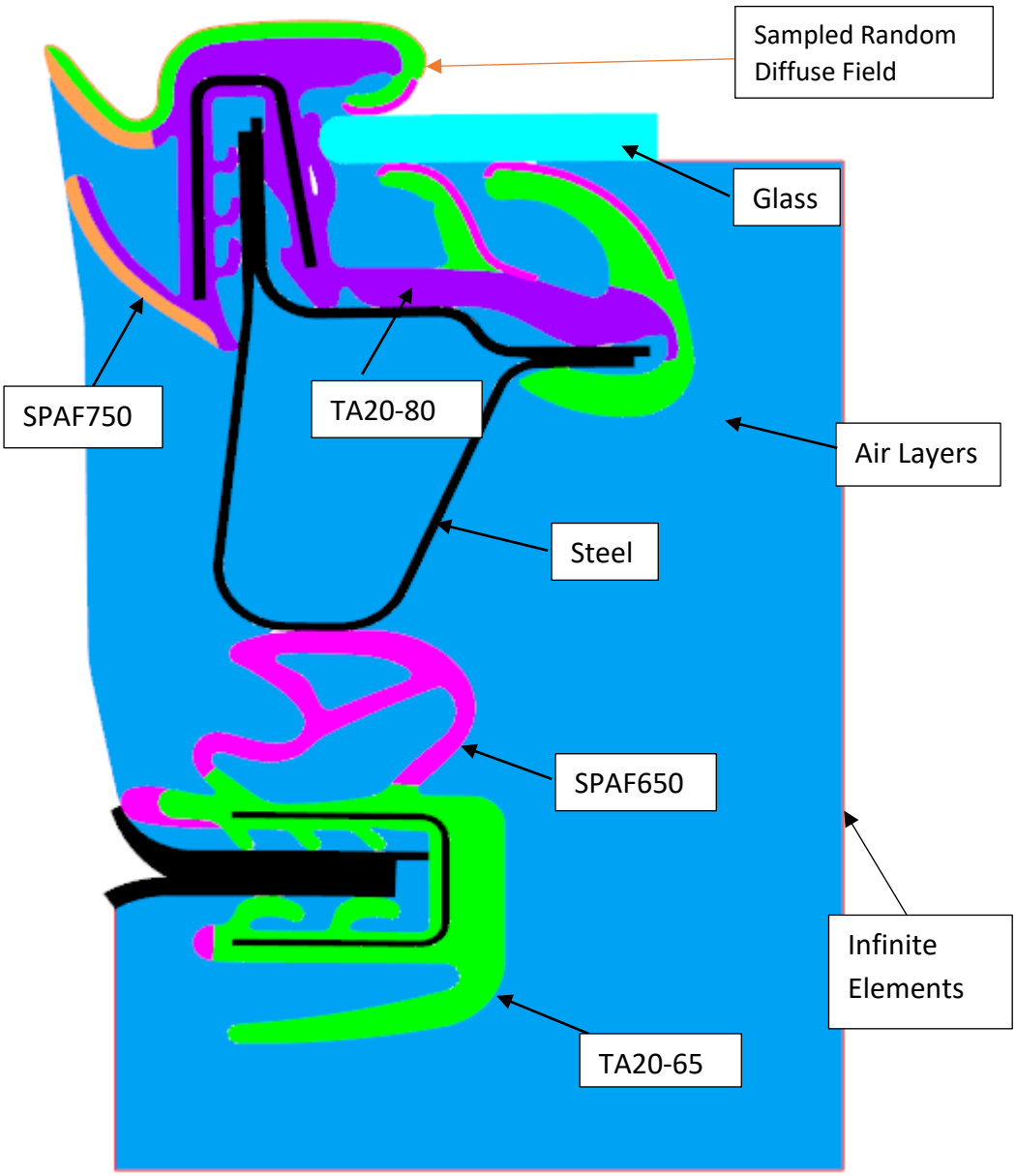

Figure 4-12 Double sealant system acoustical simulation model

Hyperelastic material properties are defined as they are defined in the validation analyses. Their modulus values are calculated by using the double transition (15 – Parameter) model as explained in section 2.1.1.5. It should be noted that TA20-70 material should be used rather than the TA20-65 material in the primary sealant. However, sample of TA20-70 cannot be physically acquired; therefore, tests for

complex modulus cannot be conducted. There is also one other important point that should be phrased. To be able to catch the sound transmission performance of the sealant system only, diffuse field boundary condition is applied on the secondary sealant only rather than the glass. However, sound transmission through the glass component is also an important phenomenon, which reduces the sound quality metrics inside the automobile. Therefore, in order to decrease the sound transmission through the automobile door, the overall glass – sealant system should be taken into account.

Upon the inspection of the specified model, it can be said that there exist three possible paths that sound waves can be transmitted. Those paths are marked in Figure 4-13.

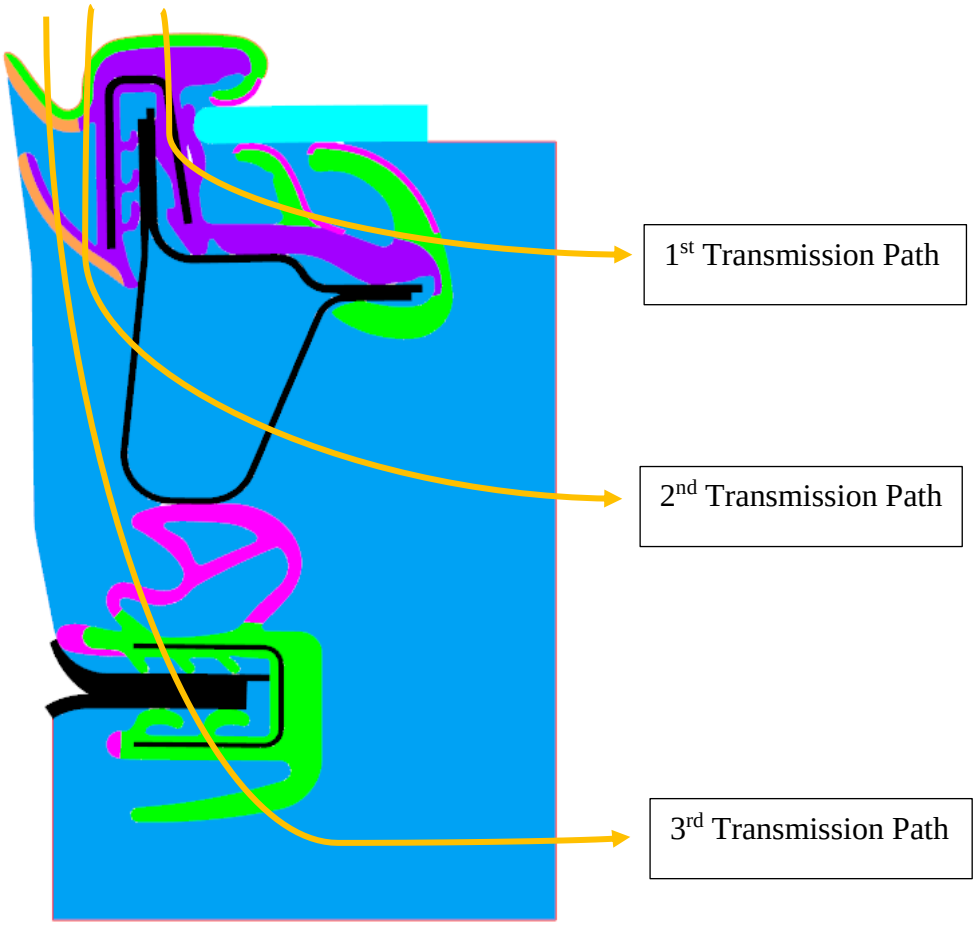

Figure 4-13 Possible sound transmission paths on dual sealant model

In order to understand effects of these different transmission paths, three different cases have been developed and acoustical simulations for those models have been carried. In the 1st case, simulations of model shown in Figure 4-12 have been performed. This model gives the actual sound insulation performance of the sealant system. As the 2nd case, door frame and corresponding air layers are not considered to eliminate the sound transmission from the 2nd path. Corresponding model to the 2nd case is illustrated in Figure 4-14.

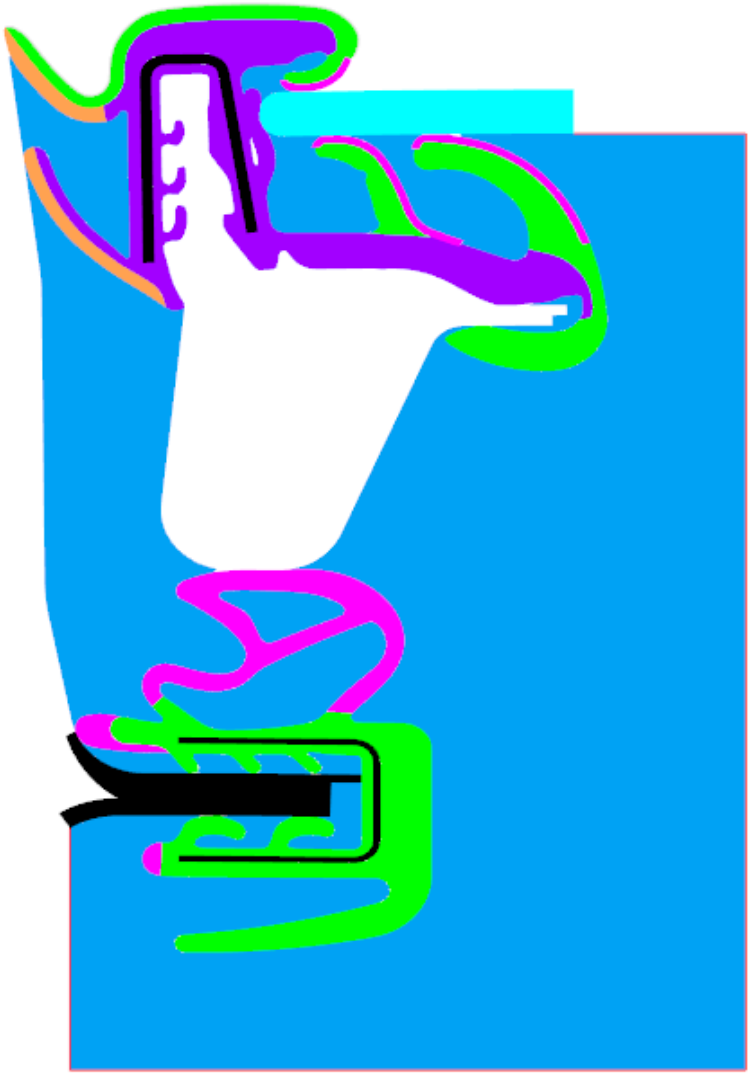

Figure 4-14 Acoustical model of the 2nd case

As the 3rd and the last case, air layer at the receiver portion and the corresponding infinite elements layer are constructed such that it only covers the primary seal. Moreover, door frame is also left out in this case. By this way, both the 1st and the 2nd transmission paths have been eliminated. From the results of the 3rd case, sound insulation performance of only these two sealants can be predicted. Model corresponds to the 3rd case is presented in Figure 4-15.

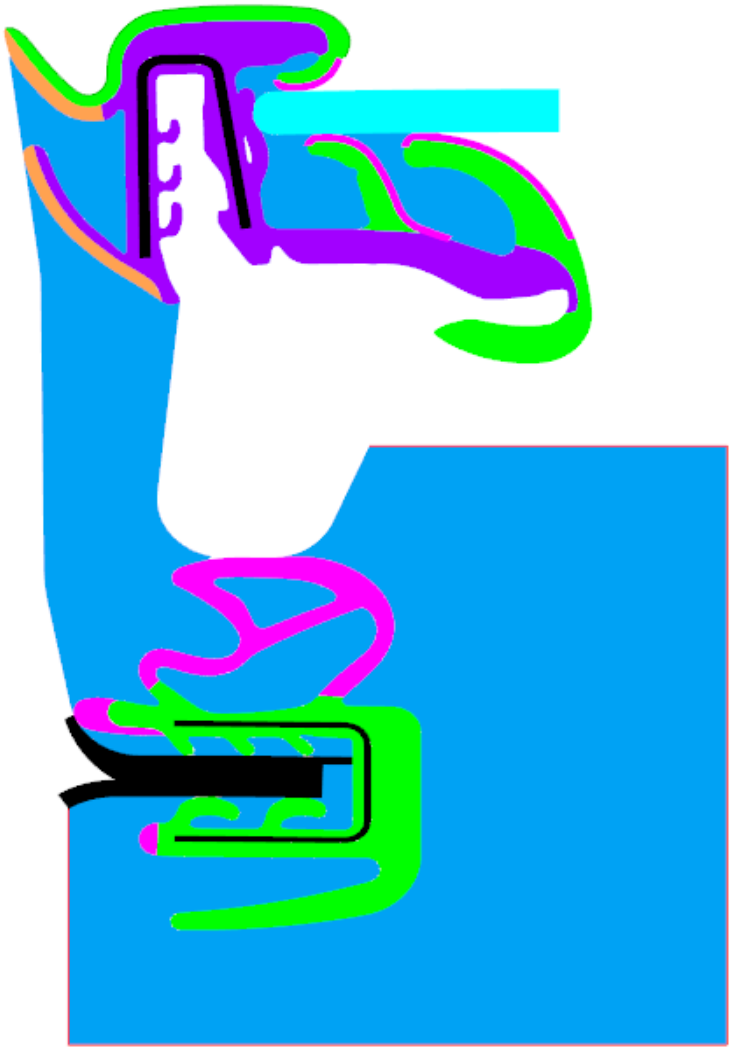

Figure 4-15 Acoustical model of the 3rd case

4.2.2 RESULTS

Sound transmission loss values are calculated for the specified frequencies as in the case of the previous acoustical analyses. Incident power by the sampled random diffuse field and radiated power from the infinite layer are used in calculations of the sound transmission loss. Furthermore, the results of each case is compared with the summation of the validation test results conducted on the primary and secondary seals. By using this superposition method, sound insulation performance of the two

sealants can be roughly predicted. Calculated sound transmission loss values are represented in 1/3 octave band center frequencies. Results of the actual system (i.e. Case 1) can be observed in Figure 4-16.

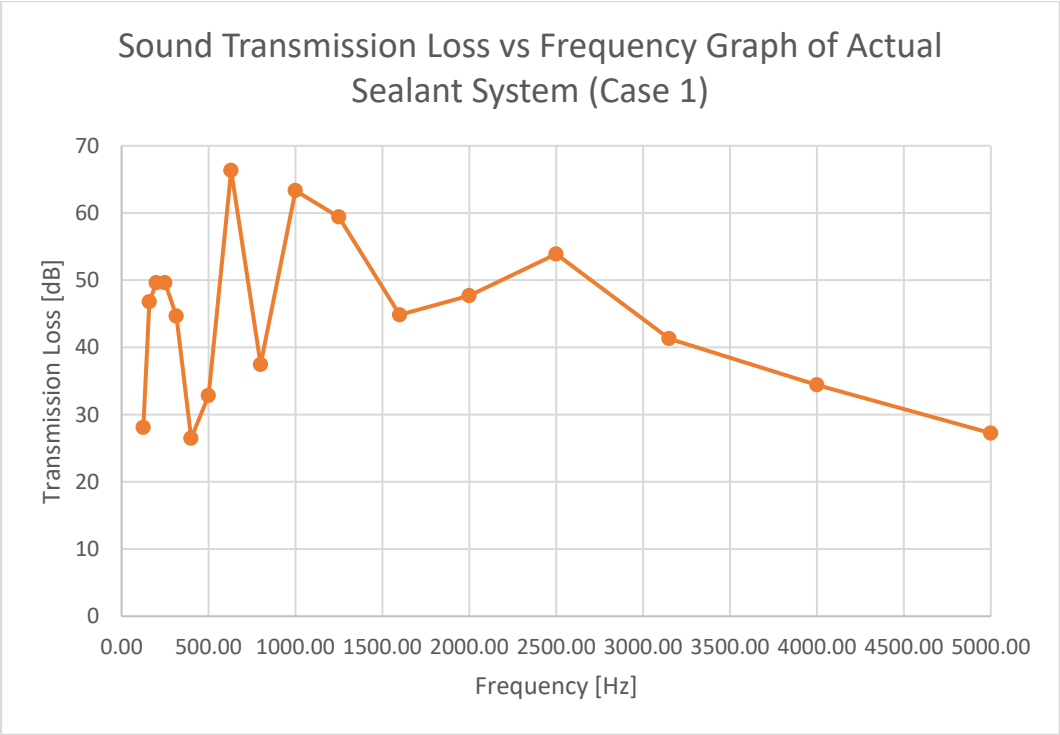

Figure 4-16 Transmission loss vs frequency graph of actual sealant system (i.e. Case 1)

As it can be seen in the Figure 4-16, the calculated sound transmission loss values for the two – sealant system are low especially for the mid – to – high frequency ranges. It is reasonable to state that according to the simulation results of the primary and secondary sealants, sound transmission values of a sealant system, which contains both of the bulb seals, should be higher. The reason of those lower results is the previously mentioned additional sound transmission paths. As the leakage from those paths are eliminated, the sound transmission loss values should get higher. This situation can be proved by comparing the results of all of the cases. In Figure 4-17

this comparison have been made and in addition to the results of the cases, summation of individual sound transmission loss values of validation test simulations is also taken into account.

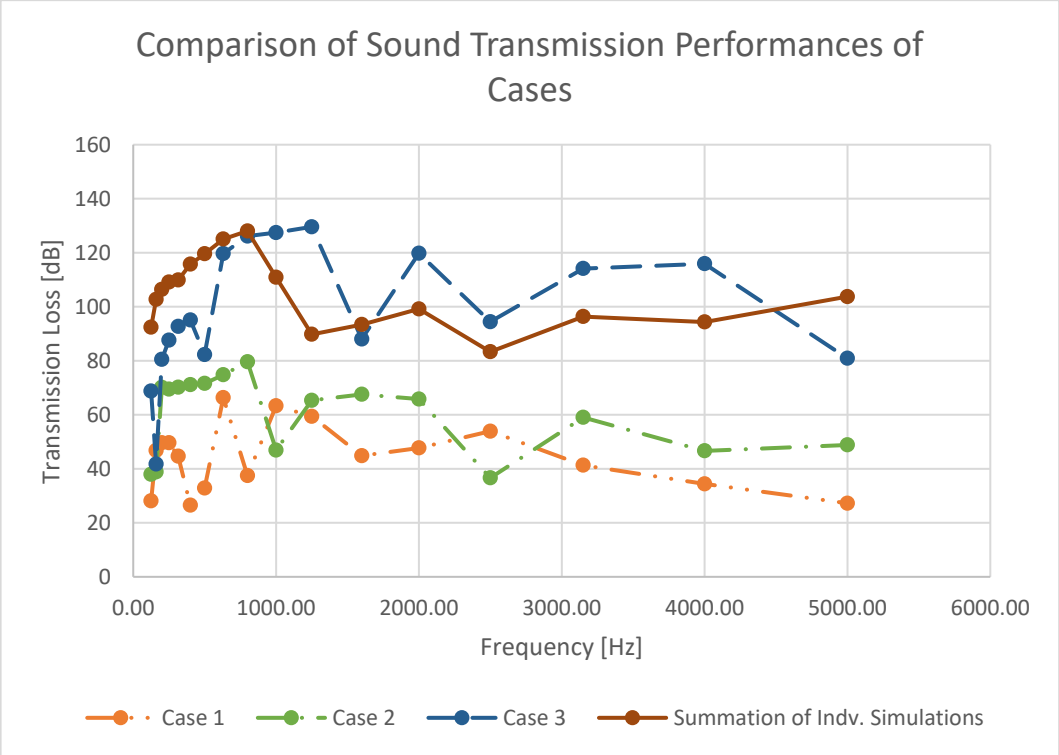

Figure 4-17 Transmission loss comparison

According to Figure 4-17 as the transmission paths are eliminated the sound transmission loss values are increasing. Moreover, for the 3rd case simulation results have same trend and close results with the summation of the individual acoustical simulation results, as it is expected. Transmission loss simulation is like springs connected in series. The week element dominates the outcome.

CHAPTER 5

SUMMARY AND CONCLUSIONS

5.1 SUMMARY

This study involves prediction of sound insulation performance of sealing system of an automobile. This has been accomplished by the aid of finite element analyses and calculation of the sound transmission loss values of the sealing system. This study is accomplished in two main steps. In the first step, deformed forms of the sealants have been obtained, and in the second step, acoustical analyses have been performed.

In order to obtain the deformed shape of the sealants, quasi – static analyses have been performed in Marc – Mentat 2016 platform. At the beginning of the study in order to acquire the suitable model for the deformation analysis, validation analyses are performed on the bulb seals, separately. Three different tests have been simulated and simulation results are compared with the experimental results. After the validation step, deformation analysis has been conducted on the sealing system, which consists of two different bulb sealants and frame components of the automobile, by using same validated model. Quasi – static analysis has been finalized with exporting the deformed geometry. Each node's position from the displacement results of the simulation has been recalculated in this process.

Next intermediate step is preparation of the exported deformed geometry for acoustical simulations. It should be noted that in the deformation analyses air layers are not considered. Therefore, air layers are added in between the solid layers to be able to perform the acoustical analyses. This task is performed in SolidWorks 2016.

Final main step is the acoustical simulations. Those simulations have been performed in Actran 15.1 and Apex Fosse is used as the pre – processor. Firstly, validation study has been conducted as in the case of the deformation analyses. In this study, three different simulations are performed for validation of the acoustical models. The first one is exercised on a simplified model and others are performed on primary and secondary seals, separately. As the first validation simulation, transmission loss values of the dual – membrane model are predicted from simulation as well as an analytical method, which is named as transfer function matrix method. Those two results are compared. For the rest of simulations, transmission loss values are calculated for 1/3 octave band center frequencies and simulation results are compared with the experimental results. After obtaining the correct model, acoustical simulation has been performed on the sealant system of a vehicle by using the resulting geometry of the deformation analysis. Moreover, three different simulations have been performed to examine the effects of three different transmission paths for the overall sealant system of an automobile.

5.2 CONCLUSIONS

Elastomeric bulb seal materials are classified as hyperelastic materials whose material properties, Young's modulus and loss factor, are highly dependent on temperature and frequency. Furthermore, there is a non – linear relationship between the stress and strain for the hyperelastic materials. Therefore, analysis performed on the hyperelastic materials are highly non – linear. During the quasi – static

deformation analyses, materials have been defined on the Marc – Mentat 2016 by using the hyperelastic material models.

Firstly, validation analyses have been performed to obtain proper model for the deformation analysis. During the validation analyses three tests, two of them on the primary seal and one of them on the secondary seal, have been simulated and force vs opening curves are compared with the experimental results. In addition, the effects of friction forces between mating bodies is also depicted. For all of the test simulations good correlation with the experimental results have been obtained. As it is expected, friction forces increase the required force to deform the bodies and simulations with the frictional effects give closer results to the experimental results. Simulation results and experimental results have yielded very close values as it can be examined in Figure 3-15, Figure 3-16 and Figure 3-17.

Most important points of simulations with the hyperelastic materials involve using the correct material model and defining contacts between two mating body correctly. Moreover, since the analyses have been performed on 2D models, correct 2D assumption should also be chosen properly. For these analyses, “plain strain” assumption has been chosen as the thickness of the samples used in the conducted experiments is relatively large. It should be noted that during the deformation analysis of the sealant system air layers are not considered.

Upon completion of deformation analyses, deformed geometry has been exported. This procedure is executed by calculating a new position of each node from the overall displacement result of the quasi – static analysis. Moreover, new elements have been set from those updated nodes and a new geometry has been formed from those elements. Therefore, the mesh resolution should be fine enough to get a proper geometry for the deformed form. As the element size is getting smaller, exported geometry becomes smoother. However, models with very fine mesh resolution need

more computational time and it may result in divergent displacement values during the calculations. Hence, element size should be chosen by considering its effects on quality of the exported geometry and on computational resource that it requires.

Exported geometries have been modified on SolidWorks 2016. Gaps between the solid bodies are filled with air layers. Then, finalized geometry is exported for the acoustical analysis.

Three different acoustical analyses have been performed to decide on the validity of the acoustical simulation model as in the case of the deformation analyses. Acoustical simulations are performed on Actran 15.1 while the meshed geometries are formed in the Apex Fossa environment. During the acoustical simulations, element shape and mesh quality are two of the most important issues to deal. If the elements are highly distorted, Actran cannot make calculations and yield zero pressure and power values although it successfully finalizes the computation without any error message.

The initial analysis is performed on a simplified model by assigning constant Young's modulus and loss factor. Results of the performed acoustical analysis are compared with the results of an analytical method named as transfer function matrix method. From the comparison, it can be concluded that transmission loss values come out very close to each other for mid – to – high frequency range. However, for low frequencies, simulation results are higher than the analytical results. Moreover, the predicted resonant frequency is very close to the air – mass – air resonance frequency calculated from Eq. (4-1). It is reasonable to state that beside the low frequencies, this model can be used to predict the sound insulation performance of a system. Second and third analyses have been performed on the primary and secondary sealants. Sound transmission loss values are predicted from the simulation results and they are compared with the experimental results for the $1/3$ octave band center frequencies. Although frequency dependent properties of some of the materials are missing and

different but similar behaving materials are assigned for those components; the calculated results from the simulations are close to the experimental results at mid – to – high frequency range as in the case of the simulations of the simplified model. In the low frequency range, the predicted sound transmission loss values are higher as it is expected. Hence, for the acoustical simulations, it can be stated that the calculated sound transmission loss values are reasonable and the model is validated.

As the final step, sound transmission loss values of sealant system composed of two different bulb seals are predicted. Finalized geometry, that is the modified version of the resultant geometry, is exported from Marc 2016 and validated model is applied during the simulations. The calculated transmission loss values from the simulation results are represented in 1/3 octave band frequencies. For the actual sealant system, overall sound transmission loss values are very low even for the low frequencies. The reason behind this issue is two additional transmission paths between the outside and the passenger side. Effects of those paths are examined with two additional simulations. One of the transmission paths is eliminated in each simulation. At the end, effect of only the main transmission path, which is the 3rd path in Figure 4-13, is acquired. As the transmission paths are eliminated, the predicted transmission loss values become higher as expected. Moreover, the results of the final simulations, carried to understand only the effect of the 3rd transmission path, possess the highest transmission loss values, as it is expected. Furthermore, those results are compared with the superposed results of the simulations performed on the primary and secondary sealants, and transmission loss values of 3rd case display the closest values to these superposed results.

REFERENCES

[1] J. Park, T. Siegmund, and L. Mongeau, "Sound Transmission Through Elastomeric Bulb Seals," *J. Sound Vib.*, vol. 259, no. 2, pp. 299–322, 2003.

[2] B. Andro, S. Chaigne, A. Diallo, and M. Mermet, "Prediction of sound transmission through automotive door seal systems," *Acoustics*, 2008.

[3] S. Atamer, M. Çalışkan, and G. O. Özgen, "Prediction of Sound Transmission through Elastomeric Bulb Seals," *Internoise 2014*, no. September, pp. 1–9, 2014.

[4] Ö. D. Okay, "Validation of Structural Analysis Model of a Layered Structure with Elastomeric Components," Middle East Technical University, 2010.

[5] MSC Software, "Nonlinear Finite Element Analysis of Elastomers."

[6] A. Stenti, D. Moens, and W. Desmet, "Dynamic modeling of car door weather seals: A first outline," *Proc. ISMA 2004 Int. Conf. Noise Vib. Eng. Vols 1-8*, pp. 1249–1261, 2005.

[7] E. Dikmen and I. Basdogan, "Material Characteristics of a Vehicle Door Seal and Its Effect on Vehicle Vibrations," *Veh. Syst. Dyn.*, vol. 46, no. 11, pp. 975–990, 2008.

[8] N. W. Tschoegl, "Constitutive Equations for Elastomers," *J. Polym. Sci.*, vol. 9, no. 9171, pp. 1959–1970, 1971.

[9] D. I. G. Jones, *Handbook of Viscoelastic Vibration Damping*. New York: Wiley, 2001.

[10] L. Rouleau, R. Pirk, B. Pluymers, and W. Desmet, "Characterization and

Modeling of the Viscoelastic Behavior of a Self-Adhesive Rubber Using Dynamic Mechanical Analysis Tests," *J. Aerosp. Technol. Manag.*, vol. 7, no. 2, pp. 200–208, 2015.

[11] R. Jakel, "Analysis of Hyperelastic Materials with MECHANICA," 2010.

[12] L. E. Kinsler, A. R. Frey, A. B. Coppens, and J. V Sanders, "Fundamentals of Acoustics," vol. 1. p. 560, 1999.

[13] J. Park, L. G. Mongeau, and T. Seigmund, "Sound Transmission Characteristics of Elastomeric Sealing Systems," *J. Can. Acoust. Assoc.*, vol. 28, no. 3, pp. 102–103, 2000.

[14] J. A. Cordioli, M. Calçada, T. Rocha, V. Cotoni, and P. Shorter, "Application of the Hybrid FE-SEA Method to Predict Sound Transmission Through Complex Sealing Systems," 2011.

[15] Y. Gur and K. N. Morman, "Sound Transmission Analysis of Vehicle Door Sealing System," in *Noise & Vibration Conference & Exposition*, 1999, no. 724, p. 12.

[16] R. H. T. Ueda, L. C. Brandão, and C. H. Lauro, "Analysis of Automotive Liftgate Seals Using Finite Element Analysis," *SciELO Anal. - Polim.*, vol. 20, pp. 301–308, 2010.

[17] C. Oliver, L. Jézéquel, and S. Besset, "Door and Window Seal Impact on Acoustic and Vibrational Behavior of Aerodynamic Noise," in *22nd International Congress on Sound and Vibration*, 2015, no. July, p. 8.

[18] Q. Li and L. Thesis, "Transmission loss of vehicle seals," Kungliga Tekniska Högskolan, 2008.

[19] L. R. G. Treloar, "The Elasticity of a Nerwork of Long-Chain Molecules. I.," *Transations Faraday Soc.*, no. 36, pp. 36–41, 1942.

[20] L. R. G. Treloar, "The Elasticity of a Nerwork of Long-Chain Molecules. II.," *Transations Faraday Soc.*, no. 241, pp. 241–246, 1943.

[21] V. Hongisto, “Sound Insulation of Doors—Part 1: Prediction Models for Structural and Leak Transmission,” *J. Sound Vib.*, vol. 230, no. 1, pp. 133–148, 2000.

[22] V. Hongisto, J. Keränen, and M. Lindgren, “Sound Insulation of Doors - Part 2: Comparison Between Measurement Results and Predictions,” *J. Sound Vib.*, vol. 230, no. 1, pp. 149–170, 2000.

[23] K. M. Morman, Y. Gur, W. Bloomfield, and A. Arbor, “Method and System for Designing Vehicle Door Seals Based on Predicted Sound Transmission Characteristics,” 5,940,788, 1999.

APPENDIX A

TRANSMISSION LOSS VS FREQUENCY GRAPHS

6.1 PRIMARY SEAL

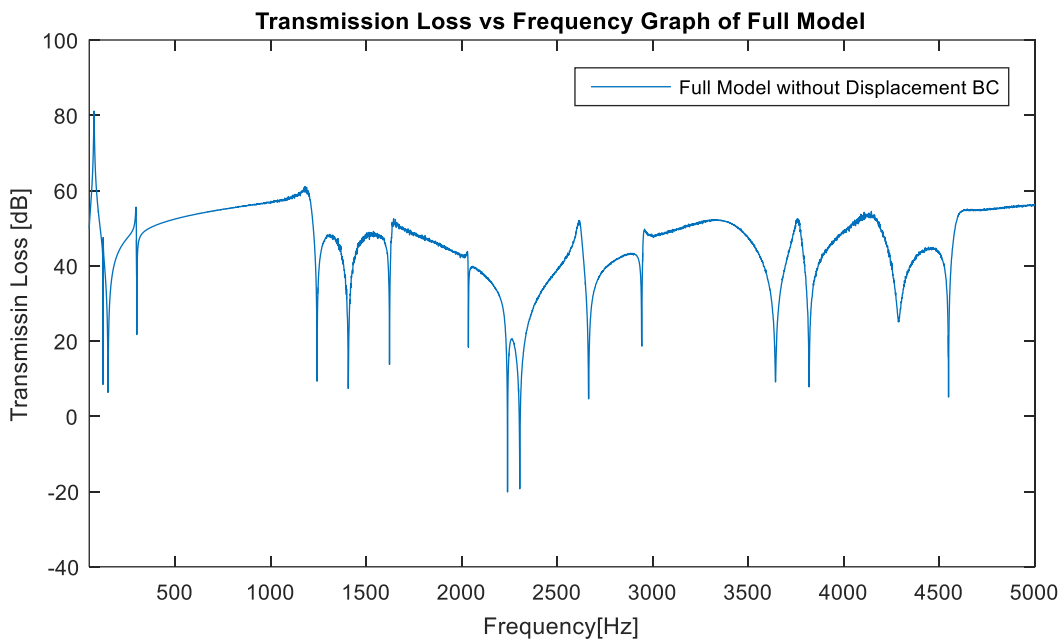

Figure 6-1 Transmission loss vs frequency graph of simulation results of primary seal

6.2 SECONDARY SEAL

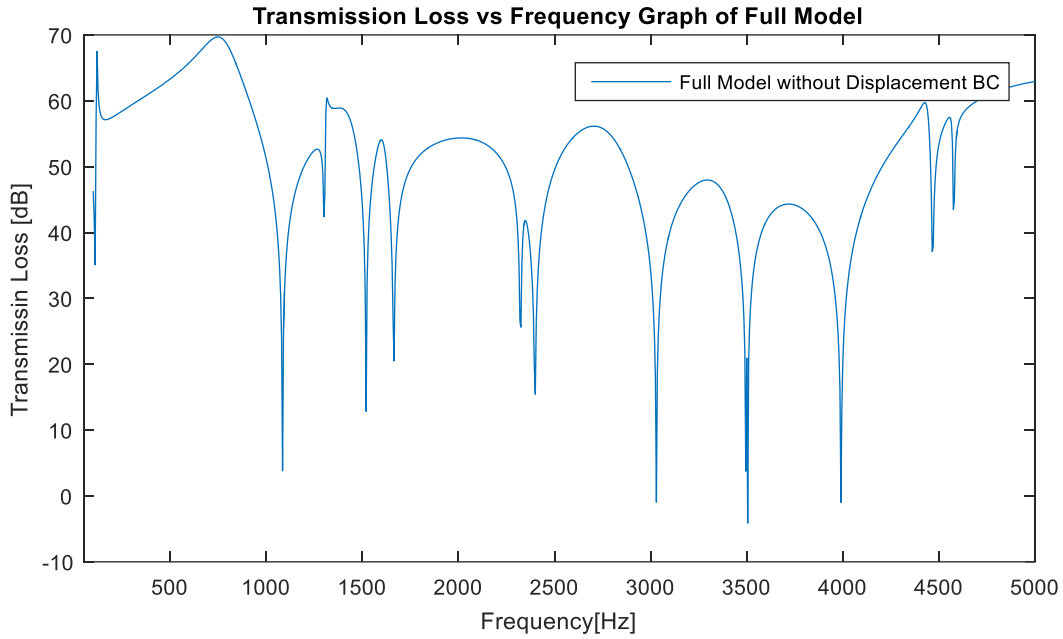

Figure 6-2 Transmission loss vs frequency graph of simulation results of secondary seal

6.3 MULTIPLE SEALANT SYSTEM

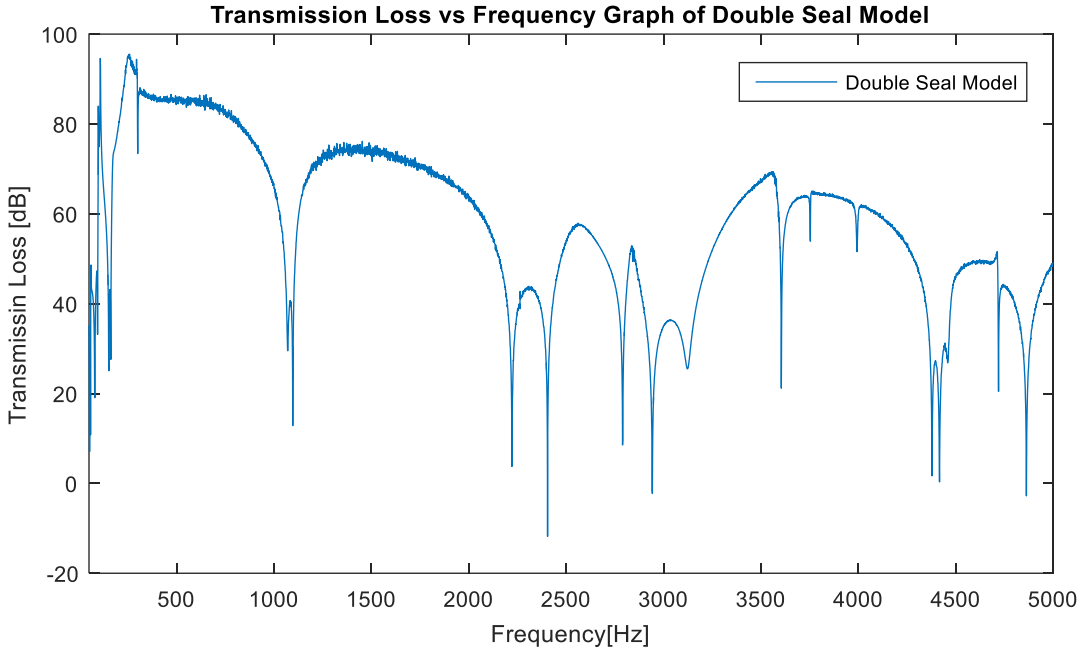

Figure 6-3 Transmission loss vs frequency graph of simulation results of multiple sealant system